Jordan-Wigner composite fermion liquids in a two-dimensional quantum spin ice

Leonardo Goller[1] and Inti Sodemann Villadiego[2,3]
[1]*SISSA, Via Bonomea 265, 34136 Trieste, Italy*
[2]*Institut für Theoretische Physik, Universität Leipzig, Brüderstraße 16, 04103, Leipzig, Germany*
[3]*Max-Planck-Institut für Physik komplexer Systeme, Nöthnitzer Straße 38, 01187 Dresden, Germany*

(Received 29 September 2023; accepted 9 January 2024; published 26 January 2024)

The Jordan-Wigner map in two dimensions is an exact lattice regularization of the 2π-flux attachment to a hard-core boson (or spin $\frac{1}{2}$) leading to a composite fermion particle. When the spin-$\frac{1}{2}$ model obeys ice rules this map preserves locality, namely, local Rohkshar-Kivelson (RK) models of spins are mapped onto local models of Jordan-Wigner composite fermions. Using this composite fermion dual representation of RK models we construct spin-liquid states by projecting Slater determinants onto the subspaces of the ice rules. Interestingly, we find that these composite fermions behave as "dipolar" partons for which the projective implementations of symmetries are very different from standard "pointlike" partons. We construct interesting examples of these composite Fermi-liquid states that respect all microscopic symmetries of the RK model. In the six-vertex subspace, we constructed a time-reversal and particle-hole-invariant state featuring two massless Dirac nodes, which is a composite fermion counterpart to the classic π-flux state of Abrikosov fermions in the square lattice. This state is a good ground-state candidate for a modified RK–type Hamiltonian of quantum spin ice. In the dimer subspace, we constructed a state featuring a composite Fermi surface but with nesting instabilities towards ordered phases such as the columnar state. We have also analyzed the low-energy emergent gauge structure. If one ignores confinement, the system would feature a $\mathrm{U}(1) \times \mathrm{U}(1)$ low-energy gauge structure with two associated gapless photon modes, but with the composite fermion carrying gauge charge only for one photon and behaving as a gauge-neutral dipole under the other. These states are also examples of pseudoscalar U(1) spin liquids where mirror and time-reversal symmetries act as composite fermion particle-hole conjugations, and the emergent magnetic fields are even under such time-reversal or lattice mirror symmetries.

DOI: 10.1103/PhysRevB.109.035162

I. INTRODUCTION

The appearance of fermionic particles in systems whose microscopic building blocks are spins or bosons is a remarkable example of the emergence of nonlocal excitations in quantum states of matter. An exact and powerful map that allows to understand this phenomenon in one dimension is the Jordan-Wigner transformation, which provides a rewriting of one-dimensional (1D) spin-$\frac{1}{2}$ models in terms of fermions. In two dimensions the Jordan-Wigner transformation is closely related to another celebrated statistical transmutation procedure known as flux attachment [1–6]. More specifically, as we will review in detail in Sec. II, a standard Jordan-Wigner fermion constructed by ordering spin-$\frac{1}{2}$ operators in a two-dimensional (2D) lattice is exactly equivalent to a hard-core boson carrying a fictitious solenoid of 2π flux. In this sense, the 2D Jordan-Wigner fermion is an exact lattice regularized version of the composite fermion particle that is commonly used to understand certain quantum Hall states emerging from microscopic bosons, such as those making the bosonic composite Fermi-liquid state at filling $\nu = 1$ [7–9].

This 2D Jordan-Wigner flux attachment has been exploited in several studies of nontrivial quantum disordered states ("spin liquids") and their competition with traditional ordered phases [4,10–17]. One of the central challenges with the models investigated in these previous studies is that the Jordan-Wigner flux-attachment map in 2D does not preserve space locality, in the sense that not all local spin-$\frac{1}{2}$ operators appearing in the Hamiltonian are mapped onto local fermionic operators. This sharply contrasts with the situation in 1D, where simply imposing a global parity symmetry guarantees that local spin Hamiltonians map onto local fermionic Hamiltonians. In most of the 2D studies this difficulty is dealt with in a nonsystematic manner by adding background magnetic fields that account for the relation between particle density and flux in an average fashion, similarly to how it is done in mean-field treatments of composite fermions in quantum Hall states [18–21].

Recently, however, it has been emphasized that another kind of exact Jordan-Wigner–type map in 2D is possible which in some sense preserves space locality [22–25]. This is achieved by imposing local conservation of certain $\mathbb{Z}_2$-valued operators and thus endowing the Hilbert space of spin $\frac{1}{2}$ with a $\mathbb{Z}_2$ lattice gauge theory structure. The gauge-invariant spin operators (namely, those commuting with the $\mathbb{Z}_2$ conservation laws) can then be mapped exactly into bilinears of fermion operators. The single-fermion creation operator remains nonlocal and can be explicitly constructed as a Jordan-Wigner–type string operator in 2D [22–25]. This construction realizes an exact lattice regularization of a different kind of flux attachment, namely, the one associated with a mutual Chern-Simons theory comprised of two U(1) gauge fields and the following K matrix:

$$K = \begin{pmatrix} 0 & 2 \\ 2 & 0 \end{pmatrix},$$

which is the Chern-Simons description of the topological order associated with Kitaev's toric code model [22–25], and the Jordan-Wigner fermions are the ϵ particles, while the operator associated with the local $\mathbb{Z}_2$ conservation law measures the parity of one of the other self-bosonic anyons, e.g., the e or m particle. For related constructions see also [26–32].

Motivated by these precedents, this work investigates systems with a different kinds of local conservation law that allow to preserve the locality of the usual Jordan-Wigner map in 2D associated with attaching 2π flux to a hard-core boson. Our local conservation laws will be associated with a two-dimensional "spin-ice rule" with a correspondingly conserved local operator that generates a U(1) gauge group, and the models of interest will be the classic 2D Rokshar-Kivelson–type (RK) Hamiltonians [33–45].[1] Similar to the situation in 1D, these models will remain local under Jordan-Wigner maps, however, the price we will have to pay for this is that the resulting fermionic model will be necessarily interacting and endowed with local conservation laws. Despite this, the advantage of rewriting the RK models in terms fermionic variables is that they are much more flexible degrees of freedom to construct nontrivial quantum disordered states than the original spin degrees of freedom. For example, simple fermionic Slater determinant states would serve already as a mean-field approximation to describe quantum spin-liquid states. There is, however, a crucial caveat to this mean-field approach, which is that generically free-fermion Slater determinant states will not obey the local spin-ice rules. In other words, the naive free-fermion states would break the local gauge invariance and violate Elitzur's theorem [47]. To remedy this, we will project the free-fermion states onto the susbpace of the Hilbert space satisfying the ice rules, in an analogous fashion to how the Gutzwiller projection is employed in parton constructions of spin-liquid states [48]. Despite the similarity of spirit, we have encountered that these states differ in crucial aspects from the standard parton constructions, such as the Abrikosov fermions [49–51].

One of the key distinctions is that the Abrikosov fermions of standard parton constructions behaves as a pointlike object under the parton gauge transformations, whereas the Jordan-Wigner fermion behaves as a dipolelike object under the local U(1) gauge transformations of the RK models. This is because the Abrikosov fermions operator at a given lattice site only transforms nontrivially under the parton gauge transformations acting on its site, but it transforms trivially under gauge transformations of different sites. In other words, the creation of a single Abrikosov fermion would violate the constraint defining the physical Hilbert space only at a single lattice site, and in this sense it is pointlike. The Jordan-Wigner fermion violates the spin-ice rule of two neighboring vertices, in such a way so as to create a dipole under of the U(1) Gauss' law of the RK–type Hamiltonians.

Because of the above, we will refer to our construction of spin-ice projected Slater determinants of the Jordan-Wigner fermions as an "extended parton construction." These differences between extended vs pointlike partons lead to crucial physical differences between the states constructed from them. Some of these differences will manifest as unconventional implementations of lattice symmetries. For example, we will show that $\pi/2$ rotation symmetries[2] do not admit an ordinary fermion implementation for the Jordan-Wigner fermions, but need to be dressed by a unitary transformation that is not part of the U(1) lattice gauge group.

But the most remarkable difference we have found between the extended partons and the pointlike partons is the nature of the gauge fluctuations around their mean-field Slater determinant states. According to the principles of the projective symmetry group constructions for ordinary pointlike partons, like Abrikosov fermions, a Slater determinant state which conserves the global particle-number fermions will describe a U(1) spin-liquid state, whenever it is stable against gauge confinement. The deconfined state has therefore an emergent U(1) photon gauge field, and the fermionic parton will carry charge under this field. As we will see, however, the Slater determinant of the Jordan-Wigner extended partons will feature a U(1) × U(1) gauge structure, namely, two distinct gapless photons. The Jordan-Wigner fermion will carry a net gauge charge under one of these two photons, but it will be gauge neutral under the other photon, for which it will only carry a gauge dipole.

Moreover, despite the fact that the Jordan-Wigner fermion is a composite fermion that can be viewed as a boson attached to 2π flux, we will see that the expected action of the two U(1) × U(1) gauge fields is an ordinary Maxwell-type action with no Chern-Simons terms, as a result of the enforcement of time-reversal and microscopic mirror symmetries of the models in question. This is interesting because it demonstrates an explicit instance of the existence of a composite Fermi-liquid-like state arising from flux attachment, for which the emergent gauge structure does not feature an explicit Chern-Simons term. This feature is somewhat reminiscent of the Dirac composite fermion theories of the half-filled Landau level [52–54], and of some of the more sophisticated composite Fermi-liquid theories of bosons at $\nu = 1$ [7–9], which contrast from the more traditional explicit forms of flux attachment in the Halperin-Lee-Read (HLR) description of composite fermions [18].

We will also construct interesting explicit examples of mean-field spin-liquid states for RK–type 2D quantum spin-ice Hamiltonians. As we will see, the sectors defined by different values of the spin-ice rules will correspond to different fillings of the Jordan-Wigner composite fermion bands. For example the sector with zero spin, which maps to the quantum six-vertex model [37,38], will correspond to half-filling of a two-band model. We will construct an explicit mean-field state that satisfies all the space symmetries of the lattice, time-reversal, and particle-hole transformations, and that features two gapless linearly dispersing Dirac fermion modes at low energy, which can be pictures as a composite fermion counterpart to the classic π-flux state of Abrikosov fermions [50,55]. Ignoring compactification-driven instabilities (see below, however), this would be therefore a specific

[1] See Ref. [46] for a recently proposed interesting variant.

[2] These are $\frac{\pi}{2}$ rotations that will be denoted by $R_{\frac{\pi}{2}}$.

kind of Dirac composite Fermi-liquid state, with an emergent low-energy $U(1) \times U(1)$ gauge structure with two massless photons, with the fermions carrying charge under only one U(1) photon and neutral under the other U(1) photon.

Field theories of massless Dirac fermions coupled to a single U(1) compact gauge field are known to remain deconfined at low energies in the limit of large-N number of Dirac fermion flavors [56,57] and to also avoid spontaneous chiral symmetry breaking [58,59]. However, understanding the ultimate infrared fate of these field theories at finite N has remained challenging [60–62]. In our case we have $N = 2$ Dirac fermions and two photons (with the fermions carrying charge under only one of these photons). We will not address systematically the impact of gauge compactification, but we expect that at least the photon under which the fermions are neutral will undergo Polyakov-type confinement [63,64], which will remove it from low energies, leaving possibly only two massless Dirac fermions coupled to a single U(1) photon at low energies, analogously to QED_3 with $N = 2$ (to the extent that this theory avoids confinement and other instabilities at low energies).

On the other hand, we will see that for the subspace of spin ice that maps onto the quantum dimer model [37], the band structure of the Jordan-Wigner composite fermions will be at quarter-filling, leading to the appearance of a composite Fermi-surface state. Moreover, the state arising when the composite fermions only hop between nearest-neighbor sites will display a perfectly nested Fermi surface. This nesting is accidental in the sense that it can be removed by adding symmetry-allowed further-neighbor hopping terms. Nevertheless, such strong tendency for perfect nesting can be viewed as related to the tendency of the quantum dimer model systems to have ordinary gauge-confined ground states (such as the resonant plaquette or the columnar phases [65–70]), which would appear if the Fermi surface is fully gapped via a composite fermion particle-hole pair condensation. This nested state could be therefore useful as a mother state to understand the descending competing broken-symmetry states of the quantum dimer model and perhaps help understand the strong tendency towards the columnar phase of the classic RK model, which has been advocated in recent studies to take over the complete phase diagram on the side of the RK point where a unique ground state exists ($v/t < 1$) [69,70].

Our paper is organized as follows: Section II reviews the one-dimensional Jordan-Wigner transformation and its interpretation as flux attachment in the 2D square lattice. Section III applies this construction to 2D quantum spin-ice models, and introduces the general extended parton construction of mean-field states. Then we apply this to the specific cases of quantum six-vertex and quantum dimer models, and construct the mean-field states with two Dirac cones and a Fermi surface for each of these models, respectively. Section IV develops a description of the gauge field fluctuations, and discusses the derivation of the effective low-energy theories for these states, demonstrating the appearance of two U(1) gauge fields with two associated gapless photons, with the fermions being charged under only one of the U(1) fields. We close then with a summary and discussion where we also comment on future research directions.

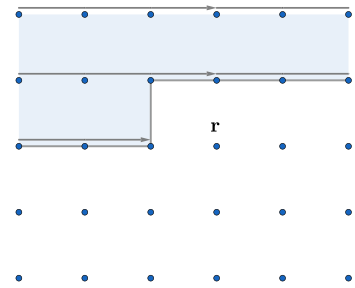

FIG. 1. Physical spin-$\frac{1}{2}$ degrees of freedom reside at the blue sites of a 2D square lattice labeled by $\mathbf{r}$. The light blue shaded region denotes the membrane operator made from the product of all the $\sigma^z(\mathbf{r}')$ spin operators in such region, associated with the Jordan-Wigner fermion creation operator at site $\mathbf{r}$ [see Eq. (1)]. The directed arrows illustrate our "western typing" convention for ordering the 2D lattice sites.

II. EQUIVALENCE OF JORDAN-WIGNER TRANSFORMATION AND FLUX ATTACHMENT IN 2D

Let us consider a two-dimensional square lattice with a spin-$\frac{1}{2}$ degree of freedom residing in each site denoted by $\mathbf{r}$, as depicted in Fig. 1. These spin-$\frac{1}{2}$ degrees of freedom can also be viewed as hard-core bosons, according to the convention of Table I. By choosing a convention for the ordering of sites, we can write the standard Jordan-Wigner fermion creation operators as follows (see Fig. 1):

$$f^\dagger(\mathbf{r}) = b^\dagger(\mathbf{r}) \prod_{1 \leqslant \mathbf{r}' < \mathbf{r}} \sigma^z(\mathbf{r}'). \tag{1}$$

We will order the sites using "western typing" convention, as depicted in Fig. 1. Since $\sigma^z(\mathbf{r}) = \exp[i\pi n(\mathbf{r})]$, it follows that for any pair of sites $\mathbf{r}, \mathbf{r}'$ the boson hopping operators can be written as

$$b^\dagger(\mathbf{r}) b(\mathbf{r}') = f^\dagger(\mathbf{r}) e^{i\pi \sum_{\mathbf{r}' \leqslant \mathbf{r}'' < \mathbf{r}} n(\mathbf{r}'')} f(\mathbf{r}'). \tag{2}$$

When $\mathbf{r}, \mathbf{r}'$ are nearby, the above operator is clearly local in its physical bosonic representation; however, it is generally nonlocal in its dual fermion representation as illustrated in Fig. 2.

Let us now demonstrate the equivalence of Eq. (2) to the 2π-flux attachment. Consider spinless fermions $f^\dagger(\mathbf{r})$ located at the sites $\mathbf{r}$ of the square lattice. We attach a thin solenoid to each of these fermions which we view as located in the

TABLE I. Dictionary spin $\frac{1}{2}$ to hard-core-boson language.

Spin $\frac{1}{2}$	Boson
$\|\uparrow\rangle$	$\|0\rangle$
$\|\downarrow\rangle$	$\|1\rangle$
σ^+	b
σ^-	$b^\dagger$
$\frac{1-\sigma^z}{2}$	n

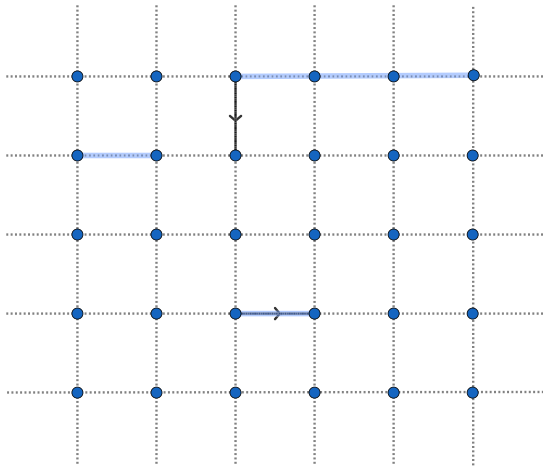

FIG. 2. Solid directed arrows represent the local boson hopping operator between sites from site $\mathbf{r}'$ towards site $\mathbf{r}$ from Eq. (2). Blue lines represent the Jordan-Wigner strings associated with the fermion representation of these same operators. We see that for our convention (see Fig. 1), the horizontal boson hoppings remain local in the fermion representation, whereas the vertical hoppings have a nonlocal fermion representation.

center of the plaquette that is northeast to the site $\mathbf{r}$ (see Fig. 3). The solenoid carries a 2π flux and we choose a gauge that concentrates its vector potential $\mathbf{A}(\mathbf{x})$ into two strings, depicted as dotted lines in Fig. 3. This gauge is chosen so that the flux attachment exactly matches our specific choice of "western typing" ordering convention of the Jordan-Wigner transformation, and different ordering conventions lead to different gauge choices for the flux attachment (see, e.g., [1–6]). Here $\mathbf{x}$ can be viewed as a coordinate on the ambient 2D space in which the lattice is embedded. Each one of these strings is chosen so that the line integral of the vector potential across a path that intersects the strings is exactly π. Therefore, when another fermion hops across a bond that intersects one of these strings, its hopping amplitude will have an extra minus sign, relative to the hopping it has when the string is not present (namely, each string acts as a "branch cut" that dresses the fermion hopping phase by π).

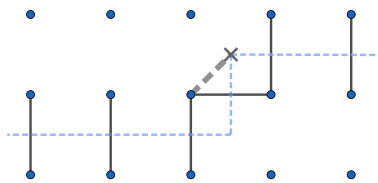

FIG. 3. Flux attachment is performed by binding to each boson (located in the sites marked by blue dots) a thin solenoid depicted by the star which is located in the plaquette northeast from the boson site. This thin solenoid carries 2π flux, whose vector potential is chosen to be concentrated in the two dotted lines connected to the star. The hopping operators (depicted by solid black lines) that intersect such dotted lines are multiplied by -1 when the solenoid is present, namely, there is an extra π phase for hopping across the dotted lines.

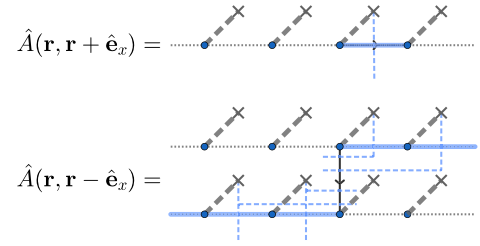

FIG. 4. A local boson hopping operator (depicted by the directed black solid line) can be equivalently represented as a fermion hopping operator with its hoppings dressed by the vector potentials that capture the 2π-flux attachment, according to the rules depicted in Fig. 3 [see Eq. (4)].

Therefore, the above convention fixes the vector potential $\mathbf{A}(\mathbf{x})$ to be a unique operator which is a function of all the fermion occupation operators $n(\mathbf{r}) = f^\dagger(\mathbf{r})f(\mathbf{r})$. Therefore, establishing the equivalence of the above flux attachment procedure to the Jordan-Wigner transformation reduces to demonstrating that the following operator identity holds:

$$\exp\left(i\pi \sum_{\mathbf{r}' \leqslant \mathbf{r}'' < \mathbf{r}} n(\mathbf{r}'')\right) = \exp\left(i \int_{\mathbf{r}'}^{\mathbf{r}} \mathbf{A}(\mathbf{x}) \cdot d\mathbf{x}\right). \quad (3)$$

To demonstrate the above relation, let us first consider the line integral of $\mathbf{A}(\mathbf{x})$ when $\mathbf{r}, \mathbf{r}'$ are nearest-neighbor sites. From Fig. 4, we can see that the following holds for the horizontal and vertical nearest-neighbor hoppings:

$$\begin{aligned} \frac{1}{\pi} \int_{\mathbf{r}}^{\mathbf{r}+\mathbf{e}_x} \mathbf{A}(\mathbf{x}) \cdot d\mathbf{x} &= n(\mathbf{r}), \\ \frac{1}{\pi} \int_{\mathbf{r}}^{\mathbf{r}-\mathbf{e}_y} \mathbf{A}(\mathbf{x}) \cdot d\mathbf{x} &= \sum_{x \leqslant x'} n(x', y) + \sum_{x' < x} n(x', y-1), \end{aligned} \quad (4)$$

where $\mathbf{r} = (x, y)$ are the coordinates of the lattice sites measured in units of lattice constant, and the integration path is chosen, respectively, to be the bonds $\{\mathbf{r}, \mathbf{r} + \mathbf{e}_x\}$ and $\{\mathbf{r}, \mathbf{r} - \mathbf{e}_y\}$ (see Fig. 4). The relations in Eq. (4) are the same expected from Eq. (3).

Let us now show that the line integral of $\mathbf{A}(\mathbf{x})$ in Eq. (3) is independent of the specific path that connects the points $\mathbf{r}, \mathbf{r}'$, modulo 2π. Let us consider two paths γ_1 and γ_2 connecting $\mathbf{r}, \mathbf{r}'$. These two paths define a closed path γ which is the boundary of a region Ω (see Fig. 5). From Stokes' theorem it follows that

$$\oint_\gamma \mathbf{A}(\mathbf{x}) \cdot d\mathbf{x} = \iint_\Omega (\nabla \times \mathbf{A})(\mathbf{x}) \cdot d\sigma = 2\pi \sum_{\mathbf{r} \in \Omega} n(\mathbf{r}). \quad (5)$$

The sum over $\mathbf{r} \in \Omega$ in the above expression is performed over those sites $\mathbf{r}$ for which the solenoid is strictly in the interior of Ω (see Fig. 5). Therefore, since the fermion-number operators $n(\mathbf{r})$ are integer valued, it follows from Eq. (5) that

$$\int_{\gamma_1} \mathbf{A}(\mathbf{x}) \cdot d\mathbf{x} = \int_{\gamma_2} \mathbf{A}(\mathbf{x}) \cdot d\mathbf{x} \mod(2\pi). \quad (6)$$

The above equation demonstrates that there is no ambiguity in the line integrals in the right-hand side of Eq. (3). A detailed

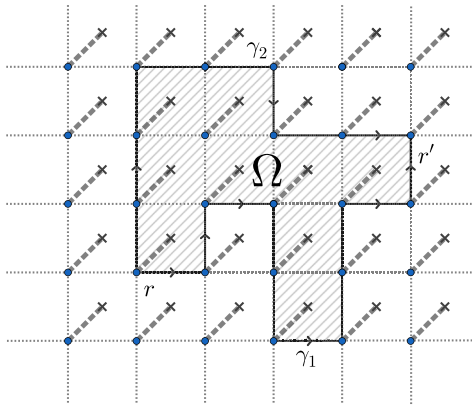

FIG. 5. Illustration of the paths used to derive Eqs. (5) and (6).

derivation that Eq. (3) holds for any pair $\mathbf{r}, \mathbf{r}'$ is presented in Appendix A.

Therefore, we see that there is a precise equivalence between the notion of the statistical transmutation of a hard-core boson and a "composite fermion" carrying a solenoid of 2π flux, and the statistical transmutation of spin-$\frac{1}{2}$ degrees of freedom onto Jordan-Wigner fermions in 2D lattices. The nonlocality of the Jordan-Wigner transformation in 2D should not be viewed as "bug" but rather as a "feature" that secretly encodes the natural nonlocality associated with flux attachment. This equivalence could also be useful to understand the precise lattice versions of transformations discussed within the web of dualities [71].

III. JORDAN-WIGNER COMPOSITE FERMIONS AS EXTENDED PARTONS IN 2D QUANTUM SPIN ICE

Quantum spin ice in the 2D square lattice is a classic example of a lattice gauge theory, namely, a model with a set of local conservation laws [19,20,33–44]. For different values for these local conservation laws the Hilbert space can be reduced to that of the quantum six-vertex model (Q6VM) or the celebrated quantum dimer model (QDM) introduced by Rokhsar and Kivelson [33]. In this section, we will develop a dual representation of these models in terms of Jordan-Wigner composite fermions, and exploit the fact that these models of spins remain local in terms of their dual Jordan-Wigner composite fermions. We will show that these Jordan-Wigner composite fermions behave in certain sense like partons, such as Abrikosov fermions [48,72], but with crucial qualitative differences arising from the fact that they carry not only lattice gauge charge, but also a lattice gauge dipole moment.

A. (2 + 1)D quantum spin ice and its Jordan-Wigner composite fermion representation

To describe quantum spin-ice models it is convenient to introduce a different lattice convention relative to that of the previous section. We first divide the plaquettes of the 2D square lattice into two sublattices, that we will now call "vertices" and "plaquettes," so that the spin-$\frac{1}{2}$ degrees of freedom are viewed as residing in the "links" connecting such vertices (see Fig. 6). These links therefore form another square lattice

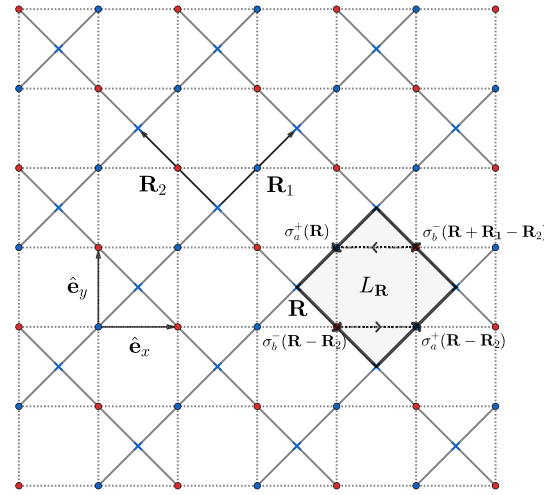

FIG. 6. The original square lattice of spins is spanned by vectors $\hat{\mathbf{e}}_x$ and $\hat{\mathbf{e}}_y$, whose sites (blue and red dots) are denoted by $\mathbf{r}$. The "spin-ice" lattice is the Bravais lattice spanned by vectors $\mathbf{R}_1$ and $\mathbf{R}_2$, and with a basis of two spin sites: the "a" sites (blue dots) and "b" sites (red dots). The plaquettes of the original square lattice are now separated into "vertices" located at $\mathbf{R}$ and "plaquettes" (e.g., the square shaded in gray) of the "spin-ice lattice." The plaquette resonance operator of the RK model, $L_{\mathbf{R}}$ from Eq. (10), is also illustrated.

which is rotated 45° relative to the original square lattice. The Bravais lattice of the spin-ice models is spanned by two vectors $\mathbf{R} = n_1\mathbf{R}_1 + n_2\mathbf{R}_2$, $n_{1,2} \in \mathbb{Z}$, which can be viewed as the position of vertices (see Fig. 6). Therefore, the unit cell has a basis with two spin-$\frac{1}{2}$ degrees of freedom, which we will distinguish by subscripts a, b. For example, $\sigma_a^i(\mathbf{R})$ will denote the ith Pauli matrix associated with the site $(\mathbf{R}, a)$ (see Fig. 6).[3] From here on, we will assume that the original square lattice has an even number of spin sites both in the x and y directions because this is needed in order to make spin ice lattice periodic in a torus (see Fig. 6).

For every vertex, we define an "ice charge operator" as the sum of the z components of the spins in its four links:

$$Q_{\text{ice}}(\mathbf{R}) \doteq \sigma_a^z(\mathbf{R}) + \sigma_b^z(\mathbf{R}) + \sigma_a^z(\mathbf{R}-\mathbf{R}_1) + \sigma_b^z(\mathbf{R}-\mathbf{R}_2). \tag{7}$$

The ice charge operators are the locally conserved quantities, and they are the generators of the following "UV lattice gauge group" of unitary transformations:

$$G[\{\theta(\mathbf{R})\}] = \exp\left(i\sum_{\mathbf{R}}\theta(\mathbf{R})Q_{\text{ice}}(\mathbf{R})\right), \tag{8}$$

where $\theta(\mathbf{R})$ are arbitrary real numbers. The lattice gauge theory structure is imposed by demanding that the Hamiltonian H is invariant under the UV lattice gauge group or, equivalently,

[3]We will also continue to label the spin sites with lowercase letter $\mathbf{r}$ when there is no need to specify its detailed Bravais lattice label, namely, $\mathbf{r}$ is also understood to be the physical coordinate of the spin site with Bravais lattice label $(\mathbf{R}, i)$ with $i = a, b$.

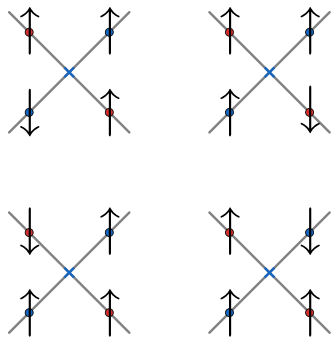

FIG. 7. The four configurations of σ^z on the links allowed by $Q_{\text{ice}}(\mathbf{R}) = 2$. This sector corresponds to the quantum dimer model, and the dimers are located at links where spins are reversed relative to the state with all spins pointing up. Therefore, the dimers also mark the location of JW composite-fermions.

that it commutes with all the ice charge operators:

$$[Q_{\text{ice}}(\mathbf{R}), H] = 0, \quad \forall\, \mathbf{R}. \tag{9}$$

The subspace with $Q_{\text{ice}}(\mathbf{R}) = 2$ at every vertex is equivalent to that of the quantum dimer model (QDM), whereas the subspace with $Q_{\text{ice}}(\mathbf{R}) = 0$ is equivalent to the quantum six-vertex model (Q6VM) (see Figs. 7 and 8 for illustration of the allowed configurations). Gauge-invariant operators include spin-diagonal operators such as $\sigma_a^z(\mathbf{R})$ (boson number), and products of spin and raising lowering operators (boson creation and annihilation) over a sequence of links forming a closed loop, the smallest of which is the "plaquette flipping" operator:

$$L_{\mathbf{R}} = \sigma_a^+(\mathbf{R})\sigma_b^-(\mathbf{R}-\mathbf{R}_2)\sigma_a^+(\mathbf{R}-\mathbf{R}_2)\sigma_b^-(\mathbf{R}+\mathbf{R}_1-\mathbf{R}_2). \tag{10}$$

The above operator can be viewed as centered around the plaquette that is neighboring to the right the vertex located at $\mathbf{R}$ as shown in Fig. 6. A classic gauge-invariant Hamiltonian is the Rokhsar-Kivelson model:

$$H = -t\sum_{\mathbf{R}} L_{\mathbf{R}} + L_{\mathbf{R}}^\dagger + v\sum_{\mathbf{R}} L_{\mathbf{R}}L_{\mathbf{R}}^\dagger + L_{\mathbf{R}}^\dagger L_{\mathbf{R}}. \tag{11}$$

Additionally, when placed in a 2D torus each gauge-invariant subspace splits into "winding" sectors, due to the existence of two conserved t'Hooft loop operators, one for each direction

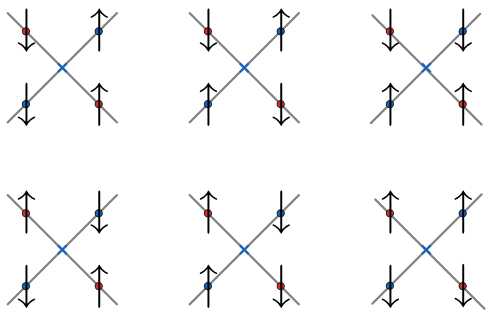

FIG. 8. The six configurations of σ^z on the links allowed by $Q_{\text{ice}}(\mathbf{R}) = 0$. This is the sector of the six-vertex model.

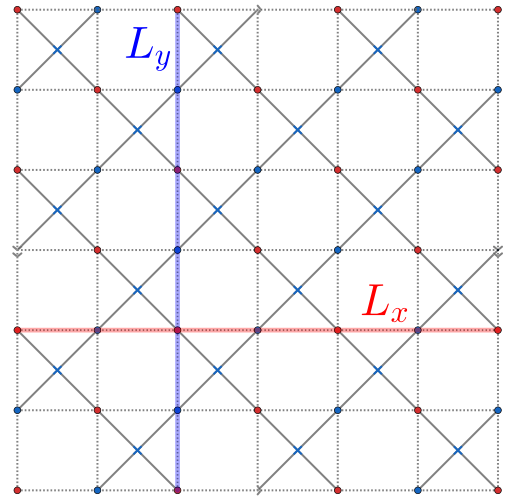

FIG. 9. Noncontractible loops $L_{x,y}$ for the definition t'Hooft operators in Eq. (12) for a lattice with periodic boundary conditions. Notice that in order to place the spin-ice lattice on a torus there needs to be an even number of spin along the x and y directions.

of the torus, defined as

$$\ell_x \doteq \sum_{\mathbf{r}\in L_x}\sigma^z(\mathbf{r}), \quad \ell_y \doteq \sum_{\mathbf{r}\in L_y}\sigma^z(\mathbf{r}), \tag{12}$$

where $\mathbf{r} \in L_{x,y}$ denotes a sum over the sites in the noncontractible loops of the torus depicted in Fig. 9.

One of the remarkable properties of the lattice gauge structure of quantum spin-ice models is that any local gauge-invariant operator remains local in its dual Jordan-Wigner (JW) composite fermion representation. For example, the elementary plaquette flipping operator from Eq. (10), after using the Jordan-Wigner transformation described in Sec. II, can be written as

$$L_{\mathbf{R}} = f_a(\mathbf{R})f_b^\dagger(\mathbf{R}+\mathbf{R}_1)f_a(\mathbf{R}+\mathbf{R}_2)f_b^\dagger(\mathbf{R}). \tag{13}$$

Therefore, we see that the RK model can be equivalently represented as a local model of interacting Jordan-Wigner composite fermions. For larger gauge-invariant loop operators (e.g., those enclosing two adjacent plaquettes), the dual fermion operators would also include the products of the fermion parities for the links inside the loop, but in general any local gauge-invariant operator of spins maps onto a local fermion operator without any leftover trace of the long-range part of the Jordan-Wigner strings.[4]

The ice charge operators are represented in terms of Jordan-Wigner composite fermions as follows:

$$Q_{\text{ice}}(\mathbf{R}) = 4 - 2\,n_{\text{ice}}(\mathbf{R}) = 4 - 2\sum_{\mathbf{r}\in\mathbf{R}} f^\dagger(\mathbf{r})f(\mathbf{r}), \tag{14}$$

[4]This follows from the fact that plaquette operators $L_{\mathbf{R}}$, $L_{\mathbf{R}}^\dagger$, and $\sigma_{\mathbf{r}}^z$ form a complete algebraic basis from which any local gauge-invariant operator can be obtained by addition and multiplication of these. Since these basis operators are mapped into local fermion operators via the JW transformation, it follows that any local gauge-invariant operator remains local in its dual JW composite fermion representation.

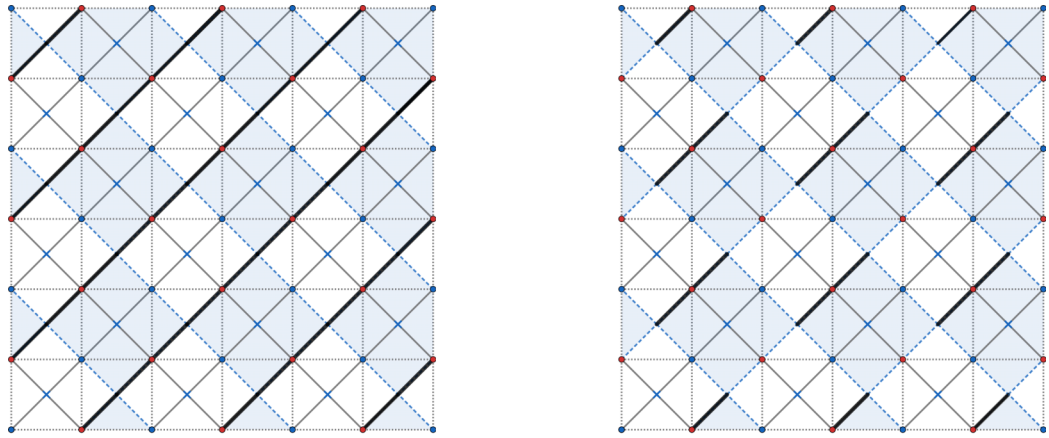

FIG. 10. Left: Depiction of a configuration with half of spins reversed (half-filling of JW composite fermions) relative to fully polarized state (denoted by solid bars) belonging to six-vertex subspace. Right: Depiction of a configuration with one quarter of spins reversed (quarter-filling of JW composite fermions) relative to fully polarized state (denoted by solid bars) belonging to quantum dimer subspace.

where $\mathbf{r} \in \mathbf{R}$ denotes the spin sites $\mathbf{r}$ in the four links connected to vertex $\mathbf{R}$, and $n_{\text{ice}}(\mathbf{R})$ is the total number of fermions in such links. From the above we see that the subspaces obeying with different values of ice charge correspond to different lattice fillings of the Jordan-Wigner composite fermions. The QDM and Q6VM spaces have $\frac{1}{4}$ and $\frac{1}{2}$ filling of the fermion sites, respectively. Some representative configurations illustrating these fillings are shown in Fig. 10.

In this work we will be interested in constructing spin-liquid states that are relevant not only for the RK model, but for the universality class that the RK Hamiltonian defines. This universality class is defined as the set of local spin Hamiltonians,[5] with the same spin-ice local conservation laws, and the same global symmetries of the RK model. Some of these global symmetries of the RK model are listed in Table II, and the notation for some of its space symmetries is also depicted in Fig. 11. The particle-hole symmetry can only be enforced for the filling associated with the subspace of the Q6VM (see Table II).

B. Review of Abrikosov parton states

Before introducing the extended parton construction of states for Jordan-Wigner composite fermions in quantum spin ice, we would like to review some of the key ideas of the more traditional construction of states for Abrikosov fermions, which we will sometimes refer to as "pointlike" partons (for more detailed discussions see, e.g., Refs. [48,72–74]). The same previously discussed physical spin-$\frac{1}{2}$ degrees of freedom at the lattice site $\mathbf{r}$ can be alternatively represented in terms of spinful Abrikosov fermions $\psi_s^\dagger(\mathbf{r})$ $(s = \uparrow, \downarrow)$:

$$\sigma^i(\mathbf{r}) = \sigma^i_{ss'} \psi_s^\dagger(\mathbf{r}) \psi_{s'}(\mathbf{r}), \tag{15}$$

where $\sigma^i_{ss'}$ is the ss' element of the ith Pauli matrix. The above representation enlarges the physical Hilbert space from a two-dimensional $\{|\uparrow\rangle, |\downarrow\rangle\}$ into a four-dimensional $\{|0\rangle, |\uparrow\rangle, |\downarrow\rangle, |\uparrow\downarrow\rangle\}$. In this case, the "UV lattice gauge group" is generated by the fermion number at each site:

$$n(\mathbf{r}) = \sum_s f_s^\dagger(\mathbf{r}) f_s(\mathbf{r}). \tag{16}$$

The above operator is the counterpart of the spin-ice charge for this lattice gauge structure. Gauge-invariant operators are defined as those commuting with $n(\mathbf{r})$, and in this case they are the spin operators themselves, $\sigma^i(\mathbf{r})$. The physical subspace is a gauge-invariant subspace satisfying

$$n(\mathbf{r})\,|\psi\rangle = |\psi\rangle\,. \tag{17}$$

Therefore, in this parton construction physical states are restricted to have $\frac{1}{2}$ fermion filling of the lattice, which is

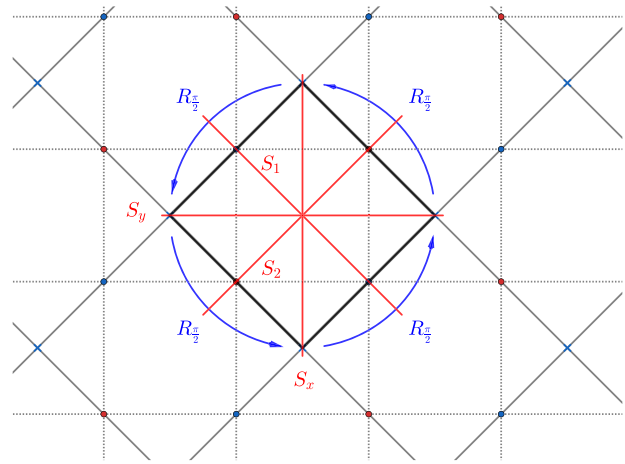

FIG. 11. Illustration of the point-group symmetry operations of the quantum spin-ice model centered on a spin-ice plaquette (corresponding to dihedral group D_8). The model also has a similar set of symmetry operations centered around the vertices, which we also consider for constructing states.

[5]The locality is defined with respect to the tensor product structure of the Hilbert space of underlying microscopic spin degrees of freedom.

TABLE II. Table of symmetries of the Rokhsar-Kivelson Hamiltonian of quantum spin ice. $U_d(\mathbf{r})$ and $U_d(\mathbf{R})$ denote the image of the site $\mathbf{r}$ and the vertex $\mathbf{R}$ under the corresponding spatial transformation. See Fig. 11 for a definition of the spatial transformations and Fig. 13 for a depiction of the action of $R_{\frac{\pi}{2}}$.

Symmetries	Symbol		Q6VM	QDM	Linear	Antilinear	Action on $b(\mathbf{r})$	Action on $Q_{\text{ice}}(\mathbf{R})$
Time reversal	Θ		✓	✓		✓	$b(\mathbf{r})$	$Q_{\text{ice}}(\mathbf{R})$
Spatial transformations	U_d	$R_{\frac{\pi}{2}}$ S_x S_y S_1 S_2	✓	✓	✓		$b(U_d(\mathbf{r}))$	$Q_{\text{ice}}(U_d(\mathbf{R}))$
Particle-hole	X		✓		✓		$b^\dagger(\mathbf{r})$	$-Q_{\text{ice}}(\mathbf{R})$

already a crucial difference with respect to the Jordan-Wigner composite fermions.

When restricted to the physical subspace $n(\mathbf{r}) = \mathbb{1}$, there is actually a SU(2) group that leaves all gauges invariant, and which is larger than the U(1) UV lattice gauge group generated by (17). Such larger group of operations that leave the gauge-invariant operators invariant is called the *parton gauge group* (PGG). To construct spin-liquid states it is convenient to introduce an auxiliary mean-field Hamiltonian that parametrizes a Slater determinant of fermions:

$$H_{\text{MF}} = \sum_{ss'} \sum_{\mathbf{r},\mathbf{r}'} t_{ss'}(\mathbf{r},\mathbf{r}') f_s^\dagger(\mathbf{r}) f_{s'}(\mathbf{r}'). \tag{18}$$

The hopping elements $t_{ss'}(\mathbf{r},\mathbf{r}')$ in the mean-field Hamiltonian can be viewed as variational parameters of its Slater determinant ground state, that we will denote by $|\Omega_0[t_{ss'}(\mathbf{r},\mathbf{r}')]\rangle$. The above mean-field Hamiltonian conserves the total fermion number and, therefore, it is invariant under a global U(1) subgroup of the PGG. More generally, the group that leaves the mean-field Hamiltonian invariant is called invariant gauge group (IGG). The importance of the IGG is that it determines the expected true low-energy emergent gauge group of the spin-liquid state [48,72] (assuming it does not suffer from instabilities such as gauge confinement). For the above mean-field Hamiltonian with a U(1) IGG we expect then to have U(1) spin liquid [48,72].[6] For concreteness in this work we will be focusing on spin liquids with low-energy emergent U(1) gauge groups.

The ground state $|\Omega_0[t_{ss'}(\mathbf{r},\mathbf{r}')]\rangle$ of the above mean-field Hamiltonian generically is not invariant under the UV gauge group and violates the constraint of Eq. (17). The correct physical mean-field state is obtained by projecting this state onto the physical gauge-invariant subspace (Gutzwiller projection), as follows:

$$|\Omega[t_{ss'}(\mathbf{r},\mathbf{r}')]\rangle = \prod_{\mathbf{r}} \left(\frac{1-(-1)^{n(\mathbf{r})}}{2} \right) |\Omega_0[t_{ss'}(\mathbf{r},\mathbf{r}')]\rangle\,. \tag{19}$$

The Gutzwiller projection is a nontrivial operation that generally makes difficult the calculation gauge-invariant operators. It is possible, however, to develop a precise understanding of the symmetry properties of the Gutzwiller projected physical state. To illustrate this, let us imagine that there is some global physical symmetry operation acting on the spins, denoted by S (e.g., a lattice translation or a mirror symmetry). We say that two operations S_1 and S_2 defined by their action on the parton fermions represent the same physical symmetry, if they have the same action on all gauge-invariant operators. However, if S_1 and S_2 differ by an element of the parton gauge group, their enforcement on $|\Omega_0\rangle$ can lead to two distinct physical states $|\Omega\rangle$. In this case, then S_1 and S_2 are said to be two distinct projective symmetry-group (PSG) implementations on the partons of the same underlying physical symmetry (for a recent discussion illustrating this, see e.g. [75]).

C. Extended parton states for quantum spin ice

We are now ready to present our extended parton construction of mean-field states for composite fermions obtained from the JW transformation applied to the quantum spin-ice Hamiltonians. The idea is to parallel the construction for Abrikosov fermions, but for the UV gauge structure defined by the ice charge operators from Eq. (7). We begin by introducing an auxiliary mean-field Hamiltonian of composite fermions:

$$H_{\text{MF}} = \sum_{\mathbf{r},\mathbf{r}'} t(\mathbf{r},\mathbf{r}') f^\dagger(\mathbf{r}) f(\mathbf{r}'). \tag{20}$$

Here $f^\dagger(\mathbf{r})$ is the creation operator of the spinless Jordan-Wigner fermion at the spin site $\mathbf{r}$. The hopping amplitudes $t(\mathbf{r},\mathbf{r}')$ are again viewed as parametrizing the Slater determinant ground state of the mean-field Hamiltonian, denoted by $|\Phi_0[t(\mathbf{r},\mathbf{r}')]\rangle$. The physical spin orientation is encoded in the composite fermion occupation at each site, and therefore there is no enlargement of the full spin Hilbert space. Nevertheless, the composite fermion hopping bilinears in the above mean-field Hamiltonian generically do not commute with the generators of the UV lattice gauge transformations, and therefore its ground state $|\Phi_0\rangle$ violates the ice rules. However, this is forbidden by Elitzur's theorem: local gauge symmetries cannot be spontaneously broken. As a consequence, the naive ground state of the above mean-field Hamiltonian is not a satisfactory approximation to the true gauge-invariant ground states of quantum spin-ice models. However, this deficiency can be cured in an analogous way as in the case of Abrikosov partons, by projecting $|\Phi_0\rangle$ onto the gauge-invariant subspaces. Therefore, in analogy to the Gutzwiller projection, we

[6]But had we chosen a BCS–type mean-field state with a $\mathbb{Z}_2$ IGG, we would expect a $\mathbb{Z}_2$ spin liquid.

introduce a projector into a gauge-invariant subspace, specified by the local ice charges $Q_{\text{ice}}(\mathbf{R})$ and the t' Hooft operators (ℓ_x, ℓ_y) (for the case of a torus), given by

$$P(\{Q_{\text{ice}}(\mathbf{R}), \ell_x, \ell_y\}) \doteq P(\ell_x)P(\ell_y)\prod_{\mathbf{R}} P(Q_{\text{ice}}(\mathbf{R})),$$
$$|\Phi[t(\mathbf{r}, \mathbf{r}')]\rangle = P(\{Q_{\text{ice}}(\mathbf{R}), \ell_x, \ell_y\})\,|\Phi_0[t(\mathbf{r}, \mathbf{r}')]\rangle\,. \tag{21}$$

The above projected state is also parametrized by the hoppings $t(\mathbf{r}, \mathbf{r}')$, that could be in principle optimized as variational parameters to minimize the energy of RK–type Hamiltonians.

1. Symmetry implementation on JW composite fermions: General considerations

Let us now consider the implementation of symmetries on these mean-field states of Jordan-Wigner composite fermions. As in the case of Abrikosov fermions, the key idea is that the task of enforcing symmetries in the physical projected states is traded by the easier task of enforcing symmetries in the unprojected mean-field Hamiltonians. However, one needs to develop a set of consistency criteria for these implementations because there are multiple ways in which one given symmetry can be implemented in the unprojected state, leading to the rich structure of projective symmetry-group implementations [48,72].

At first glance it might appear as if there was no freedom on how to implement symmetries on the Jordan-Wigner fermions because any prescription on how physical symmetries act on the underlying spin-$\frac{1}{2}$ degrees of freedom would fix a unique symmetry action of the Jordan-Wigner composite fermion operators. We will refer to this underlying symmetry implementation as the "bare" symmetry action. However, this bare symmetry implementation cannot be suitably enforced in the mean-field Hamiltonians from Eq. (20). This is because the specific choice for implementing the Jordan-Wigner ordering of the 2D lattice (e.g., the western typing convention of Sec. II) does not manifestly preserve the symmetries of the lattice and, thus, for example, the bare action of the bare implementation of a $\pi/2$ lattice rotation would map the fermion bilinear mean-field Hamiltonian from Eq. (20) onto a complex operator which is no longer fermion bilinear Hamiltonian and does not appear local in its dual fermion representation. Our goal in this subsection will be therefore to develop a precise but more flexible notion of symmetry implementations on the Jordan-Wigner composite fermions that is amenable to enforcement on mean-field Hamiltonians.

Some of these difficulties of bare symmetry actions are not peculiar to the 2D Jordan-Wigner transformation but are also reminiscent of those appearing in the 1D Jordan-Wigner transformation, e.g., in the anomalous implementation of lattice translations, which we will now discuss in order to motivate the 2D construction. For example, consider a standard 1D finite lattice with periodic boundary conditions and a standard translational symmetry implemented on the microscopic spin operators located at site r as follows:

$$T\sigma^i(r)T^\dagger = \sigma^i(r+1). \tag{22}$$

However, when this "bare" symmetry is implemented on the JW fermions it does not act like a standard fermionic lattice translation, which we denote by τ, defined as

$$\tau f^\dagger(r)\tau^\dagger = f^\dagger(r+1) \neq T f^\dagger(r)T^\dagger. \tag{23}$$

The above arises because the JW string becomes translated by T and therefore it does not follow the initial JW convention (it does not start at spin "1" anymore).[7] However, while T and τ are different operations when acting on the single-fermion operator, they would act identically on fermion bilinear operators supported in the interior of the 1D chain:

$$\tau f^\dagger(r)f(r)\tau^\dagger = T f^\dagger(r)f(r)T^\dagger = f^\dagger(r+1)f(r+1). \tag{24}$$

Therefore, we can say that when the symmetry operations T and τ are restricted to act on parity-even operators, they are essentially the same symmetry.[8] The parity restriction in 1D plays an analogous role to the spin gauge structure in 2D, in the sense that local spin operators that are invariant under the UV lattice gauge symmetry remain local in their dual fermion representation after the JW map. In other words, after a quantum spin-ice model is mapped onto fermions via the JW map, it appears to be a bona fide local fermionic model, similar to how a parity-even spin Hamiltonian looks like an ordinary fermionic model after 1D JW map.

Therefore, we define a generalized notion of equivalence among symmetries of the 2D quantum spin-ice model when these are implemented on JW transformation, as follows:

> *For a quantum spin-ice model, we say that two operators S_1 and S_2 that implement a symmetry action are equivalent, when they have the same action on all local operators that are invariant under the UV lattice gauge transformations defined in Eq. (8)* (see Fig. 12).

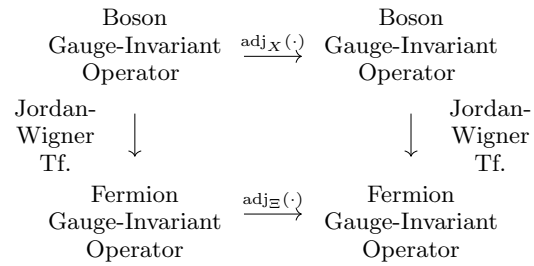

FIG. 12. Illustration of the notion of equivalence of symmetry actions of operators. Two operators X and Ξ are equivalent implementations of a symmetry, if their action is identical on all the operators that are invariant under the spin-ice UV lattice gauge transformations [defined in Eq. (8)]. This notion allows us to trade the possibly complicated "bare" action of the microscopic symmetry X on the JW composite fermions, by a simpler but equivalent symmetry implementation Ξ which maps JW fermion bilinears onto JW fermion bilinears. This is a natural extension of the notion of symmetry equivalence in standard parton constructions Abrikosov fermions (see, e.g., Refs. [48,72]).

[7]For a recent discussion of the connection between lattice translational symmetries, anomalies, and dualities associated with the 1D JW transformation, see Ref. [76].

[8]Up to corrections associated with boundary terms, but in this work we will focus on implementations of symmetry in the bulk.

The usefulness of this notion of equivalent symmetries is that instead of enforcing the nontrivial "bare" action of a symmetry S_1, we can enforce instead a simpler but equivalent symmetry implementation S_2, which maps fermion bilinear Hamiltonians onto fermion bilinear Hamiltonians. By enforcing S_2 on the fermion bilinear mean-field Hamiltonian from Eq. (20), then the expectation value of any gauge-invariant operator computed from its corresponding Gutzwiller projected state from Eq. (21) will obey the same symmetry constraints as if we had enforced the bare symmetry action S_1. In particular, if G is a lattice UV gauge transformation from Eq. (8), then S and GS are equivalent implementations of a symmetry. Interestingly, as we will see, enforcing symmetries that differ by such a pure UV lattice gauge transformation G on the mean-field Hamiltonian of Eq. (20) can lead to physically distinct states after the generalized Gutzwiller projection of Eq. (21). This situation is analogous to that of PSG implementations of symmetry on the Abrikosov partons [see discussion following Eq. (19)]. However, several interesting qualitative differences will appear between these two cases, and this is partly why we call our construction an extended projective symmetry-group implementation (see Table III).

2. *A specific implementation of symmetries of 2D quantum spin ice on JW composite fermions*

We will now construct a concrete example of extended projective symmetry implementation for the symmetries of the quantum spin-ice model (see Table II). Our objective is to illustrate the general ideas by constructing interesting and perhaps even energetically competitive spin-liquid states (although we will not compute explicitly their energy). It is clear, in analogy to ordinary parton constructions [48,72], that there is a large landscape of possible extended projective symmetry implementations beyond the ones we will illustrate concretely. We leave to future work the development of a more global understanding and classification of the large and colorful landscape of extended projective symmetry-group implementations.

TABLE III. Comparison between traditional pointlike Abrikosov fermion partons and the extended Jordan-Wigner composite fermion parton constructions for 2D quantum spin ice. Here $s \in \{\uparrow, \downarrow\}$, $\mathbf{r}$ denotes spin sites, $\mathbf{r} \in \mathbf{R}$ denotes the four spins adjacent to a quantum spin-ice vertex located at $\mathbf{R}$. See Eq. (14) and Fig. 6 for definitions and depictions.

	Abrikosov fermions	Jordan-Wigner composite fermions
Local Hilbert space enlargement	Yes	No
Internal degrees of freedom	Spin $\frac{1}{2}$	Spinless
UV gauge transformation generators	$n(\mathbf{r}) = \sum_s f_s^\dagger(\mathbf{r}) f_s(\mathbf{r})$	$Q_{\text{ice}}(\mathbf{R}) = 4 - 2\sum_{\mathbf{r}\in\mathbf{R}} f^\dagger(\mathbf{r}) f(\mathbf{r})$
Physical lattice fillings	$n(\mathbf{r}) = 1$	Any [e.g., $\langle f^\dagger(\mathbf{r}) f(\mathbf{r})\rangle = \frac{1}{4}$ for QDM]

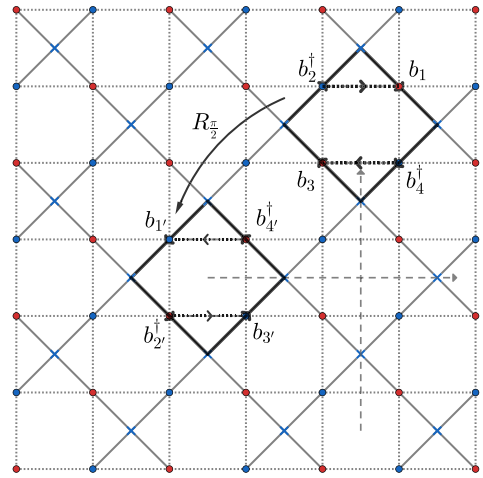

FIG. 13. Action of a 90° rotation (denoted by $R_{\frac{\pi}{2}}$) centered on the plaquette where the dashed-dotted lines intersect, acting on the plaquette resonance operators marked by thick squares (according to convention in Fig. 6).

Let us begin by considering a $\pi/2$ spatial rotation centered on a plaquette (see Fig. 13), denoted by $R_{\frac{\pi}{2}}$. We define its action on the microscopic degrees of freedom from an implementation that is natural when viewed as spinless bosons, namely, as follows:

$$R_{\frac{\pi}{2}} b^\dagger(\mathbf{r}) R_{\frac{\pi}{2}}^\dagger = b^\dagger\big(R_{\frac{\pi}{2}}\mathbf{r}\big). \tag{25}$$

Here $b^\dagger(\mathbf{r})$ is the hard-core boson equivalent of the spin-lowering operator (see Table I), and $R_{\frac{\pi}{2}}\mathbf{r}$ is the image of site $\mathbf{r}$ under the rotation. The action of $R_{\frac{\pi}{2}}$ on the gauge-invariant plaquette operator from Eq. (10) is thus simply

$$R_{\frac{\pi}{2}} (b_2^\dagger b_1 b_4^\dagger b_3) R_{\frac{\pi}{2}}^\dagger = b_{4'}^\dagger b_{1'} b_{2'}^\dagger b_{3'}, \tag{26}$$

where 1,2,3,4 denote the sites in the plaquette from Fig. 13 and $1', 2', 3', 4'$ their images after the $\frac{\pi}{2}$ rotation. As discussed in Eq. (13), this same plaquette operator can be alternatively written as a product of JW composite fermion operators. However, while the action of $R_{\frac{\pi}{2}}$ is simple on this four-fermion operator, it is complex and cumbersome on JW composite fermion operators themselves, as it involves a $\pi/2$ rotation of the JW strings. More importantly, $R_{\frac{\pi}{2}}$ does not map fermion bilinear operators onto fermion bilinears because, for example, it maps a fermion horizontal hopping into a fermion vertical hopping dressed by JW strings (see Fig. 2). Therefore, we would like to find an alternative but gauge-equivalent implementation of $R_{\frac{\pi}{2}}$ to overcome this difficulty.

To do so, we define a collection of auxiliary operators associated with each of the microscopic symmetries listed in Tables II and IV, whose action is defined by replacing the boson operator $b^\dagger(\mathbf{r})$ with the fermion operator $f^\dagger(\mathbf{r})$ in Table II. For example, for the microscopic symmetry $R_{\frac{\pi}{2}}$, we associate the auxiliary fermion operator $P_{\frac{\pi}{2}}$, whose action is obtained from Eq. (25) by replacing $b^\dagger(\mathbf{r}) \to f^\dagger(\mathbf{r})$, leading to

$$P_{\frac{\pi}{2}} f^\dagger(\mathbf{r}) P_{\frac{\pi}{2}}^\dagger = f^\dagger\big(R_{\frac{\pi}{2}}\mathbf{r}\big). \tag{27}$$

Thus, the idea is that these auxiliary fermion operators are intuitive and natural symmetry implementations on fermions,

TABLE IV. Summary of RK Hamiltonian symmetries and their implementation on bosons (spins) and JW fermions. The operations listed under the column "bare microscopic boson" are the underlying bare microscopic symmetries implemented on the boson creation operators, for example, the 90° rotation $R_{\frac{\pi}{2}}$ acts as defined in Eq. (25). For each of these we introduce an "auxiliary fermion transformation" which acts in a simple way as expected for spinless fermions, such as the fermion rotation $P_{\frac{\pi}{2}}$ defined in Eq. (27). However, this auxiliary fermion transformation is not always equivalent to the "bare microscopic boson" symmetry (see Fig. 12 for notion of equivalence), and might need to be dressed by an extra site-dependent U(1) gauge transformation to make it equivalent, as listed under "equivalent JW fermion symmetry" [see Eq. (30) as an example for the $R_{\frac{\pi}{2}}$ rotation and Fig. 14 for a definition of $U_{\frac{1}{4}}$]. The above "equivalent JW fermion symmetries" define only one possible extended projective symmetry-group implementation on the JW composite fermions. Two other examples, that are the focus of this work, are described Table V. In all the examples we implement the translations by Bravais vectors $\mathbf{R}_1, \mathbf{R}_2$ in the standard trivial nonprojective way for bosons and fermions without dressing the auxiliary fermion transformations by gauge transformations.

Symmetry	Bare microscopic boson	Auxiliary fermion transformation	Equivalent JW fermion symmetry
Time reversal	Θ	Θ	Θ
	$R_{\frac{\pi}{2}}$	$P_{\frac{\pi}{2}}$	$U_{\frac{1}{4}}P_{\frac{\pi}{2}}$
	S_x	Σ_x	Σ_x
Spatial	S_y	Σ_y	Σ_y
	S_1	Σ_1	$U_{\frac{1}{4}}\Sigma_1$
	S_2	Σ_2	$U_{\frac{1}{4}}\Sigma_2$
Particle-hole	X	Ξ	Ξ

but they are not necessarily equivalent implementations of the microscopic symmetries on gauge-invariant operators, as we now explain. This auxiliary fermion rotation acts on the same plaquette operator from Eq. (26), which can be equivalently represented with fermions using Eq. (13), as follows:

$$P_{\frac{\pi}{2}}(f_2^\dagger f_1 f_4^\dagger f_3)P_{\frac{\pi}{2}}^\dagger = -f_{4'}^\dagger f_{1'} f_{2'}^\dagger f_{3'}. \tag{28}$$

Therefore, the fermion rotation $P_{\frac{\pi}{2}}$ is not an equivalent implementation of the underlying physical symmetry $R_{\frac{\pi}{2}}$ because it additionally multiplies the gauge-invariant plaquette operator by a global minus sign. The extra minus sign can be removed by dressing $P_{\frac{\pi}{2}}$ with a staggered U(1) transformation that we call $U_{\frac{1}{4}}$, which rotates the phase of bosons with opposite signs in the a and b sublattices [see Fig. 14(a)] as follows:

$$U_{\frac{1}{4}} b_a^\dagger(\mathbf{R}) U_{\frac{1}{4}}^\dagger = e^{i\frac{\pi}{4}} b_a^\dagger(\mathbf{R}),$$

$$U_{\frac{1}{4}} b_b^\dagger(\mathbf{R}) U_{\frac{1}{4}}^\dagger = e^{-i\frac{\pi}{4}} b_b^\dagger(\mathbf{R}),$$

where we are using the Bravais labels of the sites of the model (see Sec. III A for the convention). Notice that the action of $U_{\frac{1}{4}}$ on boson and JW fermion operators is the same. Therefore, its action on the plaquette operator is

$$U_{\frac{1}{4}}(f_2^\dagger f_1 f_4^\dagger f_3)U_{\frac{1}{4}}^\dagger = -f_2^\dagger f_1 f_4^\dagger f_3. \tag{29}$$

Therefore, the action of $R_{\frac{\pi}{2}}$ and $U_{\frac{1}{4}}P_{\frac{\pi}{2}}$ on plaquette operators is identical. Moreover, their action is also identical on $\sigma^z(\mathbf{r})$ (or equivalently the onsite fermion-number operator). Since these operators together with the plaquette operators form a complete algebraic basis for all local gauge-invariant operators, it follows that $U_{\frac{1}{4}}P_{\frac{\pi}{2}}$ is an equivalent implementation of the underlying physical symmetry $R_{\frac{\pi}{2}}$ on gauge-invariant operators:

$$R_{\frac{\pi}{2}} \equiv U_{\frac{1}{4}}P_{\frac{\pi}{2}}. \tag{30}$$

Table IV presents a list of the microscopic symmetries of the quantum spin-ice model and a corresponding equivalent symmetry operation acting on the JW fermions. We see that in

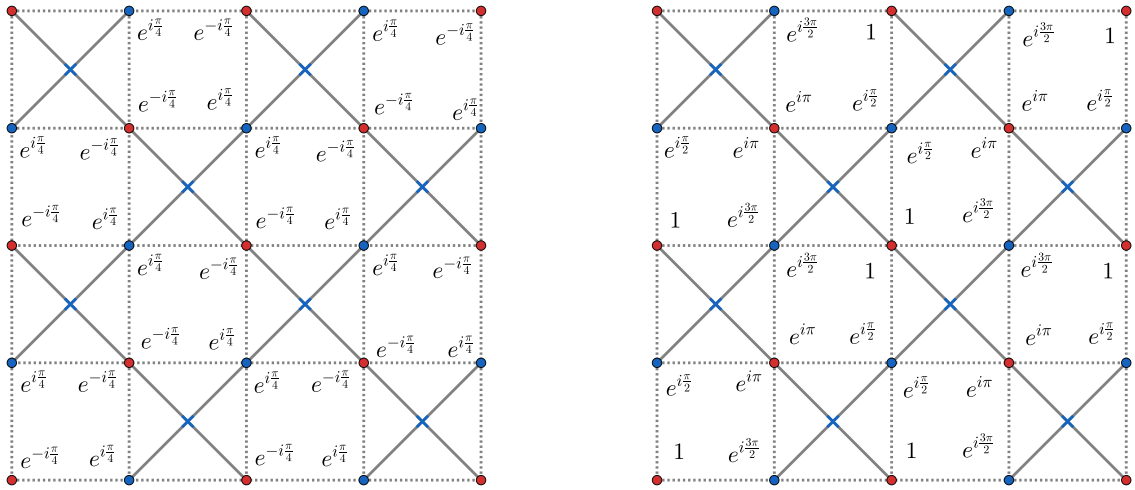

(a) $U_{\frac{1}{4}}$ (b) $V_{\frac{1}{2}}$

FIG. 14. Phases gained by creation operators $f^\dagger(\mathbf{r})$ or $b^\dagger(\mathbf{r})$ under the action of the site-dependent U(1) transformations: (a) $U_{\frac{1}{4}}$ [from Eq. (29)], (b) $V_{\frac{1}{2}}$ [from Eq. (40)].

TABLE V. The two distinct extended projective symmetry-group implementations on the JW composite fermions that are the focus of this work. These symmetries are all equivalent to the microscopic symmetries listed in Tables II and IV (see Fig. 12 for summary of notion of equivalence).

Symmetry	Θ_x (extended PSG)	Θ_y (extended PSG)
Time reversal	$G_x\Theta$	$G_y\Theta$
Spatial	$U_{\frac{1}{4}}P_{\frac{\pi}{2}}$	$U_{\frac{1}{4}}P_{\frac{\pi}{2}}$
	$G_x\Sigma_x$	$G_y\Sigma_x$
	$G_x\Sigma_y$	$G_y\Sigma_y$
	$G_yU_{\frac{1}{4}}\Sigma_1$	$G_xU_{\frac{1}{4}}\Sigma_1$
	$G_yU_{\frac{1}{4}}\Sigma_2$	$G_xU_{\frac{1}{4}}\Sigma_2$
Particle-hole	$G_y\Xi$	$G_x\Xi$

addition to the rotations, the natural fermionic implementation of diagonal mirrors S_1 and S_2 (see Fig. 11) also needs to be dressed by $U_{\frac{1}{4}}$ in order to make them equivalent to the underlying microscopic symmetries. We will also enforce Bravais lattice translational symmetries, which are understood to act identically on bosons and fermions (up to boundary terms) and thus are not listed explicitly in Table IV. Details of the derivations for these additional symmetries can be found in Appendix B.

This set of equivalent symmetries listed under the Jordan-Wigner fermion column of Table IV maps fermion bilinears onto fermion bilinears. Therefore, any such equivalent symmetry implementation, denoted by S, can be used to enforce the symmetry on the fermion mean-field Hamiltonian H_{MF} of Eq. (20), by determining the hoppings that are satisfied by the following relation:

$$SH_{\mathrm{MF}}S^{-1} = H_{\mathrm{MF}}. \tag{31}$$

Interestingly, one can show that after enforcing all the equivalent symmetries from Table IV and Bravais lattice translations, there are no allowed nearest-neighbor fermion hoppings in the lattice. For typical RK models, one expects that short-distance correlations determine a sizable portion of the energy density of the state and one would therefore expect that this projective symmetry implementation from Table IV is not a very energetically favorable choice for reasonably simple microscopic Hamiltonians. However, as mentioned before, the fermionic symmetries listed in Table IV are only one choice among a large set of possibilities.

It is therefore interesting to consider the following question: Can we construct an alternative equivalent symmetry implementation that imposes all the symmetries of the RK spin-ice model but which allows for the nearest-neighbor hoppings to be nonzero? We have found two modified symmetry implementations that allow for nonzero nearest-neighbor hoppings, which we shall denote as Θ_x and Θ_y implementations, and on which we focus for the remainder of the paper. These projective symmetry implementations are obtained by dressing the implementations of Table IV with the operations listed in Table V, which are obtained after composition with the following UV lattice gauge group elements G_x and G_y:

$$G_xb^\dagger(\mathbf{r})G_x^\dagger = (-1)^xb^\dagger(\mathbf{r}),$$
$$G_yb^\dagger(\mathbf{r})G_y^\dagger = (-1)^yb^\dagger(\mathbf{r}). \tag{32}$$

Here we write the sites as $\mathbf{r} = (x, y)$, where x, y are understood to be integers. These two transformations can be viewed as generated by the UV lattice gauge transformations from Eq. (8), by choosing $\theta(\mathbf{r})$ so that it takes the values depicted, respectively, in Figs. 15(a) and 15(b).

3. Connection to pseudoscalar spin liquids

So far we have used an implementation of microscopic symmetries which is more natural when we view the microscopic degrees of freedom as hard-core bosons, but which is not necessarily natural when we view them as spin $\frac{1}{2}$. However, thanks to the large set of microscopic symmetries of the RK model of spin ice, we are implicitly also enforcing symmetries whose action is the natural one when we view the microscopic degrees of freedom as spins.

For example, the time-reversal operator Θ, defined in Table II, acts as complex conjugation in the standard choice of Pauli matrices where only σ^y is imaginary, and $\sigma^{x,z}$ are real. Therefore, it does not square to -1. The more standard time-reversal operator of spin $\frac{1}{2}$ would act on the spin at site $\mathbf{r}$, as $\mathcal{T} = i\sigma^y(\mathbf{r})\Theta$. However, the operator $i\sigma^y(\mathbf{r})$ is equivalent to composition $U(\pi)\sigma^x(\mathbf{r})$, where $U(\pi)$ is a π-spin rotation around the z axis, which acts on the fermions as $U(\pi)f^\dagger(\mathbf{r})U^\dagger(\pi) = -f^\dagger(\mathbf{r})$. Therefore, $i\sigma^y(\mathbf{r})$ is equivalent to a composition of the particle hole X, implemented $\sigma^x(\mathbf{r})$, and a boson global U(1) symmetry operation, implemented by $U(\pi)$, which we are already enforcing, namely, we have

$$\mathcal{T} = U(\pi)X\Theta. \tag{33}$$

Therefore, we are also implicitly enforcing such standard time-reversal action $\mathcal{T}$ on spin $\frac{1}{2}$, and one can similarly understand other natural spin symmetries of the RK model, as products of the natural boson symmetries that we are already enforcing.

To determine the explicit action of $\mathcal{T}$ on JW composite fermions, let us first describe the action of Θ. On spin raising and lowering operators this acts as a trivial antiunitary operator (complex conjugation):

$$\Theta\sigma^+(\mathbf{r})\Theta^{-1} = \sigma^+(\mathbf{r}).$$

Therefore, this operator acts similarly on JW composite fermions:

$$\Theta f^\dagger(\mathbf{r})\Theta^{-1} = f^\dagger(\mathbf{r}). \tag{34}$$

Let us now describe the implementation of the particle-hole conjugation of hard-core bosons, denoted by $X = \prod_{\mathbf{r}}\sigma^x(\mathbf{r})$. From the action of this operator on spin operators, $X\sigma^+(\mathbf{r})X^\dagger = \sigma^-(\mathbf{r})$, one obtains the action on the JW composite fermions:

$$Xf^\dagger(\mathbf{r})X^\dagger = (-1)^{L_s(\mathbf{r})}f(\mathbf{r}), \tag{35}$$

where $L_s(\mathbf{r})$ is the length of the JW string. The factor $(-1)^{L_s(\mathbf{r})}$ can be viewed as pure UV gauge transformation, and therefore X is gauge equivalent to the natural JW composite fermion

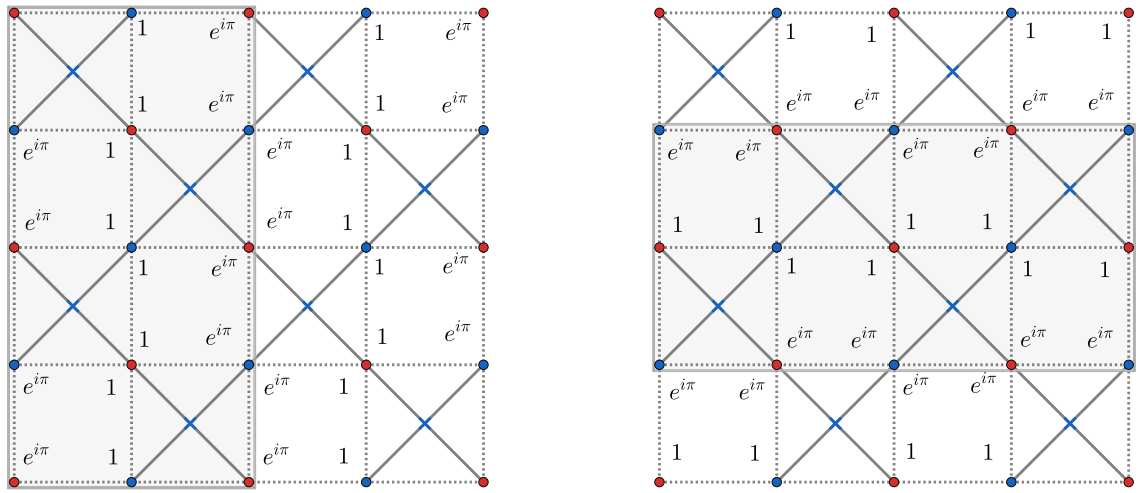

FIG. 15. Phases gained by creation operators $f^\dagger(\mathbf{r})$ or $b^\dagger(\mathbf{r})$ under the action of the UV gauge transformations: (a) G_x, (b) G_y. The transformations are obtained by choosing $\theta(\mathbf{r}) = \frac{\pi}{2}$ in Eq. (8) over the vertices contained in the gray regions and zero in the remainder.

particle-hole conjugation, denoted by Ξ (see Table IV), and defined as

$$\Xi f^\dagger(\mathbf{r})\Xi^\dagger = f(\mathbf{r}). \tag{36}$$

The spin time-reversal symmetry $\mathcal{T}$ reverses the direction of all the spin components, and in particular the z direction: $\mathcal{T}\sigma^z(\mathbf{r})\mathcal{T}^{-1} = -\sigma^z(\mathbf{r})$. Therefore, since $\sigma^z(\mathbf{r})$ encodes the information of the JW composite fermion, it is clear that $\mathcal{T}$ maps a fermion particle into a hole and vice versa. Therefore, we see that $\mathcal{T}$ is therefore a type of antiunitary particle-hole conjugation on the JW composite fermion operator, which explicitly reads as

$$\mathcal{T} f^\dagger(\mathbf{r})\mathcal{T}^{-1} = (-1)^{L_s(\mathbf{r})+1} f(\mathbf{r}), \tag{37}$$

where $L_s(\mathbf{r})$ is the length of the JW string, and the factor $(-1)^{L_s(\mathbf{r})+1}$ is a pure UV gauge transformation identical to G_x defined in Eq. (32).[9] Because of the above we see the JW composite fermion behaves under $\mathcal{T}$ as a pseudoscalar spinon, in the sense defined in Ref. [75].

We have introduced other space symmetries in their natural boson representation in Tables II and IV that also would act as particle-hole conjugations on the JW composite fermions when implemented as standard spin-$\frac{1}{2}$ symmetries. For example, for the space mirror operations S_x, S_y, S_1, S_2 $\sigma^z(\mathbf{r})$ transform as a scalar, e.g., $S_y\sigma^z(\mathbf{r})S_y^{-1} = \sigma^z(S_y\mathbf{r})$. However, its spin version would include an additional boson particle-hole conjugation, leading to the standard action of spins which are pseudovectors under mirrors, and which would reverse $\sigma^z(\mathbf{r})$ because it is parallel to these mirror planes. Therefore, these mirrors act as unitary particle-hole conjugations on the JW composite fermions, and the spin-liquid states that we will be discussing in this paper can be viewed as pseudoscalar spin liquids with respect to spin implementations of time reversal and space mirror symmetries in the sense defined in Ref. [75].

[9] Assuming the lattice has an even number of sites in the x direction, which is natural for quantum spin ice in a torus (see Fig. 9).

4. *Dirac and Fermi-surface mean-field states for the six-vertex model and quantum dimer models*

The procedure described in the previous section allows us to fix the nearest-neighbor hopping amplitudes in Eq. (20). The resulting pattern of hoppings is illustrated in Fig. 16, and the corresponding mean-field Hamiltonian reads as

$$\begin{aligned} H_{\mathrm{MF}} = \sum_{\mathbf{R}} & it^*(f_a^\dagger(\mathbf{R}-\mathbf{R}_1+\mathbf{R}_2)f_b(\mathbf{R}) + f_a^\dagger(\mathbf{R})f_b(\mathbf{R})) \\ & + t(f_a^\dagger(\mathbf{R}-\mathbf{R}_1)f_b(\mathbf{R}) + f_a^\dagger(\mathbf{R}+\mathbf{R}_2)f_b(\mathbf{R})) \\ & + \mathrm{H.c}, \end{aligned} \tag{38}$$

which in crystal momentum basis can be reexpressed as

$$H_{\mathrm{MF}} = \sum_{\mathbf{q}\in\mathrm{BZ}} (f_a^\dagger(\mathbf{q}) \quad f_b^\dagger(\mathbf{q})) \begin{pmatrix} 0 & h_{ab}(\mathbf{q}) \\ h_{ab}^*(\mathbf{q}) & 0 \end{pmatrix} \begin{pmatrix} f_a(\mathbf{q}) \\ f_b(\mathbf{q}) \end{pmatrix},$$

where we are using the crystal momentum basis $f_a^\dagger(\mathbf{R}) = N_\Lambda^{-1/2}\sum_{\mathbf{q}\in\mathrm{BZ}} e^{-i\mathbf{q}\cdot\mathbf{R}} f_a^\dagger(\mathbf{q})$, and the matrix entry is

$$h_{ab}(\mathbf{q}) = 2e^{\frac{i}{2}(q_1-q_2)}\left[it^* \cos\left(\frac{q_1-q_2}{2}\right) + t\cos\left(\frac{q_1+q_2}{2}\right)\right],$$

where $q_i = \mathbf{q}\cdot\mathbf{R_i}$, $i = 1, 2$. The associated band energy dispersion is

$$\epsilon_\pm(\mathbf{q}) = \pm 2|t|\sqrt{\cos\left(\frac{q_1-q_2}{2}\right)^2 + \cos\left(\frac{q_1+q_2}{2}\right)^2}. \tag{39}$$

These bands are illustrated in Fig. 17. The two extended projective symmetry implementations Θ_x and Θ_y (see Table V) impose different constraints on the hopping amplitude t be either purely real or purely

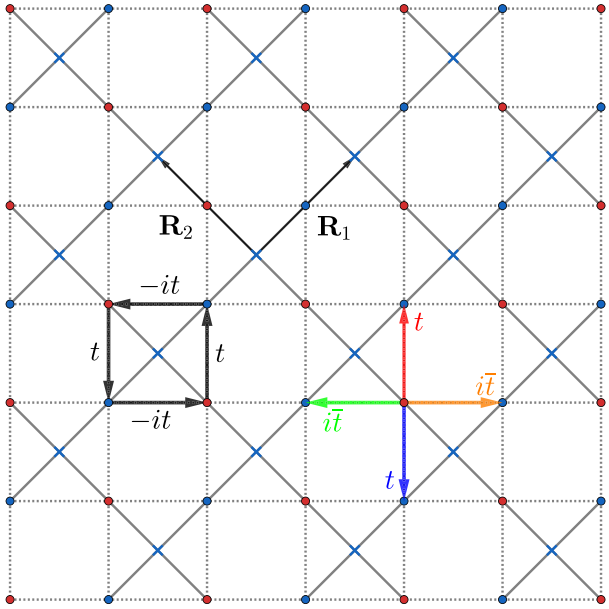

FIG. 16. Right: Depiction of the allowed nearest-neighbor JW composite fermion hoppings associated with Θ_x and Θ_y extended projective symmetry groups from Table V. Here the amplitude t is real for Θ_x and purely imaginary for Θ_y. Left: The phase of fermion hopping around a vertex or plaquette of the original square lattice (dotted line) is π. This π phase is behind the Dirac spectrum of JW composite fermions for these states (see Fig. 17).

imaginary:

$$t = t^* \quad \text{for the } \Theta_x,$$
$$t = -t^* \quad \text{for the } \Theta_y.$$

Details on how the above follows from implementing the symmetries from Table V are shown in Appendix B.

Despite their similarity, the extended projective symmetry-group implementations Θ_x and Θ_y (see Table V) are inequivalent. This can be seen by considering the action of a particular unitary transformation, denoted by $V_{\frac{1}{2}}$, which acts on the fermion operator $f^\dagger(\mathbf{r})$ as a local site-dependent U(1) transformation multiplying it by the specific phases shown in Fig. 14(b). It turns out that $V_{\frac{1}{2}}$ maps the Θ_x mean-field Hamiltonian onto the Θ_y mean-field Hamiltonian, as can be seen from its action of the following fermion bilinears (the 1,2,3,4 subindices below are the sites shown in Fig. 16):

$$t f_3^\dagger f_1 \to it f_3^\dagger f_1, \quad -it f_1^\dagger f_2 \to t f_1^\dagger f_2,$$
$$t f_2^\dagger f_4 \to it f_2^\dagger f_4, \quad -it f_4^\dagger f_3 \to t f_4^\dagger f_3. \tag{40}$$

On the other hand, the operators $L_{\mathbf{R}}$ and $L_{\mathbf{R}}^\dagger$ that enter in the microscopic RK Hamiltonian [see Eq. (10)] can be shown to be odd under the action $V_{\frac{1}{2}}$. Since $L_{\mathbf{R}}$ is invariant under the UV lattice gauge group, it follows that $V_{\frac{1}{2}}$ is not a pure gauge transformation but a transformation with nontrivial action within the gauge-invariant subspaces, and therefore the Θ_x and Θ_y mean-field Hamiltonians are not gauge equivalent, but rather realizing to two physically distinct generalized projective symmetry-group implementations. This implies that only one of them will have lower energy as a trial ground state for a specific microscopic RK Hamiltonian. Since the plaquette resonance term $L_{\mathbf{R}}$ is odd under $V_{\frac{1}{2}}$, the one that is more energetically favorable will be determined by the sign of the plaquette resonance term in the microscopic Hamiltonian.[10]

As described in Sec. III A, for the cases of the $\mathcal{H}_{\text{Q6VM}}$ and $\mathcal{H}_{\text{QDM}}$, the system is respectively at half-filling and quarter filling, therefore, as depicted in Fig. 17, these systems have a mean-field dispersion featuring two massless Dirac cones and a Fermi surface, respectively. The Dirac points are located at $\mathbf{q}_0 = (q_1, q_2) = (\pi, 0)$ and $\mathbf{q}_0 = (q_1, q_2) = (0, \pi)$. By writing $\mathbf{q} = \mathbf{q}_0 + \mathbf{p}$ and expanding the mean-field Hamiltonian to linear order in the momentum $\mathbf{p}$, we obtain the following effective Dirac Hamiltonian for the Θ_x extended PSG ($t \in \mathbb{R}$) is

$$h(\mathbf{q}_0 + \mathbf{p}) \simeq v \begin{cases} p_x\tau^x + p_y\tau^y & \text{for} \quad \mathbf{q}_0 = (\pi, 0), \\ p_x\tau^x - p_y\tau^y & \text{for} \quad \mathbf{q}_0 = (0, \pi), \end{cases} \tag{41}$$

where $\tau^{x,y}$ are Pauli matrices in the a/b sublattice space, $v = \sqrt{2}t|\mathbf{R}_1|$, and $p_x = (\mathbf{p}\cdot\hat{\mathbf{R}}_1 - \mathbf{p}\cdot\hat{\mathbf{R}}_2)/\sqrt{2}|\mathbf{R}_1|$, $p_y = (\mathbf{p}\cdot\hat{\mathbf{R}}_1 + \mathbf{p}\cdot\hat{\mathbf{R}}_2)/\sqrt{2}|\mathbf{R}_1|$. On the other hand, for the Θ_y extended PSG ($t \in i\mathbb{R}$) the linearized Hamiltonian is

$$h(\mathbf{q}_0 + \mathbf{p}) \simeq v \begin{cases} p_x\tau^y + p_y\tau^x & \text{for} \quad \mathbf{q}_0 = (\pi, 0), \\ p_x\tau^y - p_y\tau^x & \text{for} \quad \mathbf{q}_0 = (0, \pi), \end{cases} \tag{42}$$

where $v = -i\sqrt{2}t|\mathbf{R}_1|$.

Now for the case of the subspace of the QDM model which corresponds to a quarter-filling of the bands by the JW composite fermions, there is a Ferrmi surface that consists of straight lines that are perfectly nested by $(\pi, 0)$ and $(0, \pi)$ vectors (see Figs. 17 and 19). This indicates that such putative composite Fermi-liquid state would be highly unstable towards forming a state which spontaneously breaks the lattice translational symmetry and gaps the Fermi surface. This perfect nesting occurs only for the strict nearest-neighbor mean-field Hamiltonian, and therefore can be removed by adding longer-range hoppings which are allowed by the extended projective symmetry implementations under consideration (Θ_x, Θ_y from Table V). To illustrate this, we consider the further-neighbor hoppings depicted in Fig. 18. One can show that the second-neighbor hopping, denoted by t' and depicted by blue arrows in Fig. 18, vanishes for the Θ_x, Θ_y symmetry implementations. The further-neighbor hopping denoted by t_2 and depicted by green arrows in Fig. 18 is allowed by Θ_x, Θ_y symmetry implementations, and it leads to the following sublattice-diagonal entries to the mean-field Hamiltonian:

$$\Delta h_2(\mathbf{q})_{ab} \sim t_2[\cos(q_1 + q_2) + \cos(q_1 - q_2)]\delta_{ab}. \tag{43}$$

However, since $\cos(q + \pi/2) + \cos(q - \pi/2) = 0$, the above correction vanishes exactly along the lines that define

[10]Notice that $(V_{\frac{1}{2}})^2$ would map both the Θ_x and Θ_y mean-field Hamiltonians into minus themselves. However, $(V_{\frac{1}{2}})^2$ leaves all the gauge-invariant operators unchanged, and it is therefore an element of UV gauge group. Therefore, we see that changing the global sign of t in either the Θ_x or Θ_y mean-field Hamiltonians leads to the same physical state.

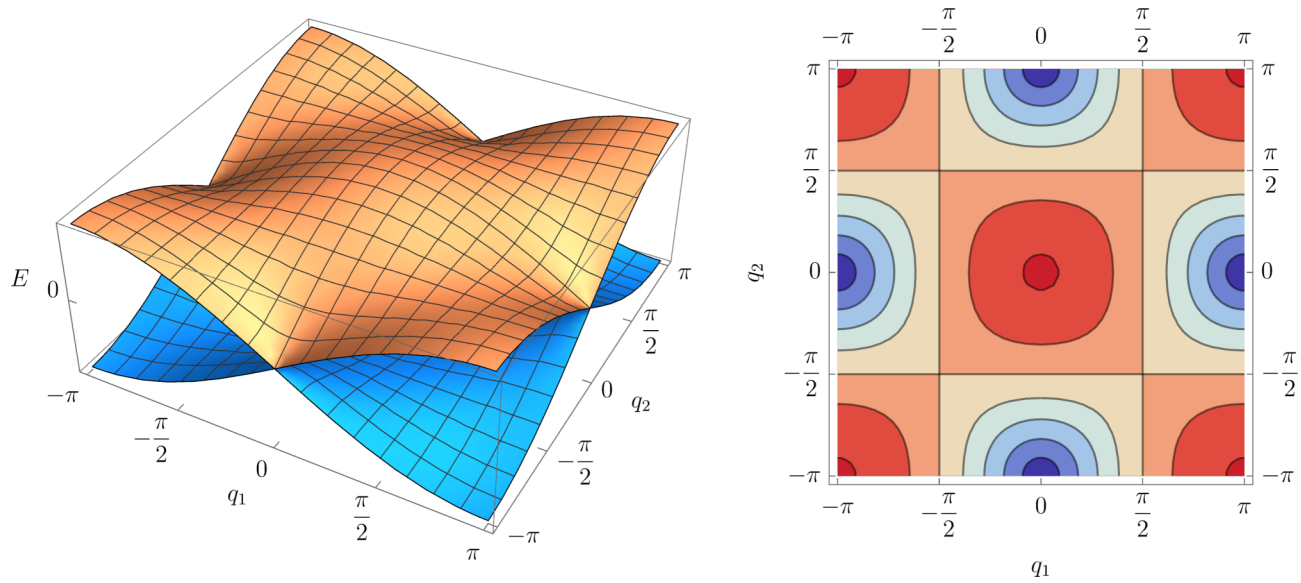

FIG. 17. Dispersions of the JW composite fermions associated with the extended projective symmetry groups Θ_x, Θ_y [see Table V for their definitions, Fig. 16 for the hoppings, and Eq. (39) for dispersion]. There are two Dirac cones at $(0,\pi)$ and $(\pi,0)$ and a Fermi surface at $\frac{1}{4}$-filling which is perfectly nested, and corresponds to the straight lines separating blue from red regions in the equal energy contours shown in the right panel. The crystal momenta are defined as $q_{1,2} = \mathbf{q}\cdot\mathbf{R}_{1,2}$ and therefore measure along the $\mathbf{R}_{1,2}$ directions (see Fig. 16).

the nested Fermi surface (see Figs. 17 and 19), and therefore does not remove the perfect nesting. Nevertheless, there are symmetry-allowed hoppings that lift the nesting. One of them is denoted by t_4 and depicted in Fig. 18 by the red arrows. This hopping adds the following sublattice-diagonal entries to the mean-field Hamiltonian:

$$\Delta h_4(\mathbf{q})_{ab} \sim t_4[\cos(2q_1+2q_2)+\cos(2q_1-2q_2)]\delta_{ab}.$$

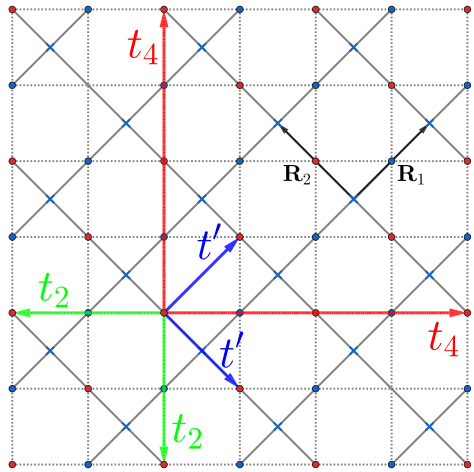

FIG. 18. Further-neighbor hoppings considered to deform the Fermi surface at $\frac{1}{4}$-filling and remove its perfect nesting. t' is forbidden by the Θ_x and Θ_y extended projective symmetry groups. t_2 and t_4 are both allowed, but t_2 alone does not remove the perfect nesting [see Eq. (43)]. Such resilience of the nesting is indicative of the fragility of the JW composite Fermi-liquid state at $\frac{1}{4}$-filling, and thus it might be a useful parent to understand the competing confined broken-symmetry states of the RK–type quantum dimer models (e.g., columnar and resonant plaquette states).

Figure 19 illustrates how the perfect nesting is destroyed as t_4 increases relative to t, leading to a composite Fermi-liquid state with two Fermi surfaces centered around $(\pi,0)$ and $(0,\pi)$. The above illustrates that a composite Fermi-liquid state at $\frac{1}{4}$-filling could be in principle a true stable spin-liquid ground state. However, the strong resilience of the nesting to near-neighbor hopping corrections is indicative that the Fermi surface has strong tendencies to be gapped out and destroyed via instabilities of composite fermion particle-hole pair condensation with finite crystal momentum, leading to ordinary confined states with spontaneously broken lattice translational symmetries, such as the columnar, staggered, and resonant

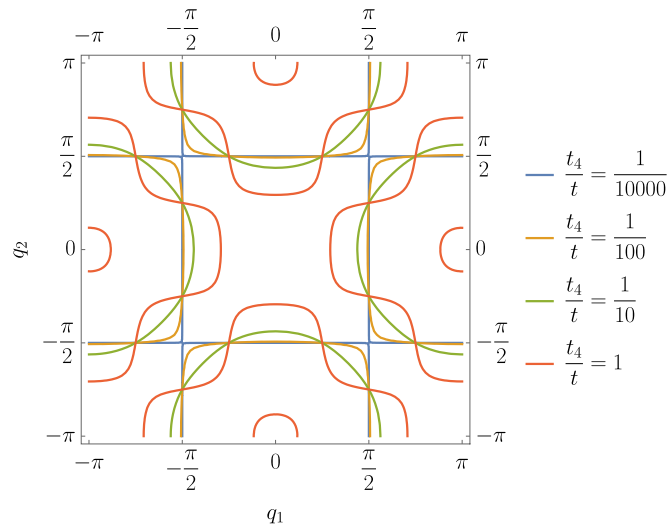

FIG. 19. Fermi surfaces at quarter-filling for various values of t_4/t, illustrating lifting the perfect nesting of the JW composite Fermi surface associated with the QDM model, by adding this further-neighbor hopping.

plaquette phases that are believed to be typically realized for RK Hamiltonians of quantum dimer models.

We would like to close this subsection by noting that our mean-field states associated with the Θ_x, Θ_y extended projective symmetry groups have a resemblance to the classic π-flux state of standard Abrikosov fermions introduced in Refs. [50,55]. In fact from Fig. 16, we see that the fermions are hopping around every plaquette of the original square lattice (which are now subdivided into vertices and plaquettes of the "spin-ice" lattice) accumulating a phase π over the closed loop. There are, however, several crucial physical differences with the classic π-flux state of Abrikosov fermions. First, the classic π-flux state is a spin singlet in which each spin species of Abrikosov fermions has the same hoppings in the square lattice, whereas in our construction the JW composite fermions are spinless with only one fermion species hopping around the plaquette, in a state that is not a spin singlet.[11] More fundamentally, an onsite U(1) transformation such as the $V_{\frac{1}{2}}$ transformation defined in Fig. 14, would be an element of the UV parton gauge of Abrikosov fermions and, therefore, the analog of the Θ_x, Θ_y projective symmetry groups would be two physically equivalent states for the classic π-flux state of Abrikosov fermions. Generally speaking, symmetries are much more constraining for the JW composite fermions relative to Abrikosov fermions, as they fix the phases of hopping and different phases might lead to physically distinct states.

Nevertheless, the fact that our mean-field Hamiltonians of JW composite fermions can be viewed as states with π flux in each plaquette of the original square lattice is useful for understanding the properties of the mean-field states. For example, for a π-flux mean-field state there exists an intra-unit-cell magnetic translation that is not part of the spin-ice Bravais lattice, which can be taken to be a translation by $(\mathbf{R}_1 + \mathbf{R}_2)/2$ (see Fig. 16). This magnetic translation would anticommute with the ordinary elementary translations along either of the two basis vectors of the Bravais lattice $\mathbf{R}_1, \mathbf{R}_2$ because the parallelogram spanned by $\mathbf{R}_1$ and $(\mathbf{R}_1 + \mathbf{R}_2)/2$ encloses π flux, and similarly for the parallelogram spanned by $\mathbf{R}_2$ and $(\mathbf{R}_1 + \mathbf{R}_2)/2$. As a consequence, this magnetic translation boosts the standard crystal momentum by $(q_1, q_2) \to (q_1 + \pi, q_2 + \pi)$, and this explains why the mean-field fermion dispersions that we have found display this translational symmetry in momentum space (see Figs. 17 and 18). However, while this magnetic translation by $(\mathbf{R}_1 + \mathbf{R}_2)/2$ is a symmetry of the unprojected mean-field Hamiltonian, this cannot be a symmetry of the microscopic RK model of quantum spin ice because a translation by $(\mathbf{R}_1 + \mathbf{R}_2)/2$ would map spin-ice vertices onto spin-ice plaquettes, which are clearly distinct in the RK model, and in any typical model with the same spin-ice rules since the ice rules themselves are incompatible with a symmetry that would exchange vertices and plaquettes (except for trivial models without quantum fluctuations). However, this symmetry of the bare-unprojected mean-field state would not be present for the full physical trial state obtained after the spin-ice Gutzwiller projection because the Gutzwiller projection operator from Eq. (21) is not invariant under such translation by $(\mathbf{R}_1 + \mathbf{R}_2)/2$ since it is defined by projecting onto the spin-ice rules associated with the vertices. As we will see, the effective Hamiltonian capturing the gauge field fluctuations that we will discuss in the next section, in fact, does not have any associated translational symmetry by $(\mathbf{R}_1 + \mathbf{R}_2)/2$, and thus this symmetry of the bare mean-field state will be lifted by gauge fluctuations.

[11]The RK Hamiltonian of quantum spin ice is highly anisotropic in spin space and far from having SU(2) symmetry.

IV. GAUGE FIELD FLUCTUATIONS AND EFFECTIVE LOW-ENERGY CONTINUUM FIELD THEORY

The Gutzwiller projection is a nontrivial operation that substantially changes the character of the un-projected mean-field state. Computing analytically the properties of the projected state is, however, a highly nontrivial task. In a sense, this projection can be viewed as giving rise to the appearance of strong gauge field fluctuations around the mean-field state [20,48,72], and, accounting for such fluctuations is necessary to capture, even qualitatively, the correct behavior of the phase of matter in question at low energies.

The mean-field description introduced in the previous section still conceals the emergence of low-energy dynamical gauge fields which can be viewed as arising from fluctuations of the hopping amplitudes of the mean-field state in Eq. (20). While a description of these gauge field fluctuations is often performed by enforcing constraints and performing saddle-point expansions in a path-integral representation (see, e.g., Refs. [77,78]), we will devise here a more phenomenological approach to infer the field content and emergent gauge structure of the low-energy field theory that describes the phase of matter for the itinerant liquids of JW composite fermions associated with the mean-field states constructed in the previous section.

We will include only the fluctuations of the phases of the complex hoppings $t(\mathbf{r}, \mathbf{r}')$ of the mean-field Hamiltonian [see Eq. (20)] but not the fluctuations of their amplitudes because we assume that the latter can be viewed as being gapped and thus not important at low energies. To capture the fluctuations of such phases, we introduce additional bosonic degrees of freedom associated with the nonzero hopping $t(\mathbf{r}, \mathbf{r}')$ of the mean-field state from Eq. (20), that connect a pair of fermion lattice sites $\mathbf{r}, \mathbf{r}'$. We denote the deviation of the phase from its mean-field value by $A(\mathbf{r}, \mathbf{r}')$, and we promote the mean-field Hamiltonian to a new Hamiltonian including this phase fluctuation variables as follows:

$$H[t] \mapsto H[t, A],$$
$$t(\mathbf{r}, \mathbf{r}')f^\dagger(\mathbf{r})f(\mathbf{r}') \to t(\mathbf{r}, \mathbf{r}')f^\dagger(\mathbf{r})e^{iA(\mathbf{r},\mathbf{r}')}f(\mathbf{r}'). \quad (44)$$

The scalar phase $A(\mathbf{r}, \mathbf{r}')$ can be interpreted as a lattice version of $\int_{\mathbf{r}'}^{\mathbf{r}} \mathbf{A} \cdot d\mathbf{x}$. Notice that Hermiticity demands that $A(\mathbf{r}, \mathbf{r}') = -A(\mathbf{r}, \mathbf{r}')$ and $t(\mathbf{r}, \mathbf{r}') = t^*(\mathbf{r}', \mathbf{r})$. The above Hamiltonian describes the coupling of the matter fields to the gauge fields, and therefore we need to provide another Hamiltonian for the "pure" gauge field sector. This Hamiltonian can be obtained by demanding invariance under a generalized version of lattice UV gauge structure and simple symmetry considerations. In Sec. IV A, we will review this construction

first for the case of usual Abrikosov partons and subsequently in Sec. IV A we will apply it to the case of the extended parton constructions for quantum spin ice.

A. Review of gauge field fluctuations for U(1) spin liquids from standard parton constructions

In this section we will derive the effective field theory governing a U(1) spin liquid associated with the standard Abrikosov parton mean-field states (see Sec. III B). The conclusion in this section will be simple and well established before, namely, when the spin-liquid state associated with a given mean-field parton state is stable, the low-energy deconfined gauge structure will be given by the invariant gauge group (IGG) [48,72]. We will illustrate this for a mean-field parton state with a global U(1) particle-conservation symmetry, and thus a U(1) IGG, leading, therefore, to a low-energy U(1) gauge group minimally coupled to the parton fermions [i.e., a standard U(1) spin liquid]. We wish, however, here to rederive these results in what is hopefully a more conceptually intuitive construction, so that we can use it as a template of reasoning for deriving the new results of the emergent low-energy gauge structure of our extended parton constructions of JW composite fermion states in the next section.

We begin by promoting the phases of the hoppings into dynamical degrees of freedom and the mean-field Hamiltonian from Eq. (18) into the following Hamiltonian capturing the field matter coupling:

$$H[t, A] \doteq \sum_{s,s'} \sum_{\mathbf{r},\mathbf{r}'} t_{ss'}(\mathbf{r}, \mathbf{r}') e^{iA(\mathbf{r},\mathbf{r}')} f_s^\dagger(\mathbf{r}) f_{s'}(\mathbf{r}'). \tag{45}$$

Here $A(\mathbf{r}, \mathbf{r}')$ is viewed as a dynamical compact periodic phase taking values $A(\mathbf{r}, \mathbf{r}') \in [0, 2\pi)$. We would like now to define an extension of the local UV parton gauge symmetry, but which acts not only on the fermions but also on the dynamical gauge fields $A(\mathbf{r}, \mathbf{r}')$. As discussed in Sec. III B, the local U(1) transformations of the parton gauge group are generated by the local fermion occupations $n(\mathbf{r})$, which transform the fermion bilinears as [see Eq. (18)]

$$f_s^\dagger(\mathbf{r}) f_s(\mathbf{r}') \xrightarrow{\text{Gauge}} e^{-i[\theta(\mathbf{r})-\theta(\mathbf{r}')]} f_s^\dagger(\mathbf{r}) f_s(\mathbf{r}') \tag{46}$$

Therefore, in order to leave the Hamiltonian from Eq. (45) invariant, we demand that these transformations act on the dynamical phase gauge degrees of freedom as follows:

$$A(\mathbf{r}, \mathbf{r}') \xrightarrow{\text{Gauge}} A(\mathbf{r}, \mathbf{r}') + \theta(\mathbf{r}) - \theta(\mathbf{r}'). \tag{47}$$

For simplicity, from now on we will assume that the hoppings only connect nearest-neighbor sites $\mathbf{r}$ and $\mathbf{r}' = \mathbf{r} + \mathbf{e}_i$ (with $i = x, y$) and we will label the bond connecting them by $(\mathbf{r}, i)$, and the gauge fields by $A(\mathbf{r}, i)$. To implement the transformation from Eq. (47) quantum mechanically, we introduce a canonically conjugate variable to the vector potentials denoted by $E(\mathbf{r}, i)$, and take these variables to satisfy the following commutation relations:

$$\begin{aligned} [A(\mathbf{x}, i), E(\mathbf{y}, j)] &= -i\delta_{\mathbf{x},\mathbf{y}}\delta_{ij}, \\ [E(\mathbf{x}, i), E(\mathbf{y}, j)] &= 0, \\ [A(\mathbf{x}, i), A(\mathbf{y}, j)] &= 0. \end{aligned} \tag{48}$$

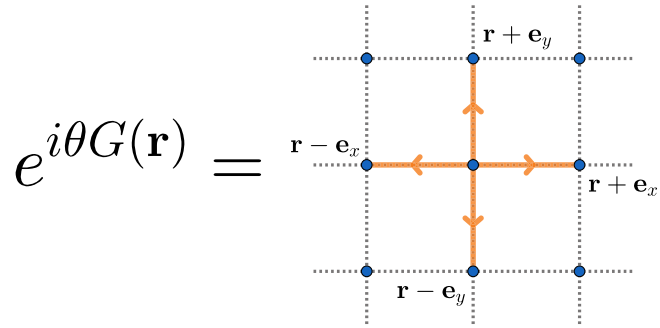

FIG. 20. Depiction of generator of generalized gauge transformations [see Eq. (49)] acting on the matter (residing on blue sites) and vector potentials (residing on links), relevant for the emergent lattice U(1) gauge theory of standard Abrikosov partons.

Since $A(\mathbf{x}, i)$ is an angle, $E(\mathbf{x}, i)$ is an angular momentum with integer-valued spectrum. It is then easy to show that the generalized UV gauge transformations acting on matter and dynamical phase gauge fields are generated by exponentials of the following operators:

$$G(\mathbf{r}) = n(\mathbf{r}) - \boldsymbol{\nabla} \cdot E(\mathbf{r}), \tag{49}$$

where

$$\boldsymbol{\nabla} \cdot E(\mathbf{r}) = E(\mathbf{r}, x) + E(\mathbf{r}, y) - E(\mathbf{r} - \mathbf{e}_x, x) - E(\mathbf{r} - \mathbf{e}_y, y). \tag{50}$$

We will demand that the combined effective Hamiltonian of matter and gauge fields is invariant under the above local gauge group, and we will interpret then the values of $G(\mathbf{r})$ as a constraint that can be consistently imposed on the states in order to represent the subspace of physical interest. The subspace of physical interest will be that for which $G(\mathbf{r}) = 0$ for all $\mathbf{r}$, and therefore this constraint can be viewed as a lattice version of Gauss's law (see Fig. 20 for a depiction).

Let us now determine the simplest operators that are made only from gauge fields which commute with every $G(\mathbf{r})$. It is easy to verify that one of them is the magnetic field operator associated with the curl of A around a plaquette (as depicted in picture Fig. 21):

$$B(\mathbf{r}) \doteq A(\mathbf{r}, x) + A(\mathbf{r} + \mathbf{e}_x, y) - A(\mathbf{r} + \mathbf{e}_y, x) - A(\mathbf{r}, y). \tag{51}$$

Here we view the plaquette of interest as being northeast from lattice site $\mathbf{r}$, and thus we are using this as a label of the plaquette as well. The canonically conjugated variable to $B(\mathbf{r})$ can be shown to be the lattice curl of E:

$$\boldsymbol{\nabla} \times E(\mathbf{r}) \doteq E(\mathbf{r}, x) + E(\mathbf{r} + \mathbf{e}_x, y) - E(\mathbf{r} + \mathbf{e}_y, x) - E(\mathbf{r}, y).$$

Notice that at any site $\mathbf{r}$, $\boldsymbol{\nabla} \times E(\mathbf{r})$ and $(\boldsymbol{\nabla} \cdot E)(\mathbf{r})$ are two independent degrees of freedom. Following an analogous reasoning to the one we did to define the action of gauge transformations on gauge fields, we extend the symmetries in Table IV onto gauge fields by requiring that the interaction Hamiltonian (46) remains invariant. Importantly, the action of symmetries on gauge fields is independent of the specific extended projective symmetry-group implementation for the fermionic matter because the "projective" factors are

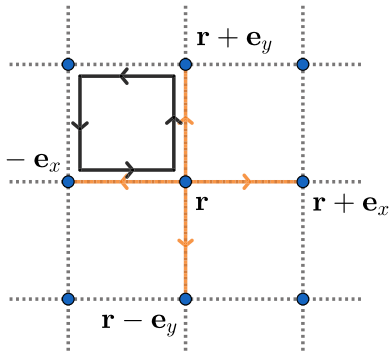

FIG. 21. The solid black lines depict the sum of vector potentials that enter the definition of the magnetic flux operator $B(\mathbf{r}-\mathbf{e}_x)$ [from Eq. (51)]. The orange lines depict the sums of electric fields that enter the divergence operator [from Eq. (50)]. The fact that these two operators commute can be visualized by noting that the number of segments in which parallel black and orange arrows overlap equals the number of segments in which antiparallel arrows overlap.

already fully taken into account in the fermion transformation rules and the choice of mean-field hopping amplitudes. Moreover, under space transformations, the vector potential $A(\mathbf{r},i)$ transforms as a vector directed along the bond $(\mathbf{r},i)$. Its transformation under time reversal Θ can be fixed by demanding that the exponent in Eq. (45) is left invariant:

$$e^{iA(\mathbf{r},i)} = \Theta e^{iA(\mathbf{r},i)}\Theta^{-1} = e^{-i\Theta A(\mathbf{r},i)\Theta^{-1}}, \tag{52}$$

thus, $\Theta A(\mathbf{r},i)\Theta^{-1} = -A(\mathbf{r},i)$.

So far we have kept track of the compactification of the A field. When the low-energy phase is deconfined, it is appropriate to simplify the description by neglecting the compactification and view the fields A as taking values on the real axis. With this simplification and after enforcing the symmetries it is easy to see that the simplest Hamiltonian that is bilinear in the local gauge-invariant fields E and B is the standard Maxwell Hamiltonian in the lattice, given by

$$H_{\text{Gauge}} = \frac{\epsilon}{2}\sum_{\mathbf{r}}[E^2(\mathbf{r},x)+E^2(\mathbf{r},y)] + \frac{1}{2\mu}\sum_{\mathbf{r}}B^2(\mathbf{r}), \tag{53}$$

where ϵ and μ are constants. The above Hamiltonian can be diagonalized in terms of "normal modes" of the pure gauge in the absence of coupling to fermionic matter. Since we have two independent scalar degrees of freedom per unit cell, associated with $A(\mathbf{r},x)$ and $A(\mathbf{r},y)$, but one nondynamical constraint per unit cell [since $\nabla\cdot E(\mathbf{r})$ commutes with H], there is only one truly dynamical harmonic oscillator degree of freedom per unit cell, associated with the magnetic field $B(\mathbf{r})$. Its equations of motion can be determined easily from the Hamiltonian using the commutators from Eq. (48) and read as follows:

$$\begin{aligned}\frac{dB(\mathbf{r})}{dt} &= -\nabla\times E(\mathbf{r}),\\ \frac{d}{dt}\nabla\times E(\mathbf{r}) &= \frac{4}{\mu\epsilon}B(\mathbf{r}) - \frac{1}{\mu\epsilon}\sum_{\substack{\xi=\pm\mathbf{e}_x\\ \xi=\pm\mathbf{e}_y}} B(\mathbf{r}+\boldsymbol{\xi}).\end{aligned} \tag{54}$$

The above can be solved by expanding fields in crystal momentum basis (Fourier transform) to obtain

$$\frac{d^2B(\mathbf{q})}{dt^2} + \frac{1}{\mu\epsilon}[4-2\cos(q_x)-2\cos(q_y)]B(\mathbf{q}) = 0, \tag{55}$$

and therefore the dispersion of the normal modes is (illustrated in Fig. 22)

$$\omega^2(\mathbf{q}) = \frac{1}{\epsilon\mu}[4-2\cos(q_x)-2\cos(q_y)]. \tag{56}$$

The above dispersion features a linearly dispersing photonlike mode centered at momentum $(q_x,q_y)=(0,0)$ with a speed of (see Fig. 22)

$$v = \frac{1}{\sqrt{\mu\epsilon}}.$$

This photon would be minimally coupled to the fermionic matter through Eq. (44). We see, therefore, that our phenomenological procedure is able to describe the low-energy field content expected at low energies for a U(1) spin liquid associated with the standard Abrikosov parton construction [48,72]. Let us pause to consider what protects the gaplessness of this photon mode? Once deconfinement is presumed, so that it is valid to replace vector potentials by continuum real-valued variables, the lattice Faraday law from Eq. (54) can be reinterpreted as a continuity equation:

$$\frac{\partial B}{\partial t}(\mathbf{r},t) + \nabla\cdot\varepsilon = 0, \tag{57}$$

where ε is a dual electric field. It is a rotated version of the previously defined electric field, so that its lattice divergence is centered on the plaquettes, and is defined as

$$\varepsilon_i = \epsilon_{ij}E_j,$$

where ϵ_{ij} is the 2D Levi-Civita symbol. The photon can be viewed as a Goldstone mode of a spontaneously broken global U(1) symmetry associated with the conservation of magnetic flux, as it is usually discussed in boson-vortex dualities in $(2+1)$D [79–81]. In the absence of gapless fermionic matter and due to compact nature of the gauge fields, the above photon would ultimately become gapped at low energies due to Polyakov confinement [63] because the global conservation law of magnetic flux would be explicitly broken by fluctuations associated with local magnetic flux creation and destruction events.

B. Gauge field fluctuations for U(1) spin liquids from extended parton constructions in 2D quantum spin ice

Let us now generalize the previous construction to try to elucidate the low-energy emergent gauge structure associated with the extended parton composite Fermi-liquid states of quantum spin-ice models discussed in Sec. III C. Just as we did for the Abrikosov fermions, we begin by writing the mean-field Hamiltonian of the composite fermions and introduce a real-valued variable that captures the fluctuations of the phase of the hopping amplitude connecting a pair of fermion sites $(\mathbf{r},\mathbf{r}')$ and denote it by $A(\mathbf{r},\mathbf{r}')$. For concreteness we will focus on the fluctuations of the mean-field states described in Sec. III C 4 which had nonzero hoppings only for $(\mathbf{r},\mathbf{r}')$

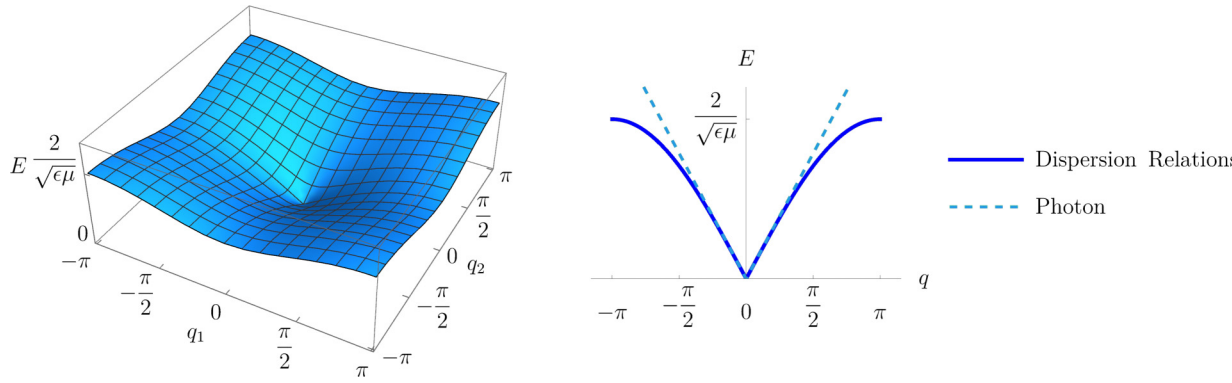

FIG. 22. Left: Dispersion relation of the standard emergent photon of a U(1) spin liquid of Abrikosov fermions, from Eq. (56). Right: Cut of the dispersion relations along $q_y = 0$, with the dashed line illustrating the linearized photon dispersion near $(q_x, q_y) = (0, 0)$.

being nearest-neighbor sites, so that the resulting mean-field Hamiltonian, analogously to (45), reads as

$$\begin{aligned} H(t,A) = \sum_{\mathbf{R}} & it^* e^{-iA_1(\mathbf{R}+\mathbf{R}_2)} f_a^\dagger(\mathbf{R}-\mathbf{R}_1+\mathbf{R}_2) f_b(\mathbf{R}) \\ & + it^* e^{iA_3(\mathbf{R})} f_a^\dagger(\mathbf{R}) f_b(\mathbf{R}) \\ & + te^{-iA_4(\mathbf{R})} f_a^\dagger(\mathbf{R}-\mathbf{R}_1) f_b(\mathbf{R}) \\ & + te^{iA_2(\mathbf{R}+\mathbf{R}_2)} f_a^\dagger(\mathbf{R}+\mathbf{R}_2) f_b(\mathbf{R}) + \text{H.c.} \end{aligned} \tag{58}$$

where the convention for the labeling of Gauge fields is depicted in Fig. 23. As before we promote the above phases into angular quantum-rotor bosonic degrees of freedom, with an associated canonically conjugate degree of freedom denoted by $E(\mathbf{r}, \mathbf{r}')$, with the same commutation relations described in Eq. (48). However, the first crucial difference that appears

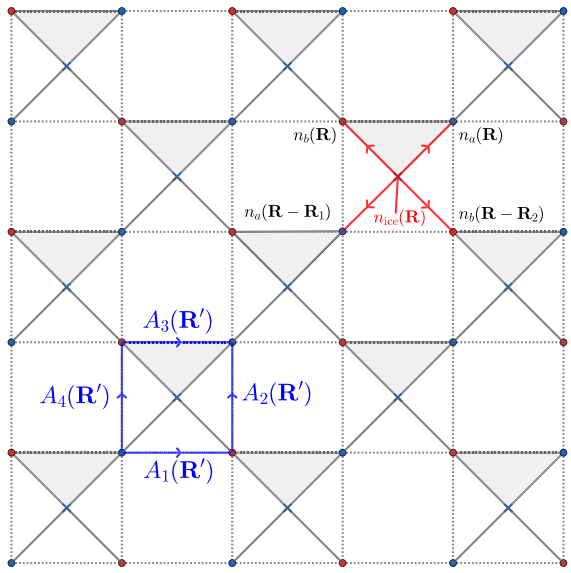

FIG. 23. Bottom left: Convention for labeling gauge fields. These reside at the links (blue lines) that connect the JW composite fermion sites (located at the solid dots). Top right: Depiction of the operators entering in the generator of generalized spin-ice gauge transformations $n_{\text{ice}}(\mathbf{R})$ from Eq. (59), which is centered at the spin-ice vertices.

for the extended partons is that the UV U(1) gauge transformations are not acting as in Eq. (46) for the Abrikosov fermions. Instead, the UV U(1) gauge transformations are generated by the spin-ice charge operators from Eqs. (7) and (14), or equivalently by the total number of fermions in the links connected to vertex $\mathbf{R}$, denoted by $n_{\text{ice}}(\mathbf{R})$, and which in Bravais lattice notation reads as (see Fig. 23)

$$n_{\text{ice}}(\mathbf{R}) = n_a(\mathbf{R}) + n_b(\mathbf{R}) + n_a(\mathbf{R}-\mathbf{R}_2) + n_b(\mathbf{R}-\mathbf{R}_1). \tag{59}$$

Therefore, the generator of the generalized lattice gauge transformations analogous to the one from Eq. (49), that also acts on the dynamical phase degrees of freedom, is a sum of the corresponding four generators from Eq. (49), and is given by

$$G_{\text{ice}}(\mathbf{R}) \doteq n_{\text{ice}}(\mathbf{R}) - \sum_{\mathbf{r}\in\mathbf{R}} (\nabla \cdot E)(\mathbf{r}), \tag{60}$$

where $\mathbf{r} \in \mathbf{R}$ denotes the four spin sites that contribute to the ice rule associated to the vertex $\mathbf{R}$, as depicted in Fig. 23, and the lattice divergence $(\nabla \cdot E)(\mathbf{r})$ is defined in the same way as in Eq. (50).

As before we demand that G_{ice} commutes with every term in the Hamiltonian and interpret the physical Hilbert space as the one satisfying the constraint $G_{\text{ice}}(\mathbf{R}) = 0$ for every $\mathbf{R}$, which can be rewritten as a Gauss law of the form

$$(\nabla \cdot E)_{\text{ice}}(\mathbf{R}) = n_{\text{ice}}(\mathbf{R}), \tag{61}$$

where $(\nabla \cdot E)_{\text{ice}}$ is given by (see Fig. 24)

$$(\nabla \cdot E)_{\text{ice}}(\mathbf{R}) = \sum_{\mathbf{r}\in\mathbf{R}} (\nabla \cdot E)(\mathbf{r}). \tag{62}$$

We can also write a canonically conjugate partner to the above gauge constraint operator, given by

$$(\nabla \cdot A)_{\text{ice}}(\mathbf{R}) = \sum_{\mathbf{r}\in\mathbf{R}} (\nabla \cdot A)(\mathbf{r}). \tag{63}$$

Let us now construct the analog of the Maxwell Hamiltonian from Eq. (53). To do so, we need to find all the linearly independent gauge field operators that commute with the gauge field part of the constraint operator $G_{\text{ice}}(\mathbf{R})$ from Eq. (60), namely, with $(\nabla \cdot E)_{\text{ice}}(\mathbf{R})$ and its canonical partner $(\nabla \cdot A)_{\text{ice}}(\mathbf{R})$. Since the Bravais unit cell contains four scalar

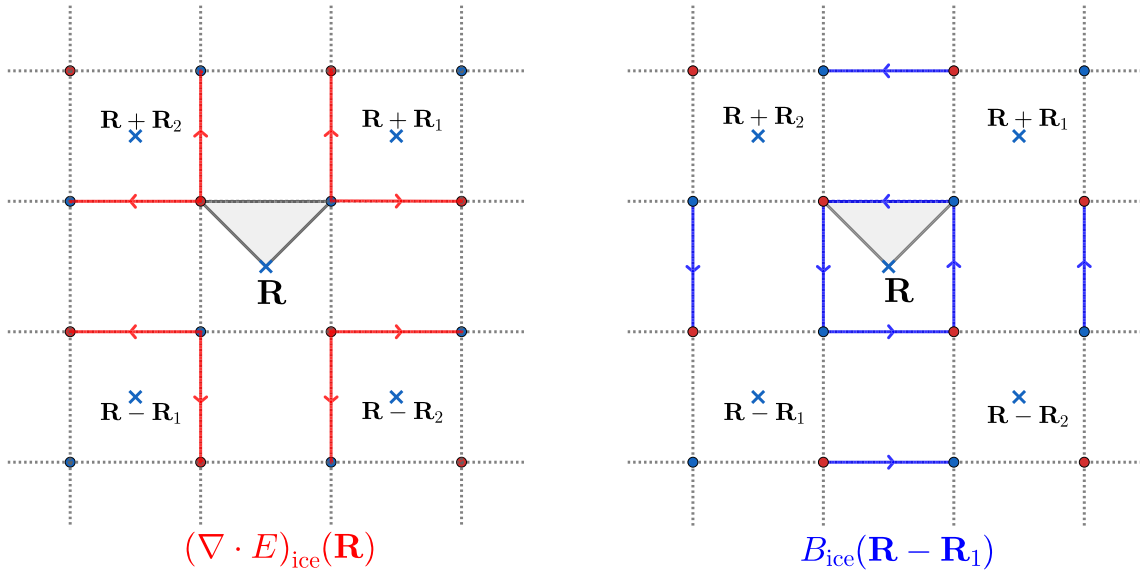

FIG. 24. Left: Depiction of generalized spin-ice electric field divergence operator $(\nabla \cdot E)_{\text{ice}} = \sum_{\mathbf{r}\in\mathbf{R}} (\nabla \cdot E)(\mathbf{r})$ from Eqs. (60) and (62). The red arrows depict the convention for adding electric fields. Right: Depiction of spin-ice magnetic field operator $B_{\text{ice}}(\mathbf{R} - \mathbf{R}_1)$ from Eq. (66). The blue arrows depict the convention for adding vector potentials. The blue crosses mark the location of the spin-ice vertices.

vector potential degrees of freedom (see Fig. 23), but there is one Gauss law constraint per unit cell, we expect three independent harmonic oscillator modes per cell and therefore three dynamical gauge field bands. To find a basis for such modes, we notice that since $(\nabla \cdot E)_{\text{ice}}(\mathbf{R})$ is a sum of divergences from the previous section on Abrikosov fermions [see Eq. (50)], the gauge-invariant operators we discussed in the previous section would also be gauge invariant in the new spin-ice construction. These include the magnetic operators $B(\mathbf{r})$ from Sec. III B, but now there are two such operators per spin-ice Bravais unit cell, one associated with the spin-ice vertex and one with the spin-ice plaquette, which we denote, respectively, by $B_V(\mathbf{R})$, $B_P(\mathbf{R})$, and together with their canonically conjugate partners are explicitly given by (see Fig. 23)

$$\begin{aligned} B_V(\mathbf{R}) &= A_1(\mathbf{R}) + A_2(\mathbf{R}) - A_3(\mathbf{R}) - A_4(\mathbf{R}), \\ (\nabla \times E)_V(\mathbf{R}) &= E_1(\mathbf{R}) + E_2(\mathbf{R}) - E_3(\mathbf{R}) - E_4(\mathbf{R}), \\ B_P(\mathbf{R}) &= A_3(\mathbf{R} - \mathbf{R}_2) + A_4(\mathbf{R} + \mathbf{R}_1 - \mathbf{R}_2) \ldots \\ &\quad - A_1(\mathbf{R} + \mathbf{R}_1) - A_2(\mathbf{R}), \\ (\nabla \times E)_P(\mathbf{R}) &= E_3(\mathbf{R} - \mathbf{R}_2) + E_4(\mathbf{R} + \mathbf{R}_1 - \mathbf{R}_2) \ldots \\ &\quad - E_1(\mathbf{R} + \mathbf{R}_1) - E_2(\mathbf{R}), \end{aligned} \tag{64}$$

where $B_V(\mathbf{R})$ can viewed as a lattice curl centered around vertex $\mathbf{R}$ and $B_P(\mathbf{R})$ as a curl centered around the plaquette which is neighboring to the right the vertex $\mathbf{R}$ (see Fig. 25). However, there are certain additional operators containing only gauge fields, that commute with every $(\nabla \cdot E)_{\text{ice}}(\mathbf{R})$, but which would not be gauge invariant under the convention of previous section, namely, they would not commute with all the divergences of electric fields defined in Eq. (50). These operators and their canonically conjugate partners (see Fig. 25) can be taken to be

$$\begin{aligned} B_x(\mathbf{R}) &= A_3(\mathbf{R} - \mathbf{R}_2) - A_1(\mathbf{R} + \mathbf{R}_1), \\ E_x(\mathbf{R}) &= E_3(\mathbf{R} - \mathbf{R}_2) - E_1(\mathbf{R} + \mathbf{R}_1), \\ B_y(\mathbf{R}) &= A_4(\mathbf{R} + \mathbf{R}_1 - \mathbf{R}_2) - A_2(\mathbf{R}), \\ E_y(\mathbf{R}) &= E_4(\mathbf{R} + \mathbf{R}_1 - \mathbf{R}_2) - E_2(\mathbf{R}), \end{aligned} \tag{65}$$

where the $B_x(\mathbf{R})$, $B_y(\mathbf{R})$ fields can viewed as centered around the plaquette of the spin-ice model which is neighboring to the right of the vertex $\mathbf{R}$ (see Fig. 25). Notice that $B_P(\mathbf{R}) = B_x(\mathbf{R}) + B_y(\mathbf{R})$. Therefore, the set of linearly independent dynamical fields could in principle be chosen to be $B_x(\mathbf{R})$, $B_y(\mathbf{R})$, $B_V(\mathbf{R})$. There is, however, a much better choice of local gauge-invariant fields that will highly simplify the dynamics and the final physical picture. The idea is that instead of $B_V(\mathbf{R})$, we would like to construct a local magnetic field strength that fits more naturally within the spin-ice gauge structure, which we will denote by $B_{\text{ice}}(\mathbf{R})$. This quantity and its canonical partner can be chosen as follows:

$$\begin{aligned} B_{\text{ice}}(\mathbf{R}) &= B_x(\mathbf{R}) + B_x(\mathbf{R} + \mathbf{R}_1 + \mathbf{R}_2) + B_y(\mathbf{R} + \mathbf{R}_2) \\ &\quad + B_y(\mathbf{R} + \mathbf{R}_1) + 2B_V(\mathbf{R} + \mathbf{R}_1), \\ (\nabla \times E)_{\text{ice}}(\mathbf{R}) &= E_x(\mathbf{R}) + E_x(\mathbf{R} + \mathbf{R}_1 + \mathbf{R}_2) + E_y(\mathbf{R} + \mathbf{R}_2) \\ &\quad + E_y(\mathbf{R} + \mathbf{R}_1) + 2(\nabla \times E)_V(\mathbf{R} + \mathbf{R}_1). \end{aligned} \tag{66}$$

Figure 24 illustrates the terms that enter into $B_{\text{ice}}(\mathbf{R})$ making more clear why it has a natural interpretation of a spin-ice lattice curl. Notice that $B_{\text{ice}}(\mathbf{R})$ is naturally viewed as centered around the vertex $\mathbf{R} + \mathbf{R}_1$ (see Fig. 24), but it will be convenient to keep its position label as $\mathbf{R}$ as we will see later on. The three fields $B_x(\mathbf{R})$, $B_y(\mathbf{R})$, $B_{\text{ice}}(\mathbf{R})$ and their canonical conjugate partners $E_x(\mathbf{R})$, $E_y(\mathbf{R})$, $(\nabla \times E)_{\text{ice}}(\mathbf{R})$ commute with the gauge constraint field $(\nabla \cdot E)_{\text{ice}}(\mathbf{R})$ and its canonical partner $(\nabla \cdot A)_{\text{ice}}(\mathbf{R})$, and thus form a basis for the three independent

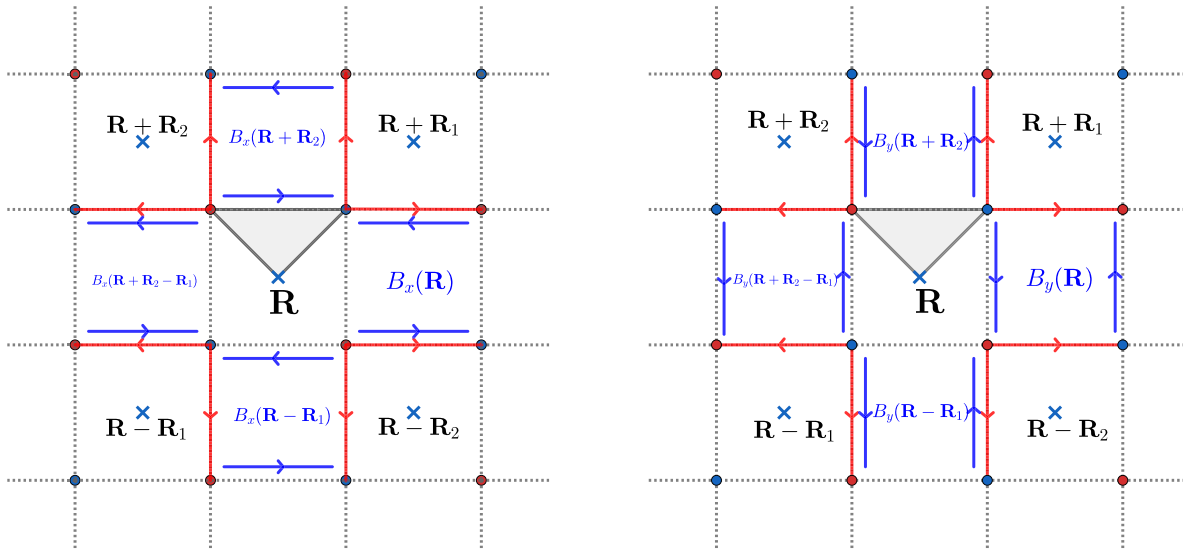

FIG. 25. Left: Depiction of B_x operators [from Eq. (65)], as pairs of blue arrows. Notice that whenever the blue arrows (vector potentials) of a B_x operator overlap with the red arrows (electric fields) of a $(\nabla \cdot E)_{\text{ice}}$ operator, there are always an equal number of parallel and antiparallel arrows, illustrating that these operators commute. Right: Analogous depictions for the B_y operators [from Eq. (65)]. The blue crosses mark the location of the spin-ice vertices.

modes of physical gauge fluctuations. The advantage of this basis over the $B_x(\mathbf{R}), B_y(\mathbf{R}), B_V(\mathbf{R})$ basis is that these fields form a set of decoupled canonical coordinates, namely, their mutual commutators vanish:

$$\begin{aligned}
[B_x(\mathbf{R}), E_y(\mathbf{R}')] = [B_x(\mathbf{R}), \quad (\nabla \times E)_{\text{ice}}(\mathbf{R}')] = 0,\\
[B_y(\mathbf{R}), E_x(\mathbf{R}')] = [B_y(\mathbf{R}), \quad (\nabla \times E)_{\text{ice}}(\mathbf{R}')] = 0,\\
[B_{\text{ice}}(\mathbf{R}), E_x(\mathbf{R}')] = [B_{\text{ice}}(\mathbf{R}), \quad E_y(\mathbf{R}')] = 0.
\end{aligned}$$

The action of the microscopic lattice space symmetries on these fields is the same as in the case of Abrikosov fermions, and the additional pure gauge group transformation that enters into the extended projective symmetry-group implementation on the fermions does not affect the gauge fields, therefore, the fields $A_i(\mathbf{R})$ transform as ordinary vectors according to the directions specified by the sites they connect, which is depicted in Fig. 23. From this the transformations of dynamical fields under space symmetries follow easily. The action of time reversal (Θ in Table II) can be also inferred analogously to Eq. (52), and one concludes that

$$\begin{aligned}
\Theta A_i(\mathbf{R})\Theta^{-1} &= -A_i(\mathbf{R}),\\
\Theta E_i(\mathbf{R})\Theta^{-1} &= E_i(\mathbf{R}),
\end{aligned} \tag{67}$$

where $i = 1, 2, 3, 4$ are the components depicted in Fig. 23, and the transformations of $E_i(\mathbf{R})$ can be inferred from its canonical commutator with $A_i(\mathbf{R})$. Let us now consider the action of the microscopic particle-hole conjugation of hard-core bosons, denoted by X (see Table II). From its action on JW composite fermions [see Eq. (35)] we obtain that the phases dressing the mean-field Hamiltonian should transform as

$$X e^{iA(\mathbf{r},\mathbf{r}')} X^\dagger = e^{iA(\mathbf{r}',\mathbf{r})} = e^{-iA(\mathbf{r},\mathbf{r}')}, \tag{68}$$

where we used that $A(\mathbf{r}', \mathbf{r}) = -A(\mathbf{r}, \mathbf{r}')$ (Hermiticity). Therefore, the fields transform as

$$\begin{aligned}
X A_i(\mathbf{R}) X^\dagger &= -A_i(\mathbf{R}),\\
X E_i(\mathbf{R}) X^\dagger &= -E_i(\mathbf{R}).
\end{aligned} \tag{69}$$

It is interesting to note that under the natural microscopic time-reversal symmetry of spin $\frac{1}{2}$ denoted by $\mathcal{T}$ (see Sec. III C 3), it follows from Eqs. (33) and (67) and (69) that the gauge fields transform as

$$\begin{aligned}
\mathcal{T} A_i(\mathbf{R}) \mathcal{T}^{-1} &= A_i(\mathbf{R}),\\
\mathcal{T} E_i(\mathbf{R}) \mathcal{T}^{-1} &= -E_i(\mathbf{R}),
\end{aligned} \tag{70}$$

and, therefore, interestingly, all the magnetic fields $B_x(\mathbf{R}), B_y(\mathbf{R}), B_{\text{ice}}(\mathbf{R})$ are even and the electric fields are odd under this time reversal, which is opposite to the standard situation in QED. This is a manifestation of the pseudoscalar transformation of the JW composite fermions under this symmetry, as discussed in Sec. III C 3 and Ref. [75]. Similar considerations also apply to other space symmetries such as mirrors, which in order to be implemented as natural spin-$\frac{1}{2}$ symmetries need to be dressed by the hard-core boson particle-hole conjugation X, which would lead to transformations on gauge fields opposite to those of ordinary QED (e.g., the electric field transforming as a pseudovector under mirrors).

We are now in a position to write a simple bilinear Maxwell-type model Hamiltonian for the pure gauge field part invariant under all microscopic symmetries of the RK model, which we write as

$$\begin{aligned}
H_{\text{Gauge}} = &\frac{\epsilon}{2} \sum_{\mathbf{R}} \sum_{i=1}^{4} E_i^2(\mathbf{R}) + \frac{\chi_B}{2} \sum_{\mathbf{R}} B_{\text{ice}}^2(\mathbf{R})\\
&+ \frac{\chi_P}{2} \sum_{\mathbf{R}} \left[B_x^2(\mathbf{R}) + B_y^2(\mathbf{R}) \right].
\end{aligned} \tag{71}$$

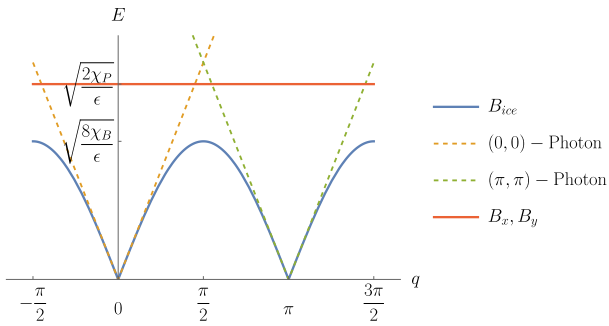

FIG. 26. Dispersion relations of the gauge fields obtained from the pure Maxwell-type Hamiltonian (i.e., ignoring coupling to matter fermions), along a cut with $q_1 = q_2$. There are two linearly dispersing photonlike modes near $(q_1, q_2) = (0, 0)$ and $(q_1, q_2) = (\pi, \pi)$, with their dispersion shown in blue obtained from Eq. (74) (the dashed lines are linearized approximations of the photon dispersions). There are also two fully gapped gauge fluctuation modes associated with the B_x, B_y fields (red lines), which are localized modes and hence have strictly flat dispersions for the ideal Maxwell-type Hamiltonian from Eq. (71).

Here we have ignored again for simplicity the compactification of gauge fields, and ϵ, χ_B, χ_P are phenomenological coupling constants. The equations of motion for the Hamiltonian from Eq. (71) are

$$\begin{aligned}
\frac{d^2B_x}{dt^2}(\mathbf{R}) &= -2\frac{\chi_P}{\epsilon}B_x(\mathbf{R}),\\
\frac{d^2B_y}{dt^2}(\mathbf{R}) &= -2\frac{\chi_P}{\epsilon}B_y(\mathbf{R}),\\
\frac{d^2B_{\rm ice}}{dt^2}(\mathbf{R}) &= -\frac{2\chi_B}{\epsilon}\left[4B_{\rm ice}(\mathbf{R}) - \sum_{\substack{\xi=\pm\mathbf{R}_1\\ \mu=\pm\mathbf{R}_2}} B_{\rm ice}(\mathbf{R}+\xi+\mu)\right],
\end{aligned} \tag{72}$$

which in crystal momentum basis reduce to

$$\begin{aligned}
\frac{d^2B_x}{dt^2}(\mathbf{q}) &= -\frac{2\chi_P}{\epsilon}B_x(\mathbf{q}),\\
\frac{d^2B_y}{dt^2}(\mathbf{q}) &= -\frac{2\chi_P}{\epsilon}B_y(\mathbf{q}),\\
\frac{d^2B_{\rm ice}}{dt^2}(\mathbf{q}) &= -\omega^2(\mathbf{q})B_{\rm ice}(\mathbf{q}),
\end{aligned} \tag{73}$$

where

$$\omega^2(\mathbf{q}) \doteq \frac{4\chi_B}{\epsilon}[2-\cos(q_1+q_2)-\cos(q_1-q_2)] \tag{74}$$

and $q_i \doteq \mathbf{q}\cdot\mathbf{R}_i$, $i = 1, 2$. The dispersion relations show features that are crucially different with respect to the case of usual lattice QED and the emergent gauge fields discussed in Sec. IV A in the context of Abrikosov fermions. The $B_{x/y}$ modes display a fully gapped and dispersiveless flat band with energy $\sqrt{2\chi_P/\epsilon}$, as depicted in Fig. 26. While the exact flatness is a consequence of our simple model, the fact that these modes are gapped is a generic feature. Therefore, the fluctuations associated with these modes are expected to be irrelevant at low energies, and they can be safely neglected from the low-energy effective theory. On the other hand, the $B_{\rm ice}$ mode displays two distinct gapless photonlike (74) linearly dispersing modes centered around $\mathbf{q} = (0, 0)$ and $\mathbf{q} = (\pi, \pi)$ as depicted in Fig. 26.

To close this section, we would like to remark that the Maxwell-type Hamiltonian of Eq. (71) does not have the half-translational symmetry by $(\mathbf{R}_1 + \mathbf{R}_2)/2$, that we encountered in the bare mean-field fermion Hamiltonian. This can be easily seen by noting that this symmetry would exchange the spin-ice vertices with the spin-ice plaquettes. However, the $B_x(\mathbf{R})$, $B_y^2(\mathbf{R})$ fields are only centered around the spin-ice plaquettes, whereas the fields $B_{\rm ice}(\mathbf{R})$ are centered only around vertices, and therefore clearly the Hamiltonian of Eq. (71) has no symmetry relating spin-ice vertices and spin-ice plaquettes. The apparent translational symmetry in momentum space by (π, π) of the pure gauge field modes that we see in Fig. 26 is a result of fine tuning of the model, which we have done for simplicity. For example, gauge-invariant terms can be easily added to the Maxwell-Hamiltonian that would delocalize the $B_x(\mathbf{R})$, $B_y(\mathbf{R})$ modes and make them itinerant and with dispersions that would have different energies near (0,0) vs near (π, π). Similarly, it is possible to add gauge-invariant terms to the Hamiltonian that would make the photons originating from fluctuations of $B_{\rm ice}(\mathbf{R})$ to have different speeds near (0,0) vs near (π, π). Therefore, the full theory of fermions coupled to gauge field fluctuations does not have the translational symmetry by $(\mathbf{R}_1 + \mathbf{R}_2)/2$ that we saw in the bare mean-field fermion Hamiltonian, reflecting the fact that this is not a true microscopic symmetry of the underlying RK Hamiltonian of spin ice.

C. Gauge field and matter couplings, low-energy effective field theory, and dipolar nature of composite fermions

Let us now determine the matter coupling to the low-energy gauge fields and the low-energy effective field theory. For concreteness we will focus on the case of gapless Dirac fermions obtained for the six-vertex subspace, but similar considerations would apply to the Fermi-surface state of the quantum dimer model. Ignoring compactification and expanding Eq. (58) up to linear order on the vector potentials, we obtain the following:

$$\begin{aligned}
H(t,A) = \sum_{\mathbf{R}} & it^*[1-iA_1(\mathbf{R}+\mathbf{R}_2)]f_a^\dagger(\mathbf{R}-\mathbf{R}_1+\mathbf{R}_2)f_b(\mathbf{R})\\
&+it^*[1+iA_3(\mathbf{R})]f_a^\dagger(\mathbf{R})f_b(\mathbf{R})\\
&+t[1-iA_4(\mathbf{R})]f_a^\dagger(\mathbf{R}-\mathbf{R}_1)f_b(\mathbf{R})\\
&+t[1+iA_2(\mathbf{R}+\mathbf{R}_2)]f_a^\dagger(\mathbf{R}+\mathbf{R}_2)f_b(\mathbf{R})\\
&+\text{H.c.}+O(A^2).
\end{aligned} \tag{75}$$

As discussed in Sec. III C 4, the fermions have gapless Dirac nodes at the two valleys $(\pi, 0)$ and $(0, \pi)$ while the gauge field has gapless photonlike modes at (0,0) and (π, π). Therefore, we expect that the dominant effects at low energy include the following:

(1) Intravalley scattering within each Dirac cone mediated by exchange of long-wavelength gauge field fluctuations with momenta near (0,0).

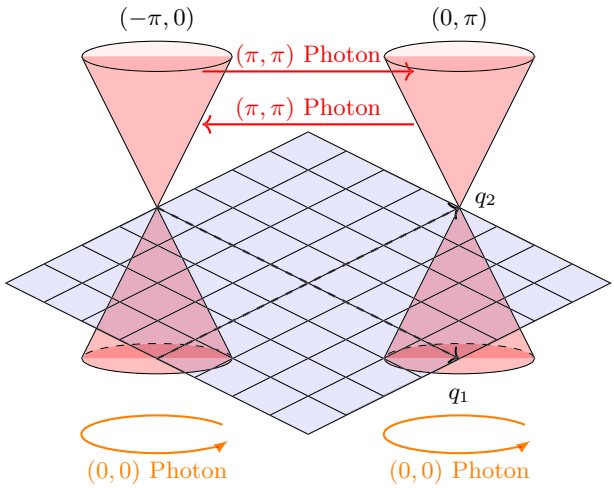

FIG. 27. Illustration of the two types of fermion scattering processes arising from their coupling to gauge fields. The gauge modes near $q = (0, 0)$ mediate "intravalley" fermion scattering processes (depicted by orange circles), and the gauge modes near $q = (\pi, \pi)$ mediate "intervalley" scattering processes (depicted by red straight arrows).

(2) Intervalley scattering process connecting the two Dirac cones mediated by the exchange of gauge fluctuations with momenta near (π, π).

These two kinds of processes are depicted in Fig. 27. Therefore, in the spirit of $k \cdot p$ theory, we define the following fields by expanding the fermion and gauge fields around their different respective gapless points:

$$\Psi(\mathbf{q}) \doteq \begin{pmatrix} f_a[\mathbf{p} + (\pi, 0)] \\ f_b[\mathbf{p} + (\pi, 0)] \\ f_a[\mathbf{p} + (0, \pi)] \\ f_b[\mathbf{p} + (0, \pi)] \end{pmatrix},$$

$$A_j^0(\mathbf{p}) \doteq A_j(\mathbf{p}), \quad j \in \{1, 2, 3, 4\}$$

$$A_j^\pi(\mathbf{p}) \doteq A_j[\mathbf{p} + (\pi, \pi)], \quad j \in \{1, 2, 3, 4\}$$

where $\mathbf{p}$ is understood to be "small" with respect to the size of the Brillouin zone, so that we can expand the Hamiltonian (75) to the first order (for the convention sublattice indices, see Fig. 23). Details of the derivations of the small momentum expansion can be found in Appendix C, we will here summarize the final results next.

1. $\mathbf{p} = (0, 0)$ *scattering terms*

The Hamiltonian density describing processes of the first type for the state with Θ_x extended PSG ($t \in \mathbb{R}$) is

$$H = v\Psi^\dagger(\mathbf{x})\big[\big(p_x - A_x^0(\mathbf{x})\big)\tau^x + \big(p_y - A_y^0(\mathbf{x})\big)\tau^y\rho^z\big]\Psi(\mathbf{x}),$$

and for the state with Θ_y extended PSG ($t \in i\mathbb{R}$) is

$$H = v\Psi^\dagger(\mathbf{x})\big[\big(p_x - A_x^0(\mathbf{x})\big)\tau^y + \big(p_y - A_y^0(\mathbf{x})\big)\tau^x\rho^z\big]\Psi(\mathbf{x}),$$

where the convention of momenta is the same as in Eq. (41), and τ^i, ρ^i denote Pauli matrices in $\{a, b\}$ sublattice and on $\{(\pi, 0), (0, \pi)\}$ valley spaces, respectively, and we have defined continuum vector potential fields as follows:

$$A_x^0(\mathbf{x}) \doteq \frac{A_1^0(\mathbf{x}) + A_3^0(\mathbf{x})}{\sqrt{2}|\mathbf{R}_1|},$$
$$A_y^0(\mathbf{x}) \doteq \frac{A_2^0(\mathbf{x}) + A_4^0(\mathbf{x})}{\sqrt{2}|\mathbf{R}_1|}. \tag{76}$$

Therefore, we see that the long-wavelength gauge fluctuations that are gapless near (0,0) simply behave as the standard minimal coupling of a photonlike mode to the matter fields [compare with mean-field Hamiltonian from Eq. (41)].

2. $\mathbf{p} = (\pi, \pi)$ *scattering terms*

The contribution to the Hamiltonian density accounting processes of the second type, for the state with Θ_x extended PSG ($t \in \mathbb{R}$), is

$$\delta H = -v\Psi^\dagger(\mathbf{x})\big[B_x^\pi(\mathbf{x})\tau^x\rho^1 + B_y^\pi(\mathbf{x})\tau^x\rho^2\big]\Psi(\mathbf{x}), \tag{77}$$

and for the state with Θ_y extended PSG ($t \in i\mathbb{R}$) is

$$\delta H = -v\Psi^\dagger(\mathbf{x})\big[B_x^\pi(\mathbf{x})\tau^y\rho^1 - B_y^\pi(\mathbf{x})\tau^y\rho^2\big]\Psi(\mathbf{x}), \tag{78}$$

where the continuum vector potential fields are defined as follows:

$$B_x^\pi(\mathbf{x}) = \frac{A_3^\pi(\mathbf{x}) - A_1^\pi(\mathbf{x})}{\sqrt{2}|\mathbf{R}_1|},$$
$$B_y^\pi(\mathbf{x}) = \frac{A_4^\pi(\mathbf{x}) - A_2^\pi(\mathbf{x})}{\sqrt{2}|\mathbf{R}_1|}. \tag{79}$$

Notice that the fields B_x^π, B_y^π are the continuum limits of the fields defined in Eq. (65) expanded around momentum (π, π). Therefore, remarkably, what we are finding here is that to linear order in vector potentials, there is no coupling to the linearly dispersing gapless photon modes near (π, π), but instead the intervalley scattering processes are only mediated by gauge fields associated with the B_x and B_y modes, which are fully gapped throughout the entire Brillouin zone. Therefore, at low energies compared to the gap of the B_x, B_y modes and the bandwidth of the photon modes, we have two emergent massless photon modes, and two massless Dirac fermions. But the fermions only carry gauge charge under the (0,0) photon but appear as gauge neutral under the (π, π) photon.

D. U(1) × U(1) gauge structure

In this section we will explain why the occurrence of two gapless photon modes and the gauge coupling of the Dirac composite fermions to only one of them, that we encountered in Secs. IV B and IV B, is not accidental. We will show there are two emergent U(1) gauge structures with independent local Gauss laws and two global flux conservations, as if we had two copies of ordinary lattice QED.

To see this it is convenient to split the Bravais lattice of vertices of the spin-ice model, which are located at vectors $\mathbf{R}$, into two sublattices denoted by Λ_A and Λ_B, as depicted in Fig. 29. The sublattice Λ_B can be obtained by displacing the Λ_A by either the Bravais vector $\mathbf{R}_1$ or $\mathbf{R}_2$, and vice versa. Therefore, the Bravais unit vectors of the lattice Λ_A can be taken to be $\{\mathbf{R}_1 - \mathbf{R}_2, \mathbf{R}_1 + \mathbf{R}_2\}$, and similarly for Λ_B (see Fig. 29). Notice that the operators that measure the divergence

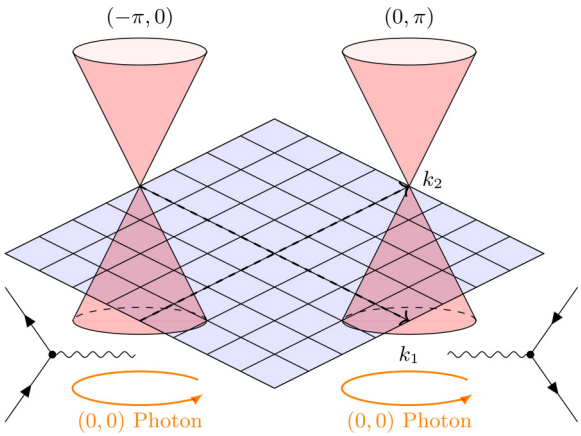

FIG. 28. Depiction of the expected infrared effective low-energy theory, which is a U(1) compact QED in $2 + 1$ dimensions minimally coupled to two massless Dirac fermions. The Dirac fermions are centered at $(0, \pi)$ and $(\pi, 0)$, and they are minimally coupled to the single U(1) photon gapless at (0,0). The photon at (π, π) likely undergoes Polyakov-style confinement, hence disappearing at low energies.

of the dynamical emergent fields $(\nabla \cdot E)_{\text{ice}}(\mathbf{R})$, defined in Eq. (62) and illustrated in Fig. 24, behave as two independent divergences obeying separate Gauss' laws. Namely, when we sum $(\nabla \cdot E)_{\text{ice}}(\mathbf{R})$ over $\mathbf{R}$ restricted to region of points residing only on sublattice Λ_A, we will get a sum of electric

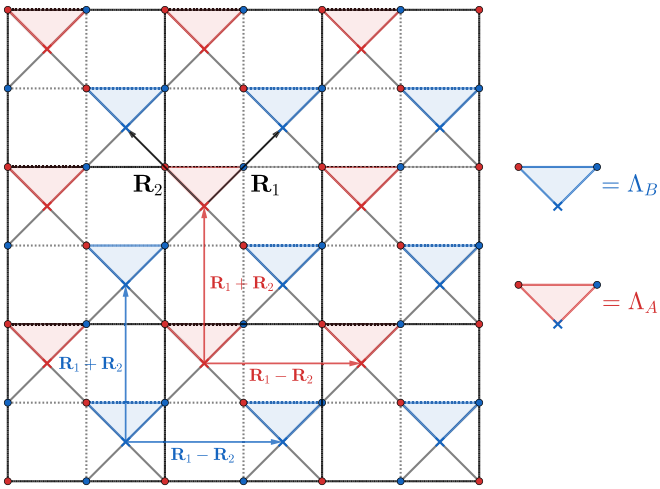

FIG. 29. Separation of the lattice of vertices into Λ_A and Λ_B sublattices, which allows to understand the $\text{U(1)}_\text{A} \times \text{U(1)}_\text{B}$ gauge structure. The JW composite fermions are located at the dots and carry equal charge $(q_A, q_B) = (1, 1)$ under these $\text{U(1)}_\text{A} \times \text{U(1)}_\text{B}$ gauge transformations. The photon that is gapless near (0,0) (see Fig. 26) corresponds to the sublattice-symmetric gauge transformation, for which the fermions are charged. This is why the JW composite fermions are minimally coupled to this photon at low energies (see Fig. 28). The photon that is gapless near (π, π) (see Fig. 26) corresponds to the sublattice-asymmetric gauge transformations (i.e., staggered), for which these asymmetric gauge transformations the JW composite fermions are not charged (behave instead as a gauge dipole) and this is why it is not minimally coupled to the (π, π) photon.

fields residing only at the boundary of such region and normal to the boundary, as expected for a lattice divergence, and similarly for regions of points contained only in sublattice Λ_B. Moreover, we can also restrict the operators $G_{\text{ice}}(\mathbf{R})$ to reside over either of the sublattices and in this way we can view the U(1) gauge group as a product $\text{U(1)}_A \times \text{U(1)}_B$. We can assign a pair charges (q_A, q_B) with $q_{A,B} \in \mathbb{Z}$ to matter operators (namely, those constructed as products of fermion creation and destruction operators) under this $\text{U(1)}_\text{A} \times \text{U(1)}_\text{B}$ gauge group. In particular, the JW composite fermion creation operator would transform as a charge $(q_A, q_B) = (1, 1)$ under such sublattice gauge groups.

There are also two independent global flux conservation symmetries (when ignoring gauge field compactification), one associated with sublattice Λ_A and the other with sublattice Λ_B, which are responsible for the gaplessness of the two photons. This can be seen by adding the operators $dB_{\text{ice}}(\mathbf{R})/dt$, defined in Eq. (66) and illustrated in Fig. 24, over some region of $\mathbf{R}$ that only contains points in the sublattice Λ_A, resulting into a boundary operator, that can be viewed as a line integral of the operator $(\nabla \times E)_{\text{ice}}(\mathbf{R})$ from Eq. (66). This can be interpreted as a conservation law analogous to the lattice Faraday law of QED from Eq. (57), except that now there are two such conservation laws, one for the Λ_A and another one for the Λ_B sublattice.

Moreover, our choice of Maxwell Hamiltonian in Eq. (71) has actually been made so that the two photons of the $\text{U(1)}_A \times \text{U(1)}_B$ gauge structure are also dynamically decoupled. This can be seen by noticing that the commutator of $B_{\text{ice}}(\mathbf{R})$ and $(\nabla \times E)_{\text{ice}}(\mathbf{R}')$ vanishes whenever $\mathbf{R}$ and $\mathbf{R}'$ belong to different Λ_A, Λ_B sublattices. The set of operators $B_{\text{ice}}(\mathbf{R})$ and their canonical partner $(\nabla \times E)_{\text{ice}}(\mathbf{R})$ with $\mathbf{R}$ restricted to a given sublattice Λ_A, Λ_B have indeed exactly the same equations of motion of ordinary QED with a single photon that we reviewed in Sec. IV A. If we expand these operators in the crystal momentum basis of each Λ_A, Λ_B sublattice, associated with Bravais vectors $\{\mathbf{R}_1 - \mathbf{R}_2, \mathbf{R}_1 + \mathbf{R}_2\}$, then we would obtain the following decoupled equations of motion:

$$\frac{d^2 B^A_{\text{ice}}(\mathbf{k})}{dt^2} = -\omega^2(\mathbf{k}) B^A_{\text{ice}}(\mathbf{k}),$$
$$\frac{d^2 B^B_{\text{ice}}(\mathbf{k})}{dt^2} = -\omega^2(\mathbf{k}) B^B_{\text{ice}}(\mathbf{k}),$$

where each of the above equations is now identical to the ordinary Maxwell theory in the square lattice from Eq. (55), with the dispersion $\omega^2(\mathbf{k})$ given by the same expression as in Eq. (56). Here the wave vector k is defined for the Bravais vectors spanned by vectors $\{\mathbf{R}_1 - \mathbf{R}_2, \mathbf{R}_1 + \mathbf{R}_2\}$, and therefore its Brillouin zone is half of the size of the Brillouin zone associated with the full translational symmetry of the lattice.

We therefore see that we have two decoupled copies of standard lattice QED, featuring linearly dispersing photon modes at $\mathbf{k} = (0, 0)$ for each of the sublattices Λ_A and Λ_B. The underlying model has a translational symmetry that exchanges these two sublattices. Therefore, in the lattice momentum convention that exploits the full lattice translational symmetry that was employed in deriving the dispersions from Eq. (71), those two modes combine into a symmetric one and

an antisymmetric one[12] to give rise, respectively, to the $\mathbf{q} = (0, 0)$ mode and $\mathbf{q} = (\pi, \pi)$ mode in Fig. 26. Now since the fermion carries charge $(q_A, q_B) = (1, 1)$ for the gauge fields associated with the two sublattices, it will therefore carry total gauge charge under the sublattice symmetric combination of those fields, associated with the photon $\mathbf{q} = (0, 0)$, and carry zero charge under their sublattice antisymmetric (staggered) combination, associated with the photon $\mathbf{q} = (\pi, \pi)$, explaining the result we encountered in the previous section by direct calculation.

While the above structure is certainly remarkable, its appearance can be intuitively understood by simply appealing to the interplay of the local conservation laws of the spin-ice models and the nature of the Jordan-Wigner composite fermion. Notice that the creation of a Jordan-Wigner composite fermion, which involves the reversal of the z direction of a single spin, violates necessarily two ice rules associated to two vertices that are connected by the link in which such spin resides. One of these vertices is located in the Λ_A sublatice and the other in the Λ_B sublatice. Thus, it is natural to see the Jordan-Wigner composite fermion as an extended dipolelike object which has two charges located at the end of the link that connects the two vertices (see Fig. 23), which will be charged under the sublattice symmetry local gauge transformations, but will be a neutral dipole under the staggered antisymmetric gauge transformation.[13] This is why we have called it an "extended parton" to emphasize the distinction with a "pointlike parton," such as the Abrikosov fermion.

V. SUMMARY AND DISCUSSION

We have built upon the idea that the standard Jordan-Wigner transmutation that maps spin-$\frac{1}{2}$ degrees of freedom onto spinless fermions in a 2D lattice is exactly equivalent to another celebrated statistical transmutation of attaching a 2π flux to a spinless hard-core boson that maps these onto spinless composite fermions. In one-dimensional chains, such Jordan-Wigner transformation has the property that it maps local Hamiltonians of spins that are symmetric under a global parity onto local Hamiltonian of fermions. However, in 2D models, simply imposing a global symmetry is not enough to preserve locality on both the *physical side* (the spin representation) and the *dual side* (the fermion representation). Nevertheless, this should not be viewed as a *bug* but rather as a *feature* of the mapping: the nonlocality is expressing the fact that the fermion is not the underlying microscopic local particle of the Hilbert space of interest, but instead it is a nonlocal composite fermion object obtained from attaching a 2π flux to the underlying microscopic particles.

One *ad hoc* approach to handle the above inherent nonlocality of Jordan-Wigner composite fermions in 2D, that is often used in mean-field treatments, is to simply ignore the detailed structure of nonlocality by replacing the gauge fields associated with the flux attachment by averaged "smeared" values that can be chosen to match the net background magnetic field which is given by the composite fermion density. However, in this work we have advanced a completely different route to capture this nonlocality of the Jordan-Wigner composite fermions. Namely, we have exploited the fact that Hamiltonians of spin-$\frac{1}{2}$ degrees of freedom that respect certain local symmetries do remain local in their dual Jordan-Wigner composite fermions representation. The local symmetries that we have focused on are the U(1) symmetries associated with ice rules in 2D quantum spin-ice models which allow to map Rokshar-Kivelson–type models of spins onto local models of Jordan-Wigner composite fermions. The local gauge symmetry structure in these 2D models therefore plays an analog role to the global symmetries in 1D that allows to keep the models local in the *physical* (spin) and *dual* (fermion) representations.

The main difficulty for constructing interesting quantum disordered 2D states within our approach is that quantum spin-ice models with RK–type Hamiltonians would necessarily map onto interacting Hamiltonians of fermions (e.g., the plaquette resonance term maps onto a quartic fermion interaction). Therefore, we do not have the luxury of 1D where nontrivial spin models can be exactly mapped onto purely free-fermion models. More fundamentally, we have seen that even though Slater determinants of fermions can be viewed as a zeroth-order mean-field approximations to the ground states of quantum spin-ice Hamiltonians (which only satisfy the ice rules in a global averaged sense), such Slater determinants necessarily violate the exact local ice rules, and therefore are not satisfactory approximations to their true ground states satisfying the local ice rules. This obstacle can, however, be naturally overcome by acting on these Slater determinants with a Gutzwiller projector that enforces the local ice rules, making such projected states satisfactory trial ground states of 2D quantum spin-ice Hamiltonians. Computing local spin operators exactly, such as those that enter the RK Hamiltonian, is however a hard analytic task, but it should be possible to efficiently implement these constraints numerically, as it has been done successfully in previous studies of the more common Gutzwiller projected states of Abrikosov fermions (see, e.g., [82–85]). This is an interesting direction that we hope future studies will further explore.

However, while explicit analytic calculations of ground-state energies for these states are challenging, it is possible to develop a precise understanding of the implementation of the global physical symmetries of the spin model in their dual Jordan-Wigner composite fermion representation, which is one of the central themes in this study. For the RK–type models such global symmetries include lattice space symmetries, time-reversal and onsite spin symmetries (e.g., unitary particle-hole conjugation of hard-core bosons). While the implementation of these symmetries is simple and standard in the physical spin-$\frac{1}{2}$ degrees of freedom, their implementations in the dual Jordan-Wigner composite fermion degrees of freedom can look fairly unusual, which is not surprising because of the nonlocal nature of the operators creating the composite fermion particles. However, because the Jordan-Wigner transformation is an explicit operator map, it is straightforward to

[12]Namely, with staggered alternating signs $+1, -1$ the Λ_A and Λ_B sublattices.

[13]Notice that interestingly the global operator associated with the staggered sum of the spin-ice charges over all the lattices in a periodic torus is identically zero. This global subgroup of the staggered gauge group acts therefore trivially within the physical Hilbert space.

determine the exact symmetry action on the Jordan-Wigner composite fermions.

Nevertheless, as a result of the additional local symmetry structure that we have imposed on the Jordan-Wigner composite fermions in spin-ice models, a kind of freedom appears on how the symmetry is implemented that bears a resemblance to the problem of implementing physical symmetries on the standard parton constructions of Abrikosov fermions. Such implementation of symmetries on Gutzwiller projected states of Abrikosov fermions leads naturally to the notions of the projective symmetry groups [48,72]. A remarkable fact about such projective symmetry-group implementations is that a given specific microscopic symmetry acting on the physical spins can be implemented in many inequivalent ways on the parton fermions, but these distinct implementations can lead to sharply physically distinct quantum disordered spin liquids of the underlying physical spins (all still obeying the same microscopic symmetries) [48,72]. We have seen that an analogous situation arises in our construction of Jordan-Wigner composite fermion states that are Gutzwiller projected to satisfy the ice rules of 2D RK–type models. Namely, gauge-inequivalent symmetry implementations on the Jordan-Wigner composite fermions can act identically on all the gauge-invariant operators within a given subspace with definite values of the ice rules, but which will lead to sharply physically distinct quantum disordered states of the Jordan-Wigner composite fermions. This freedom of symmetry implementations turns also to be a very valuable resource. For example, it is very difficult to enforce the $\pi/2$ rotational symmetry on the mean-field states, by using the fully microscopically explicit "bare" action of this symmetry on the Jordan-Wigner creation operators that include the full string ordering of the 2D lattice. However, we have seen that there are alternative projective symmetry implementations of the $\pi/2$ rotation symmetry that act as effectively local operations on the Jordan-Wigner composite fermions, and which have exactly the same action on all the spin-ice gauge-invariant operators, which lead therefore to satisfactory and much simpler implementations of this microscopic symmetry on the Gutzwiller projected states.

We have not attempted to classify all the possible spin-liquid states that can result from this *extended parton construction* of Jordan-Wigner composite fermions. From the precedents in Abrikosov fermions [48,72] it is only natural to expect that it will also have a diverse and colorful variety of possibilities, which we hope future studies can investigate. We have instead focused on constructing interesting concrete examples that satisfy the following criteria: (1) a projective symmetry implementation of all the physical global symmetries of the classic RK model for 2D quantum spin-ice applicable to the six-vertex and quantum dimer subspaces, (2) that the implementation allows for nonzero value of the nearest-neighbor hopping of fermions. The first demand guarantees that the composite fermion liquid is a fully symmetric spin liquid that does not break any of the symmetries of the model. Notice in particular that we have enforced time reversal for both six-vertex and quantum dimers and also the particle-hole symmetry of the six-vertex model, which often are neglected in *ad hoc* mean-field constructions of composite fermions based on flux smearing at fractional filling of the lattice. The second requirement is a desirable requirement to make the states potentially energetically competitive trial ground states of microscopic RK–type Hamiltonians with short-range couplings since in these models a big portion of the energy density is determined typically by optimal short-distance correlations.

We have successfully constructed two explicit examples of projective symmetry implementations of Jordan-Wigner composite fermions based on this *extended parton construction*. For the quantum six-vertex model (realized when the Jordan-Wigner composite fermions are at half-filling of the lattice) these states feature two massless Dirac cones centered at $(\pi, 0)$ and $(0, \pi)$, and thus the state is a putative composite fermion Dirac spin liquid. For the quantum dimer model (realized when the Jordan-Wigner composite fermions are at quarter-filling of the lattice) these states display a Fermi surface of the size of half of the Brillouin zone, and thus the state is a putative composite Fermi-liquid state. This Fermi surface is perfectly nested when the mean-field state only includes nearest-neighbor composite fermion hopping, but further-neighbor hoppings remove the perfect nesting and could stabilize this state. Because of this strong tendency to being unstable from nesting, this composite Fermi liquid could be a useful parent state to understand the descending ordered states and their competitions in the RK model, which is another interesting direction for future studies.

We have also developed a simplified description of the gauge field fluctuations around these mean-field states, aimed at qualitatively capturing the nature of the low-energy field theories emerging in the infrared limit (i.e., low energy and long wavelengths compared to lattice scales) and particularly the nature of the potentially deconfined low-energy gauge structure. As it is well known from Abrikosov fermions, the low-energy gauge structure can be different from the UV parton gauge. We have seen that the low-energy gauge structure differs from the UV spin-ice gauge structure, although they have some precise relations. To determine this structure, we have performed an analysis in two stages.

In the first stage, for a given bare mean-field Hamiltonian (not Gutzwiller projected) which has some specific nonzero hopping elements Jordan-Wigner composite fermions in the lattice, we consider trial Hamiltonians in which only the phases of these nonzero hopping elements are allowed to fluctuate. The spirit behind this is that the amplitude fluctuations should be generically gapped but the fluctuations of the phases could possibly be soft. We then promote these fluctuating phases to become local quantum bosonic degrees of freedom residing on the links connecting the spin sites (or equivalently the links associated with Jordan-Wigner composite fermion hopping). Such fluctuating phases of hopping can be viewed as emergent vector potentials and their canonically conjugate momentum as emergent electric fields. We then generalize the action of UV gauge symmetry group, which is generated by the local operators determining the spin-ice rule constraints, to act not only on the Jordan-Wigner composite fermions, but also on these bosonic phases and vector potential degrees of freedom, by demanding that the combination of the fermion bilinear operators and exponential of the vector potential degrees of freedom associated with hoppings are invariant under the UV spin-ice gauge group and, therefore, in a sense, the

phase fluctuations dress the mean-field state so as to become locally gauge invariant and thus become a more satisfactory approximation to the fully Gutzwiller projected trial state. With these gauge transformation rules, we then write a simple lattice model for the leading bilinear order Hamiltonian in powers of gauge fields, namely, the analog of the usual Maxwell action, that is consistent with the microscopic global symmetries of the model, while neglecting their compactification [whose potential impact is to be reconsidered at the end of the analysis (see following)]. For the RK–type models of 2D spin ice this pure gauge field Hamiltonian features four-vector potentials per Bravais unit cell, but there is a local constraint analogous to the zero divergence of electric field, leading to three truly dynamical gauge fields with associated energy bands. Out of these three, two are fully gapped over the entire Brillouin zone (and thus unimportant at low energies) while one band features two linearly dispersing U(1) photonlike modes that are gapless at (0,0) and (π, π) momentum in the Brillouin zone. This suggests a U(1) × U(1) low-energy gauge structure when compactification is neglected (but seefollowing for discussion of its important impacts).

In the second stage we determine the minimal coupling of the Jordan-Wigner composite fermion to this U(1) × U(1) low-energy gauge structure. To do so, we Taylor expand the exponential coupling of the Jordan-Wigner composite fermions to the gauge fluctuation fields to linear order in vector potentials, giving us the lattice analog of the minimal jA coupling. We have found that the fermions couple minimally to only one of the U(1) gauge fields associated with the massless photon at (0,0) momentum, while they have zero gauge charge under the (π, π) photon. There is a simple intuitive picture, closely related to the UV gauge structure of the spin ice, that sheds light on this seemingly peculiar low-energy structure. The creation of a composite fermion, which locally reverses one spin along z, violates the two ice rules associated to the vertices connected to such reversed spin. In the lattice gauge theory convention, the lattice of spin-ice vertices is separated into two sublattices and the Gauss law is conventionally taken as a staggered ice rule with alternating signs in the sublattices. In this convention, the spin reversal is viewed as creating a dipole pair of gauge charges but which is in total gauge neutral. Similarly, in our construction we could separate the spin-ice rules into two sublattices, and we could say that the Jordan-Wigner composite fermion is charged under a symmetric combination of the ice rules of the two sublattices and neutral dipole-pair object under a staggered antisymmetric combination. These two sublattices are related by a lattice translational symmetry, and since we enforce such symmetry, we encounter that the photon at (0,0) is associated with the sublattice-symmetric combination of these ice rules while the sublattice-staggered-antisymmetric combination is associated with the photon at (π, π). Because the creation of the Jordan-Wigner composite fermion violates the ice rules symmetrically, the particle only carries gauge charge under the symmetric photon at (0,0), but behaves as a neutral gauge dipolar object with respect to the antisymmetric photon (π, π).

We have therefore obtained a low-energy gauge structure of two massless Dirac fermions minimally coupled to a U(1) massless photon, and neutral under another U(1) massless photon. We would like now reconsider qualitatively the impact of gauge field compactification on this low-energy structure. The photon that "sees" the fermions as neutral dipoles propagates in this medium as if it was an insulating dielectric liquid. This is not very different from a how a photon would "see" a gapped insulating charged fermionic matter. Monopole fluctuations are therefore expected to be relevant and lead to Polyakov-style confiment for this U(1) sublattice antisymmetric photon at (π, π), as it is generically expected in $(2 + 1)$D for a compact U(1) gauge field when the matter that carries its gauge charge is gapped. We thus expect that compactification gaps out this (π, π) photon and that it is not relevant at low energies. However, since the fermion is already a short-distance neutral dipole object with respect to this gauge field, such gauge confinement is not expected to confine the fermions themselves. We are thus left with a low-energy structure in which we have two gapless Dirac nodes minimally coupled to a single U(1) photon, the one gapless at momentum (0,0). The ultimate details of the infrared behavior and strict stability of such $N = 2$ QED in $2 + 1$ dimensions is still an open problem [60–62], but provided such theory flows to a stable fixed point, our state would be therefore an analog of a Dirac spin liquid of composite fermions (but with a pseudoscalar symmetry implementation [75], see following). We hope that future studies can investigate in more detail this qualitative argument on the nature of the low-energy effective field theory.

Finally, we would like comment on the connections between our construction and the pseudoscalar spin liquids introduced in Ref. [75]. The Jordan-Wigner composite fermion can be naturally understood to behave as a pseudoscalar spinon under symmetries that reverse the direction of the z spin because this is equivalent to the Jordan-Wigner composite fermion occupation on a site. Therefore, the ordinary spin time-reversal symmetry that squares to -1 and space operations such as mirrors that reverse the z spin would act as particle-hole conjugations on the Jordan-Wigner composite fermion. The emergent magnetic and electric fields would also have opposite transformation laws to those of ordinary QED, for example, being even and odd, respectively, under such spin time-reversal operation. Therefore, we see that the U(1) gauge structure is pseudoscalar in the sense described in Ref. [75]. This can also be understood in very direct microscopic terms. For example, magnetic field operator associated with the simplest gauge-invariant loop of quantum spin ice is the four-spin operator composed of alternating spin raising and lowering operators in a plaquette [properly symmetrized so as to make the analog of $\sin(B)$ combination of lattice gauge theory]. It is easy to see that this operator is even under the previously mentioned mirrors and time-reversal operations. This magnetic field operator can be viewed as a measure of a local correlation for the XY projection of the spins to spiral around a small closed loop, and thus is physically very different from those of more traditional U(1) spin liquids, such as the triple product correlator associated spin chirality around triangles [86–88] which transforms in the similar way as the usual magnetic field experienced by electrons under point-group and time-reversal symmetries. Therefore, our current construction of Jordan-Wigner composite fermion provides a different and

perhaps more intuitive way to describe certain pseudoscalar spin liquids which illuminates on the kind of correlations associated the appearance of their magnetic fields, namely, a kind of tendency towards short-distance spin spiraling on loops. Understanding more precisely these connections is another interesting avenue of future research, which could help understand how to realize such spin liquids in real materials, such as α-$RuCl_3$, where the oscillations of thermal conductivity seen in experiments [89–92] are consistent with the expected quantum oscillations of pseudoscalar U(1) spin liquid [75].

ACKNOWLEDGMENTS

We are thankful to H.-H. Tu, D. Banerjee, K. Penc, N. Shannon, X.-F. Zhang, and R. Moessner for stimulating discussions. I.S. is especially thankful to Z. Wang for discussions and performing unpublished analysis in a preliminary stage of the project. L.G. would like to thank D. Morgante for his help with TikZ pictures. We acknowledge support by the Deutsche Forschungsgemeinschaft (DFG) through research Grant No. 518372354.

APPENDIX A: 2π -FLUX ATTACHMENT EQUIVALENCE

We adopt the same labeling convention defined in the main text in Sec. II, namely, sites are ordered according to western typing convention. We take the lattice sites of the original square lattice to be labeled by $\mathbf{r} = (x, y)$, where x, y are integers running from $1, \ldots, N$. We would like to show here for any site $\mathbf{r}$ in the lattice the following equations hold:

(1)

$$f^\dagger(\mathbf{r}+\mathbf{e}_x+\mathbf{e}_y)\, e^{i\pi \sum_{\mathbf{r}\preceq\mathbf{r}''\prec\mathbf{r}+\mathbf{e}_x+\mathbf{e}_y} n(\mathbf{r}'')} f(\mathbf{r}) = f^\dagger(\mathbf{r}+\mathbf{e}_x+\mathbf{e}_y) \exp\left(i\int_{\mathbf{r}}^{\mathbf{r}+\mathbf{e}_x+\mathbf{e}_y} \mathbf{A}(\mathbf{x})\cdot d\mathbf{x}\right) f(\mathbf{r}).$$

(2)

$$f^\dagger(\mathbf{r}-\mathbf{e}_x+\mathbf{e}_y)\, e^{i\pi \sum_{\mathbf{r}\preceq\mathbf{r}''\prec\mathbf{r}-\mathbf{e}_x+\mathbf{e}_y} n(\mathbf{r}'')} f(\mathbf{r}) = f^\dagger(\mathbf{r}-\mathbf{e}_x+\mathbf{e}_y) \exp\left(i\int_{\mathbf{r}}^{\mathbf{r}-\mathbf{e}_x+\mathbf{e}_y} \mathbf{A}(\mathbf{x})\cdot d\mathbf{x}\right) f(\mathbf{r}).$$

(3)

$$f^\dagger(\mathbf{r})\, e^{i\pi \sum_{\mathbf{r}+\mathbf{e}_x-\mathbf{e}_y\preceq\mathbf{r}''\prec\mathbf{r}} n(\mathbf{r}'')} f(\mathbf{r}+\mathbf{e}_x-\mathbf{e}_y) = f^\dagger(\mathbf{r}) \exp\left(i\int_{\mathbf{r}+\mathbf{e}_x-\mathbf{e}_y}^{\mathbf{r}} \mathbf{A}(\mathbf{x})\cdot d\mathbf{x}\right) f(\mathbf{r}+\mathbf{e}_x-\mathbf{e}_y).$$

(4)

$$f^\dagger(\mathbf{r})\, e^{i\pi \sum_{\mathbf{r}-\mathbf{e}_x-\mathbf{e}_y\preceq\mathbf{r}''\prec\mathbf{r}} n(\mathbf{r}'')} f(\mathbf{r}-\mathbf{e}_x-\mathbf{e}_y) = f^\dagger(\mathbf{r}) \exp\left(i\int_{\mathbf{r}-\mathbf{e}_x-\mathbf{e}_y}^{\mathbf{r}} \mathbf{A}(\mathbf{x})\cdot d\mathbf{x}\right) f(\mathbf{r}-\mathbf{e}_x-\mathbf{e}_y).$$

To demonstrate the above, it is sufficient to demonstrate only 1 and 2 because the other two cases follow from the previous ones by globally translating the initial and final sites of the hopping. Following, we show the arguments then for 1 and 2:

(1) The sites involved in the 2D Jordan-Wigner transformation for the hopping term $b^\dagger(\mathbf{r}+\mathbf{e}_x+\mathbf{e}_y)b_{\mathbf{r}}$ are, by (2),

$$(r_x, r_y) \to (r_x+1, r_y) \to \cdots \to (N, r_y) \to (1, r_y+1) \to \cdots \to (r_x, r_y+1).$$

Thus, the phase gained is

$$\exp[i\pi[n(r_x, r_y) + n(r_x+1, r_y) + \cdots + n(N, r_y) + n(1, r_y+1) + \cdots + n(r_x-1, r_y+1) + n(r_x, r_y+1)]].$$

Let us focus now on the gauge potential. We are free to choose the path $\mathbf{r} \to \mathbf{r}+\mathbf{e}_y \to \mathbf{r}+\mathbf{e}_y+\mathbf{e}_x$. Since

$$\exp\left(i\int_{\mathbf{r}}^{\mathbf{r}+\mathbf{e}_x+\mathbf{e}_y} \mathbf{A}(\mathbf{x})\cdot d\mathbf{x}\right) = \exp\left(i\int_{\mathbf{r}}^{\mathbf{r}+\mathbf{e}_y} \mathbf{A}(\mathbf{x})\cdot d\mathbf{x}\right) \exp\left(i\int_{\mathbf{r}+\mathbf{e}_y}^{\mathbf{r}+\mathbf{e}_y+\mathbf{e}_x} \mathbf{A}(\mathbf{x})\cdot d\mathbf{x}\right)$$

we have, using the previously established equations, that

$$\exp\left(i\int_{\mathbf{r}}^{\mathbf{r}+\mathbf{e}_x+\mathbf{e}_y} \mathbf{A}(\mathbf{x})\cdot d\mathbf{x}\right) = (e^{i\pi \sum_{\mathbf{r}\preceq\mathbf{r}''\prec\mathbf{r}+\mathbf{e}_y-\mathbf{e}_x} n(\mathbf{r})''})(e^{i\pi n(\mathbf{r}+\mathbf{e}_y)}) = \exp\left[i\pi \sum_{\mathbf{r}\preceq\mathbf{r}''\prec\mathbf{r}+\mathbf{e}_y} n(\mathbf{r}'')\right].$$

(2) The sites involved in the 2D Jordan-Wigner transformation for the hopping term $b^\dagger(\mathbf{r}-\mathbf{e}_x+\mathbf{e}_y)b(\mathbf{r})$ are, by (2),

$$(r_x, r_y) \to (r_x+1, r_y) \to \cdots \to (N, r_y) \to (1, r_y+1) \to (r_x-2, r_y+1).$$

Thus, the phase gained is

$$\exp[i\pi[n(r_x, r_y) + n(r_x+1, r_y) + \cdots + n(N, r_y) + n(1, r_y+1) + \cdots + n(r_x-2, r_y+1)]].$$

Let us focus now on the gauge potential. We are free to choose the path $\mathbf{r} \to \mathbf{r}+\mathbf{e}_y \to \mathbf{r}+\mathbf{e}_y-\mathbf{e}_x$. The result is not affected by the orientation in which the integral is taken, as a simple change in orientation of the contour would just give the complex

conjugate of the phase gained on any link and each of them can only be ± 1. Thus,

$$\exp\left(i\int_{\mathbf{r}}^{\mathbf{r}-\mathbf{e}_x+\mathbf{e}_y}\mathbf{A}(\mathbf{x})\cdot d\mathbf{x}\right)=\exp\left(i\int_{\mathbf{r}}^{\mathbf{r}+\mathbf{e}_y}\mathbf{A}(\mathbf{x})\cdot d\mathbf{x}\right)\exp\left(i\int_{\mathbf{r}+\mathbf{e}_y}^{\mathbf{r}+\mathbf{e}_y-\mathbf{e}_x}\mathbf{A}(\mathbf{x})\cdot d\mathbf{x}\right).$$

Using the previously established equations, we get

$$\begin{aligned}\exp\left(i\int_{\mathbf{r}}^{\mathbf{r}-\mathbf{e}_x+\mathbf{e}_y}\mathbf{A}(\mathbf{x})\cdot d\mathbf{x}\right)&=(e^{i\pi\sum_{\mathbf{r}\preceq\mathbf{r}''\prec\mathbf{r}+\mathbf{e}_y}n(\mathbf{r}'')})(e^{i\pi n(\mathbf{r}-\mathbf{e}_x+\mathbf{e}_y)})\\&=\exp[i\pi[n(r_x,r_y)+\cdots+n(r_x-2,r_y+1)+n(r_x-1,r_y+1)+n(r_x-1,r_y+1)]]\\&=\exp[i\pi[n(r_x,r_y)+\cdots+n(r_x-2,r_y+1)+\cancel{2n(r_x-1,r_y+1)}]]\\&=\exp\left[i\pi\sum_{\mathbf{r}\preceq\mathbf{r}''\prec\mathbf{r}+\mathbf{e}_y-\mathbf{e}_x}n(\mathbf{r}'')\right].\end{aligned}$$

We are now ready to prove Eq. (4) of the main text, which states that for any sites $\mathbf{r}$, $\mathbf{r}'$ in the lattice, it holds that

$$f^\dagger(\mathbf{r}')e^{i\pi\sum_{\mathbf{r}\preceq\mathbf{r}''\prec\mathbf{r}'}n(\mathbf{r}'')}f(\mathbf{r})=f^\dagger(\mathbf{r}')\exp\left[i\int_{\mathbf{r}}^{\mathbf{r}'}\mathbf{A}(\mathbf{x})\cdot d\mathbf{x}\right]f(\mathbf{r}).$$

Proof. The sites involved in the 2D Jordan-Wigner transformation for the hopping term $b^\dagger(\mathbf{r}')b(\mathbf{r})$ are (without loss of generality we will assume $r'_y > r_y+1$), by (2),

$$\begin{aligned}&(r_x,r_y)\to(r_x+1,r_y)\to\cdots\to(N,r_y)\to(1,r_y+1)\to\cdots\to(N,r_y+1)\to\cdots\\&\quad\to(N,r'_y-1)\to(1,r'_y)\to\cdots\to(r'_x-1,r'_y).\end{aligned}$$

Thus, the phase gained is

$$\exp\left[i\pi\sum_{\mathbf{r}\preceq\mathbf{r}''\prec\mathbf{r}'}n(\mathbf{r}'')\right].$$

Let usfocus now on the gauge potential. We are free to choose the L-shaped path that connects $\mathbf{r}$ to $\mathbf{r}'$ for $r'_x \geqslant r_x$ (Fig. 30):

Since the phases factorizes, we have

$$\exp\left(i\int_{(r_x,r_y)}^{(r'_x,r'_y)}\mathbf{A}(\mathbf{x})\cdot d\mathbf{x}\right)$$

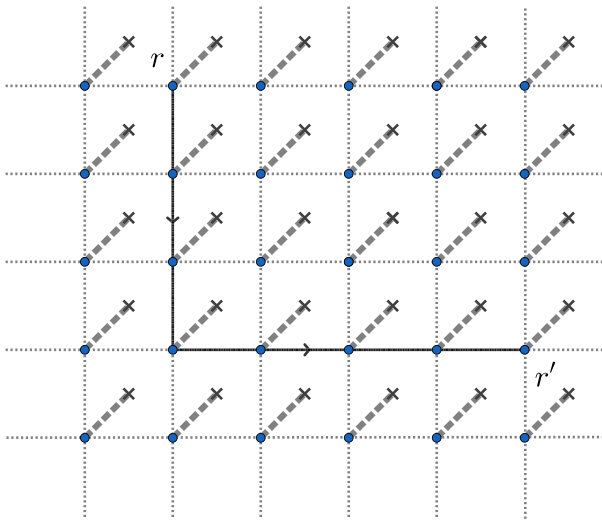

FIG. 30. L-shaped path that connects $\mathbf{r}$ to $\mathbf{r}'$ for $r_x \leqslant r'_x$.

$$\begin{aligned}&=\exp\left(i\int_{(r_x,r_y)}^{(r_x,r'_y)}\mathbf{A}(\mathbf{x})\cdot d\mathbf{x}\right)\\&\quad\times\exp\left(i\int_{(r_x,r'_y)}^{(r'_x,r'_y)}\mathbf{A}(\mathbf{x})\cdot d\mathbf{x}\right)\\&=\left(e^{i\pi\sum_{\mathbf{r}\preceq\mathbf{r}''\prec(x,y')}n(\mathbf{r}'')}\right)\left(e^{i\pi\sum_{x\leqslant x''<x'}n(r''_x,r'_y)}\right)\\&=\exp\left[i\pi\sum_{\mathbf{r}\preceq\mathbf{r}''\prec\mathbf{r}'}n(\mathbf{r}'')\right].\end{aligned}$$

For $r'_x < r_x$, the phase gained is

$$\exp\left[i\pi\sum_{\mathbf{r}\preceq\mathbf{r}''\prec\mathbf{r}'}n(\mathbf{r}'')\right].$$

We can argue similarly, choosing the path, Fig. 31, and we find

$$\begin{aligned}&\exp\left(i\int_{(r_x,r_y)}^{(r'_x,r'_y)}\mathbf{A}(\mathbf{x})\cdot d\mathbf{x}\right)\\&=\exp\left(i\int_{(r_x,r_y)}^{(r_x,r'_y)}\mathbf{A}(\mathbf{x})\cdot d\mathbf{x}\right)\exp\left(i\int_{(r_x,r'_y)}^{(r'_x,r'_y)}\mathbf{A}(\mathbf{x})\cdot d\mathbf{x}\right)\\&=\left(e^{i\pi\sum_{\mathbf{r}\preceq\mathbf{r}''\prec(x,y')}n(\mathbf{r}'')}\right)\left(e^{i\pi\sum_{x'\leqslant x''<x}n(r''_x,r'_y)}\right)\\&=\exp\left[i\pi\sum_{\mathbf{r}\preceq\mathbf{r}''\prec\mathbf{r}'}n(\mathbf{r}'')\right].\end{aligned}$$

■

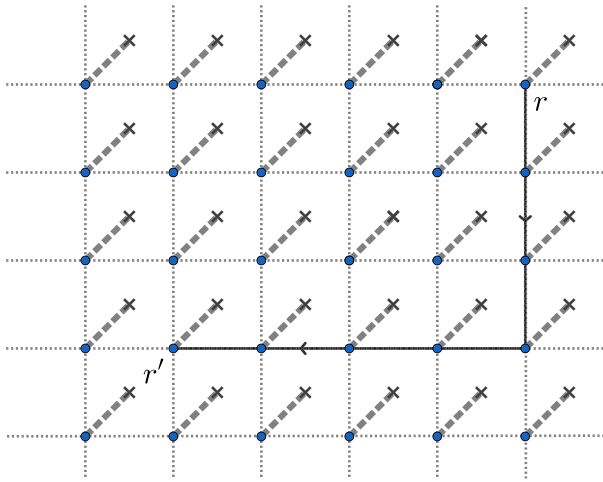

FIG. 31. L-shaped path that connects $\mathbf{r}$ to $\mathbf{r}'$ for $r'_x < r_x$.

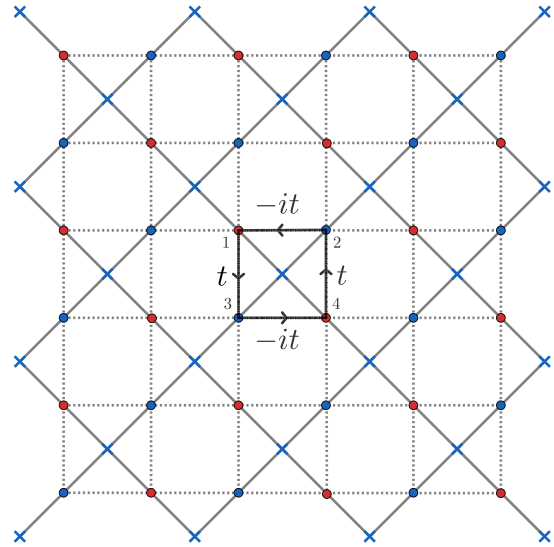

FIG. 32. The arrow indicates in which direction the hopping happens, namely, in the site where the arrow points a fermion just created.

APPENDIX B: PROJECTIVE SYMMETRY IMPLEMENTATIONS

1. $\frac{\pi}{2}$ rotation enforcement

In Sec. III C 2, we worked out the form of fermion transformation under $U_{\frac{1}{4}} R_{\frac{\pi}{2}}$ (...), then for the particular case of the mean-field nearest-neighbor hoppings:

$$t_{31} f_3^\dagger f_1 + t_{12} f_1^\dagger f_2 + t_{24} f_2^\dagger f_4 + t_{43} f_4^\dagger f_3 \xrightarrow{\mathrm{adj}_{U_{\frac{1}{4}} R_{\frac{\pi}{2}}}(\cdot)} -it_{31} f_4^\dagger f_3 + it_{12} f_3^\dagger f_1 - it_{24} f_1^\dagger f_2 + it_{43} f_2^\dagger f_4$$

which gives the following system of constraints:

$$\begin{aligned} it_{31} &= -t_{43}, \\ it_{12} &= t_{31}, \\ it_{24} &= -t_{12}, \\ it_{43} &= t_{24}. \end{aligned}$$

If we call $t_{31} \doteq t$, the solution of the system is given by the hoppings depicted in Fig. 32. Therefore, we see that the $\pi/2$ rotation is highly constraining as its combination with translations implemented in a nonprojective way would fix all the hoppings up to a global complex phase.

2. Time-reversal enforcement

The bare time-reversal operation, denoted by Θ, is defined in Table IV and Eq. (34). If we then try to enforce invariance under such bare time-reversal operation on the hopping terms, we get the following set of constraints:

$$\begin{aligned} t &= t^*, \\ -it &= it^* \end{aligned}$$

which can be solved only by $t = 0$. We are then led to conclude that the bare representation of time-reversal symmetry makes all the nearest-neighbor hopping terms vanish.

Inspired by projective symmetry-group construction, we can try to represent differently the time-reversal symmetry, dressing it with a unitary map in the gauge group. Let us consider, for example, the following gauge transformations:

$$\begin{aligned} G_x b^\dagger(\mathbf{r}) G_x^\dagger &= (-1)^{r_x} b^\dagger(\mathbf{r}), \\ G_y b^\dagger(\mathbf{r}) G_y^\dagger &= (-1)^{r_y} b^\dagger(\mathbf{r}). \end{aligned}$$

It is clear that on boson plaquette operators, $\mathrm{adj}_{G_i}(L_{\mathbf{R}}) = L_{\mathbf{R}}$ $(i = x, y)$ because it is built by two terms with even i coordinate and two terms with odd i coordinate. Moreover, since

$$\begin{aligned} G_i \sigma^z(\mathbf{r}) G_i^\dagger &= G_i [b(\mathbf{r}), b^\dagger(\mathbf{r})] G_i^\dagger \\ &= [G_i b(\mathbf{r}) G_i^\dagger, G_i b^\dagger(\mathbf{r}) G_i^\dagger] \\ &= [b(\mathbf{r}), b^\dagger(\mathbf{r})] = \sigma^z(\mathbf{r}) \end{aligned}$$

the invariance under the action of G_i applies to any gauge-invariant operator, thus, it is a UV gauge transformation. The two gauge transformations have the following action on fermion operators:

$$\begin{aligned} G_x f^\dagger(\mathbf{r}) G_x^\dagger &= (-1)^{r_x} f^\dagger(\mathbf{r}), \\ G_y f^\dagger(\mathbf{r}) G_y^\dagger &= (-1)^{r_y} f^\dagger(\mathbf{r}). \end{aligned}$$

Let us see now the dressed time-reversal transformations $\Theta_i \doteq G_i \Theta$ constrain the hoppings. For the horizontal hoppings, the additional actions of G_x and G_y, respectively, does not change the value (as both sites have the x coordinate) and make them acquire a minus sign (as the sites have a different parity y coordinate). For the vertical hoppings, conversely, the additional actions of G_x and G_y, respectively, make them acquire a minus sign (as the sites have a different parity x coordinate) and does not change the value (as both sites have the y coordinate). In the end, the constraints imposed by Θ_x and Θ_y are, respectively,

$$\begin{aligned} t &= t^*, \\ -it &= -it^*, \end{aligned}$$

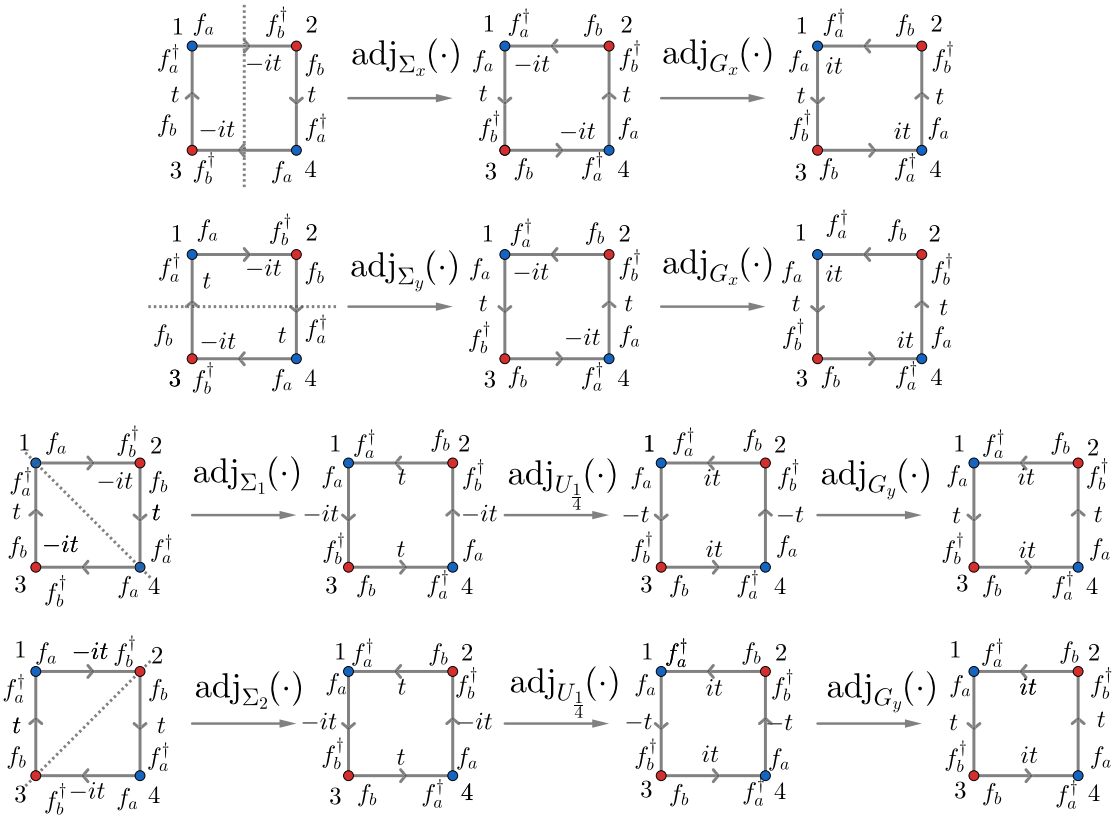

FIG. 33. Reflection action on nearest-neighbor hoppings for Θ_x extended projective symmetry group.

i.e., $t \in \mathbb{R}$, and

$$t = -t^*,$$
$$-it = it^*,$$

i.e., $t \in i\,\mathbb{R}$. And therefore we conclude that time-reversal symmetry Θ can be implemented on the JW composite fermions by two different extended projective symmetry groups Θ_x and Θ_y.

3. Reflection symmetry enforcement

We enforce now reflection symmetries on Θ_x and Θ_y extended projective symmetry groups, with the condition that all nearest-neighbor hopping (already fixed by in the previous two subsections) are nonvanishing. For the Θ_x extended projective symmetry group ($t \in \mathbb{R}$), reflection symmetries are realized in the following way on the JW composite fermions (see Tables II, IV, and V and Fig. 11 for conventions):

$$\begin{aligned} S_x &\leftrightarrow G_x \Sigma_x, \\ S_y &\leftrightarrow G_x \Sigma_y, \\ S_1 &\leftrightarrow G_y U_{\frac{1}{4}} \Sigma_1, \\ S_2 &\leftrightarrow G_y U_{\frac{1}{4}} \Sigma_2. \end{aligned} \tag{B1}$$

Figure 33 shows why the above action allows for the nearest-neighbor hopping of JW composite fermion for the Θ_x extended projective symmetry group.

On the other hand, for the Θ_y extended projective symmetry group ($t \in i\mathbb{R}$), reflection symmetries are realized in the following way:

$$\begin{aligned} S_x &\leftrightarrow G_y \Sigma_x, \\ S_y &\leftrightarrow G_y \Sigma_y, \\ S_1 &\leftrightarrow G_x U_{\frac{1}{4}} \Sigma_1, \\ S_2 &\leftrightarrow G_x U_{\frac{1}{4}} \Sigma_2. \end{aligned} \tag{B2}$$

Figure 34 shows why the above action allows for the nearest-neighbor hopping of JW composite fermion for the Θ_y extended projective symmetry group.

4. Particle-hole enforcement

Similarly to reflection symmetries, particle-hole symmetry is enforced on Θ_x and Θ_y extended projective symmetry groups, with the condition that all nearest-neighbor hoppings are nonvanishing. For the Θ_x and Θ_y extended projective symmetry group ($t \in \mathbb{R}$), particle-hole symmetry is, respectively, realized in the following way on the JW composite fermions (see Tables II, IV, and V and Fig. 11 for conventions):

$$\begin{aligned} X &\leftrightarrow G_x \Xi, \\ Xl &\leftrightarrow G_y \Xi. \end{aligned}$$

Figure 35 shows why the above action allows for the nearest-neighbor hopping of JW composite fermion for the Θ_x and Θ_y extended projective symmetry group.

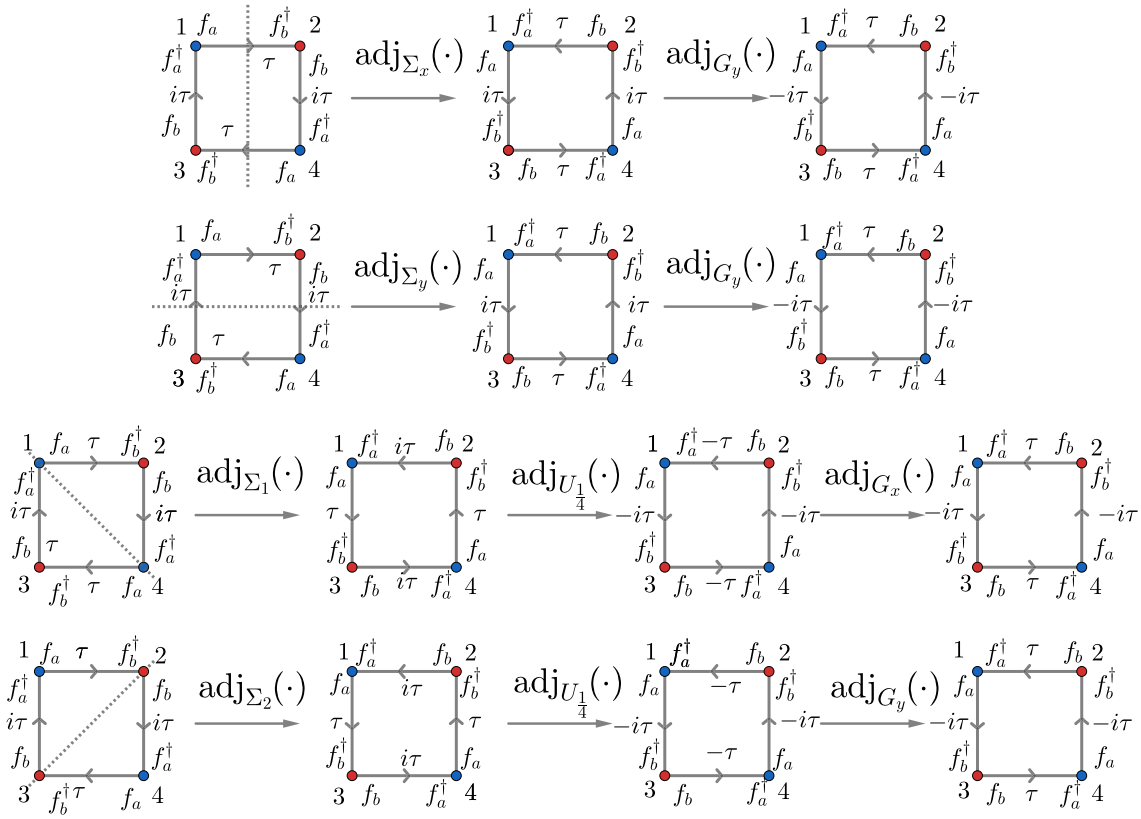

FIG. 34. Reflection action on nearest-neighbor hoppings for Θ_y extended projective symmetry group ($t = i\tau$ with $\tau \in \mathbb{R}$).

APPENDIX C: LOW-ENERGY EFFECTIVE THEORY DERIVATION

After linearizing in vector potentials, the Fourier transform of Eq. (58) is given by

$$H(t,A) = \sum_{\mathbf{q},\mathbf{p}\in \mathrm{BZ}} it^*([\delta_{\mathbf{p}\mathbf{0}} + iA_3(\mathbf{p})] + [\delta_{\mathbf{p}\mathbf{0}} - iA_1(\mathbf{p})e^{-i\mathbf{p}\cdot\mathbf{R}_2}]e^{-i\mathbf{q}\cdot(\mathbf{R}_2-\mathbf{R}_1)})f_a^\dagger(\mathbf{q})f_b(\mathbf{q}+\mathbf{p})$$
$$+ t([\delta_{\mathbf{p}\mathbf{0}} - iA_4(\mathbf{p})]e^{i\mathbf{q}\cdot\mathbf{R}_1} + [\delta_{\mathbf{p}\mathbf{0}} + iA_2(\mathbf{p})e^{-i\mathbf{p}\cdot\mathbf{R}_2}]e^{-i\mathbf{q}_2})f_a^\dagger(\mathbf{q})f_b(\mathbf{q}+\mathbf{p}). \tag{C1}$$

Following discussion in Sec. IV C, we define the following set of operators:

$$\Psi(\mathbf{q}) \doteq \begin{pmatrix} f_a[\mathbf{p}+(\pi,0)] \\ f_b[\mathbf{p}+(\pi,0)] \\ f_a[\mathbf{p}+(0,\pi)] \\ f_b[\mathbf{p}+(0,\pi)] \end{pmatrix},$$
$$A_j^0(\mathbf{p}) \doteq A_j(\mathbf{p}), \quad j \in \{1,2,3,4\}$$
$$A_j^\pi(\mathbf{p}) \doteq A_j[\mathbf{p}+(\pi,\pi)], \quad j \in \{1,2,3,4\}$$

where $\mathbf{p}$ has to be understood as "small" momentum with respect to Brillouin zone size, so that we can expand the Hamiltonian (75) to the first order in $\boldsymbol{R}_i \cdot \boldsymbol{p}$.

a. $\mathbf{q} = (0,0)$ *scattering processes analysis*

In the limit of $\mathbf{q}\cdot\mathbf{R}_i \ll 1$ and to first order in crystal momenta, the Hamiltonian describing $\mathbf{q} = (0,0)$ scattering processes is

$$H(t,A^0)|_{(0,0)} \simeq \sqrt{2}|\mathbf{R}_1| \sum_{\mathbf{q},\mathbf{p}\in\mathrm{BZ}} t^*\big[\mathbf{q}_x\delta_{\mathbf{p}\mathbf{0}} - A_x^0(\mathbf{p})\big](f_a^\dagger[(\pi,0)+\mathbf{q}]f_b[(\pi,0)+\mathbf{q}+\mathbf{p}] + f_a^\dagger[(0,\pi)+\mathbf{q}]f_b[(0,\pi)+\mathbf{q}+\mathbf{p}])$$
$$+ it\big[\mathbf{q}_y\delta_{\mathbf{p}\mathbf{0}} - A_y^0(\mathbf{p})\big](f_a^\dagger[(0,\pi)+\mathbf{q}]f_b[(0,\pi)+\mathbf{q}+\mathbf{p}] - f_a^\dagger[(\pi,0)+\mathbf{q})]f_b[(\pi,0)+\mathbf{q}+\mathbf{p}]) + \mathrm{H.c.},$$

where

$$A_x^0(\mathbf{p}) \doteq \frac{A_1^0(\mathbf{p}) + A_3^0(\mathbf{p})}{\sqrt{2}|\mathbf{R}_1|}, \quad A_y^0(\mathbf{p}) \doteq \frac{A_2^0(\mathbf{p}) + A_4^0(\mathbf{p})}{\sqrt{2}|\mathbf{R}_1|}.$$

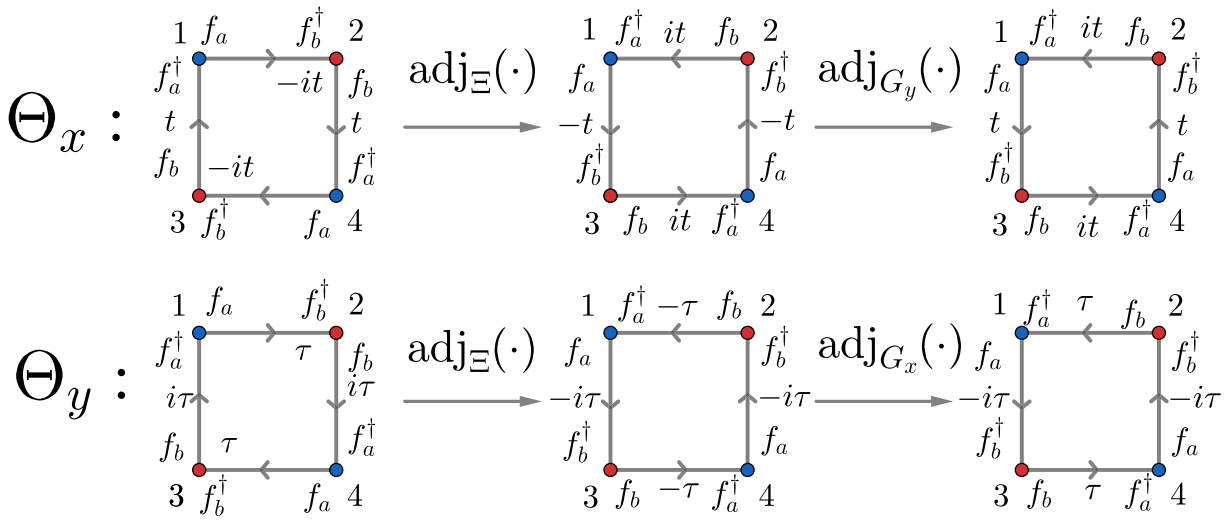

FIG. 35. Particle-hole action on nearest-neighbor hoppings for Θ_x ($t \in \mathbb{R}$) and Θ_y extended projective symmetry group ($\tau \in \mathbb{R}$).

Thus,

$$H(t, A^0)|_{(0,0)} = \sum_{\mathbf{q},\mathbf{p}\in \mathrm{BZ}} v \begin{cases} \Psi^\dagger(\boldsymbol{q})\big[\big(\mathbf{q}_x\delta_{\mathbf{p0}} - A^0_x(\mathbf{p})\big)\mathbb{1}\otimes\tau^x + \big(\mathbf{q}_y\delta_{\mathbf{p0}} - A^0_y(\mathbf{p})\big)\rho^z\otimes\tau^y\big]\Psi(\boldsymbol{q}+\boldsymbol{p}), & t\in\mathbb{R} \\ \Psi^\dagger(\boldsymbol{q})\big[\big(\mathbf{q}_x\delta_{\mathbf{p0}} - A^0_x(\mathbf{p})\big)\mathbb{1}\otimes\tau^y + \big(\mathbf{q}_y\delta_{\mathbf{p0}} - A^0_y(\mathbf{p})\big)\rho^z\otimes\tau^x\big]\Psi(\boldsymbol{q}+\boldsymbol{p}), & t\in i\mathbb{R} \end{cases}$$

where $v \doteq \sqrt{2}|t||\mathbf{R}_1|$ and the sets of τ^i and ρ^j Pauli matrices are understood to act, respectively, on $\{a, b\}$ sublattice spaces and on $\{(\pi, 0), (0, \pi)\}$ valley space.

b. $\mathbf{q} = (\pi, \pi)$ momentum scattering processes

To first order in crystal momenta, the Hamiltonian describing $\mathbf{q} = (\pi, \pi)$ scattering processes is

$$\begin{aligned} H(t, A^\pi)|_{(\pi,\pi)} \simeq \sqrt{2}|\mathbf{R}_1| \sum_{\mathbf{q},\mathbf{p}\in\mathrm{BZ}} &\big(-t^* B^\pi_x(\mathbf{p}) + itB^\pi_y(\mathbf{p})\big) f^\dagger_a[(\pi,0)+\mathbf{q}] f_b[(0,\pi)+\mathbf{q}+\mathbf{p}] \\ &- \big(t^* B^\pi_x(\mathbf{p}) + itB^\pi_y(\mathbf{p})\big) f^\dagger_a[(0,\pi)+\mathbf{q}] f_b[(\pi,0)+\mathbf{q}+\mathbf{p}] + \mathrm{H.c.}, \end{aligned}$$

where

$$B^\pi_x(\mathbf{x}) = \frac{A^\pi_3(\mathbf{x}) - A^\pi_1(\mathbf{x})}{\sqrt{2}|\mathbf{R}_1|}, \quad B^\pi_y(\mathbf{x}) = \frac{A^\pi_4(\mathbf{x}) - A^\pi_2(\mathbf{x})}{\sqrt{2}|\mathbf{R}_1|}. \tag{C2}$$

In the limit of $\mathbf{q}\cdot\mathbf{R}_i \ll 1$, and following a similar procedure as before we can write the Hamiltonian above in a matrix form

$$H(t, A^\pi)|_{(\pi,\pi)} = -v \sum_{\mathbf{q},\mathbf{p}\in\mathrm{BZ}} \begin{cases} \Psi^\dagger(\boldsymbol{q})\rho^x \otimes \big[B^\pi_x(\mathbf{p})\tau^x + B^\pi_y(\mathbf{p})\tau^y\big]\Psi(\boldsymbol{q}+\boldsymbol{p}), & t\in\mathbb{R} \\ \Psi^\dagger(\boldsymbol{q})\rho^y \otimes \big[B^\pi_x(\mathbf{p})\tau^x - B^\pi_y(\mathbf{p})\tau^y\big]\Psi(\boldsymbol{q}+\boldsymbol{p}), & t\in i\mathbb{R}. \end{cases}$$

[1] E. Fradkin, Jordan-Wigner transformation for quantum-spin systems in two dimensions and fractional statistics, Phys. Rev. Lett. **63**, 322 (1989).

[2] G. W. Semenoff, Canonical quantum field theory with exotic statistics, Phys. Rev. Lett. **61**, 517 (1988).

[3] D. Eliezer and G. W. Semenoff, Intersection forms and the geometry of lattice Chern-Simons theory, Phys. Lett. B **286**, 118 (1992).

[4] M. Azzouz, Interchain-coupling effect on the one-dimensional spin-$\frac{1}{2}$ antiferromagnetic Heisenberg model, Phys. Rev. B **48**, 6136 (1993).

[5] K. Sun, K. Kumar, and E. Fradkin, Discretized Abelian Chern-Simons gauge theory on arbitrary graphs, Phys. Rev. B **92**, 115148 (2015).

[6] O. Derzhko, Jordan-Wigner fermionization for spin-$\frac{1}{2}$ systems in two dimensions: A brief review, J. Phys. Studies **5**, 49 (2001).

[7] N. Read, Lowest-Landau-level theory of the quantum Hall effect: The Fermi-liquid-like state of bosons at filling factor one, Phys. Rev. B **58**, 16262 (1998).

[8] V. Pasquier and F. Haldane, A dipole interpretation of the $\nu = 12$ state, Nucl. Phys. B **516**, 719 (1998).

[9] Z. Dong and T. Senthil, Noncommutative field theory and composite Fermi liquids in some quantum Hall systems, Phys. Rev. B **102**, 205126 (2020).

[10] Y. R. Wang, Ground state of the two-dimensional antiferromagnetic Heisenberg model studied using an extended Wigner-Jordan transformation, Phys. Rev. B **43**, 3786 (1991).

[11] Y. R. Wang, In-phase flux state of the two-dimensional antiferromagnetic Heisenberg model and the Raman spectrum of La_2CuO_4, Phys. Rev. B **43**, 13774 (1991).

[12] Y. R. Wang, Low-dimensional quantum antiferromagnetic Heisenberg model studied using Wigner-Jordan transformations, Phys. Rev. B **46**, 151 (1992).

[13] A. Lopez, A. G. Rojo, and E. Fradkin, Chern-Simons theory of the anisotropic quantum Heisenberg antiferromagnet on a square lattice, Phys. Rev. B **49**, 15139 (1994).

[14] Y. Ji, J. Qi, J.-X. Li, and C.-D. Gong, The stepped spin - Peierls phase transition in the quasi-one-dimensional spin-$\frac{1}{2}$ quantum XY-model, J. Phys.: Condens. Matter **9**, 2259 (1997).

[15] Q. Yuan, Y. Zhang, and H. Chen, Spin-Peierls transition in an anisotropic two-dimensional XY model, Phys. Rev. B **64**, 012414 (2001).

[16] K. Kumar, K. Sun, and E. Fradkin, Chern-Simons theory of magnetization plateaus of the spin-$\frac{1}{2}$ Quantum XXZ Heisenberg model on the kagome lattice, Phys. Rev. B **90**, 174409 (2014).

[17] T. A. Sedrakyan, V. M. Galitski, and A. Kamenev, Topological spin ordering via Chern-Simons superconductivity, Phys. Rev. B **95**, 094511 (2017).

[18] B. I. Halperin, P. A. Lee, and N. Read, Theory of the half-filled Landau level, Phys. Rev. B **47**, 7312 (1993).

[19] E. Fradkin, *Field Theories of Condensed Matter Physics* (Cambridge University Press, Cambridge, 2013).

[20] X.-G. Wen, *Quantum Field Theory of Many-body Systems: From the Origin of Sound to an Origin of Light and Electrons* (Oxford University Press, Oxford, 2004).

[21] J. K. Jain, *Composite Fermions* (Cambridge University Press, Cambridge, 2007).

[22] Y.-A. Chen, A. Kapustin, and D. Radičević, Exact bosonization in two spatial dimensions and a new class of lattice gauge theories, Ann. Phys. **393**, 234 (2018).

[23] O. Pozo, P. Rao, C. Chen, and I. Sodemann, Anatomy of $\mathbb{Z}_2$ fluxes in anyon Fermi liquids and Bose condensates, Phys. Rev. B **103**, 035145 (2021).

[24] C. Chen, P. Rao, and I. Sodemann, Berry phases of vison transport in $\mathbb{Z}_2$ topologically ordered states from exact Fermion-flux lattice dualities, Phys. Rev. Res. **4**, 043003 (2022).

[25] P. Rao and I. Sodemann, Theory of weak symmetry breaking of translations in $\mathbb{Z}_2$ topologically ordered states and its relation to topological superconductivity from an exact lattice $\mathbb{Z}_2$ charge-flux attachment, Phys. Rev. Res. **3**, 023120 (2021).

[26] A. Kitaev, Anyons in an exactly solved model and beyond, Ann. Phys. **321**, 2 (2006).

[27] H.-D. Chen and J. Hu, Exact mapping between classical and topological orders in two-dimensional spin systems, Phys. Rev. B **76**, 193101 (2007).

[28] H.-D. Chen and Z. Nussinov, Exact results of the Kitaev model on a hexagonal lattice: Spin states, string and brane correlators, and anyonic excitations, J. Phys. A: Math. Theor. **41**, 075001 (2008).

[29] E. Cobanera, G. Ortiz, and Z. Nussinov, Unified approach to quantum and classical dualities, Phys. Rev. Lett. **104**, 020402 (2010).

[30] E. Cobanera, G. Ortiz, and Z. Nussinov, The bond-algebraic approach to dualities, Adv. Phys. **60**, 679 (2011).

[31] Z. Nussinov, G. Ortiz, and E. Cobanera, Arbitrary dimensional Majorana dualities and architectures for topological matter, Phys. Rev. B **86**, 085415 (2012).

[32] C. Chen and I. S. Villadiego, Nature of visons in the perturbed ferromagnetic and antiferromagnetic Kitaev honeycomb models, Phys. Rev. B **107**, 045114 (2023).

[33] D. S. Rokhsar and S. A. Kivelson, Superconductivity and thequantum hard-core dimer gas, Phys. Rev. Lett. **61**, 2376 (1988).

[34] R. Moessner, O. Tchernyshyov, and S. L. Sondhi, Planar Pyrochlore, Quantum Ice and Sliding Ice, J. Stat. Phys. **116**, 755 (2004).

[35] Y. Wan and O. Tchernyshyov, Quantum strings in quantum spin Ice, Phys. Rev. Lett. **108**, 247210 (2012).

[36] L.-P. Henry and T. Roscilde, Order-by-disorder and quantum coulomb phase in quantum square Ice, Phys. Rev. Lett. **113**, 027204 (2014).

[37] J. Herzog-Arbeitman, S. Mantilla, and I. Sodemann, Solving the Quantum Dimer and Six-Vertex Models one electric field line at a time, Phys. Rev. B **99**, 245108 (2019).

[38] N. Shannon, G. Misguich, and K. Penc, Cyclic exchange, isolated states, and spinon deconfinement in an XXZ Heisenberg model on the checkerboard lattice, Phys. Rev. B **69**, 220403(R) (2004).

[39] R. Moessner, S. L. Sondhi, and E. Fradkin, Short-ranged resonating valence bond physics, quantum dimer models, and Ising gauge theories, Phys. Rev. B **65**, 024504 (2001).

[40] D. Banerjee, F.-J. Jiang, P. Widmer, and U.-J. Wiese, The (2+1)-d $U(1)$ quantum link model masquerading as deconfined criticality, J. Stat. Mech. (2013) P12010.

[41] F. Tschirsich, S. Montangero, and M. Dalmonte, Phase diagram and conformal string excitations of square ice using gauge invariant matrix product states, SciPost Phys. **6**, 028 (2019).

[42] X. Ran, Z. Yan, Y.-C. Wang, J. Rong, Y. Qi, and Z. Y. Meng, Fully packed quantum loop model on the square lattice: Phase diagram and application for Rydberg atoms, Phys. Rev. B **107**, 125134 (2023).

[43] P. Stornati, P. Krah, K. Jansen, and D. Banerjee, Crystalline phases at finite winding densities in a quantum link ladder, Phys. Rev. D **107**, L031504 (2023).

[44] D. Banerjee and A. Sen, Quantum scars from zero modes in an abelian lattice gauge theory on ladders, Phys. Rev. Lett. **126**, 220601 (2021).

[45] S. Biswas, D. Banerjee, and A. Sen, Scars from protected zero modes and beyond in $U(1)$ quantum link and quantum dimer models, SciPost Phys. **12**, 148 (2022).

[46] Z. Yan, Z. Y. Meng, D. A. Huse, and A. Chan, Height-conserving quantum dimer models, Phys. Rev. B **106**, L041115 (2022).

[47] S. Elitzur, Impossibility of spontaneously breaking local symmetries, Phys. Rev. D **12**, 3978 (1975).

[48] X.-G. Wen, Quantum orders and symmetric spin liquids, Phys. Rev. B **65**, 165113 (2002).

[49] G. Baskaran and P. W. Anderson, Gauge theory of high-temperature superconductors and strongly correlated Fermi systems, Phys. Rev. B **37**, 580 (1988).

[50] I. Affleck and J. B. Marston, Large-n limit of the Heisenberg-Hubbard model: Implications for high-T_c superconductors, Phys. Rev. B **37**, 3774 (1988).

[51] I. Affleck, Large-n limit of SU(n) quantum "spin" chains, Phys. Rev. Lett. **54**, 966 (1985).

[52] D. T. Son, Is the composite fermion a Dirac particle?, Phys. Rev. X **5**, 031027 (2015).

[53] D. T. Son, The Dirac Composite Fermion of the fractional quantum Hall effect, Annu. Rev. Condens. Matter Phys. **9**, 397 (2018).

[54] S. D. Geraedts, M. P. Zaletel, R. S. K. Mong, M. A. Metlitski, A. Vishwanath, and O. I. Motrunich, The half-filled Landau level: The case for Dirac composite fermions, Science **352**, 197 (2016).

[55] G. Kotliar, Resonating valence bonds and d-wave superconductivity, Phys. Rev. B **37**, 3664 (1988).

[56] V. Borokhov, A. Kapustin, and X. Wu, Topological disorder operators in three-dimensional conformal field theory, J. High Energy Phys. 11 (2002) 049.

[57] M. Hermele, T. Senthil, M. P. A. Fisher, P. A. Lee, N. Nagaosa, and X.-G. Wen, Stability of $U(1)$ spin liquids in two dimensions, Phys. Rev. B **70**, 214437 (2004).

[58] T. Appelquist, D. Nash, and L. C. R. Wijewardhana, Critical behavior in (2+1)-dimensional QED, Phys. Rev. Lett. **60**, 2575 (1988).

[59] D. Nash, Higher-order corrections in (2+1)-dimensional QED, Phys. Rev. Lett. **62**, 3024 (1989).

[60] S. Albayrak, R. S. Erramilli, Z. Li, D. Poland, and Y. Xin, Bootstrapping $N_f = 4$ conformal QED_3, Phys. Rev. D **105**, 085008 (2022).

[61] N. Karthik and R. Narayanan, Numerical determination of monopole scaling dimension in parity-invariant three-dimensional noncompact QED, Phys. Rev. D **100**, 054514 (2019).

[62] S. M. Chester and S. S. Pufu, Towards bootstrapping QED_3, J. High Energy Phys. 08 (2016) 019.

[63] A. Polyakov, Compact gauge fields and the infrared catastrophe, Phys. Lett. B **59**, 82 (1975).

[64] A. Polyakov, Quark confinement and topology of gauge theories, Nucl. Phys. B **120**, 429 (1977).

[65] S. Sachdev, Spin-Peierls ground states of the quantum dimer model: A finite-size study, Phys. Rev. B **40**, 5204 (1989).

[66] P. W. Leung, K. C. Chiu, and K. J. Runge, Columnar dimer and plaquette resonating-valence-bond orders in the quantum dimer model, Phys. Rev. B **54**, 12938 (1996).

[67] O. F. Syljuåsen, Plaquette phase of the square-lattice quantum dimer model: Quantum Monte Carlo calculations, Phys. Rev. B **73**, 245105 (2006).

[68] A. Ralko, D. Poilblanc, and R. Moessner, Generic mixed columnar-plaquette phases in Rokhsar-Kivelson models, Phys. Rev. Lett. **100**, 037201 (2008).

[69] D. Banerjee, M. Bögli, C. P. Hofmann, F.-J. Jiang, P. Widmer, and U.-J. Wiese, Interfaces, strings, and a soft mode in the square lattice quantum Dimer model, Phys. Rev. B **90**, 245143 (2014).

[70] T. Oakes, S. Powell, C. Castelnovo, A. Lamacraft, and J. P. Garrahan, Phases of quantum dimers from ensembles of classical stochastic trajectories, Phys. Rev. B **98**, 064302 (2018).

[71] N. Seiberg, T. Senthil, C. Wang, and E. Witten, A duality web in 2+1 dimensions and condensed matter physics, Ann. Phys. **374**, 395 (2016).

[72] X.-G. Wen, Quantum order: A quantum entanglement of many particles, Phys. Lett. A **300**, 175 (2002).

[73] I. Affleck, Z. Zou, T. Hsu, and P. W. Anderson, $SU(2)$ gauge symmetry of the large-U limit of the Hubbard model, Phys. Rev. B **38**, 745 (1988).

[74] E. Dagotto, E. Fradkin, and A. Moreo, SU(2) gauge invariance and order parameters in strongly coupled electronic systems, Phys. Rev. B **38**, 2926 (1988).

[75] I. S. Villadiego, Pseudoscalar $U(1)$ spin liquids in α-$RuCl_3$, Phys. Rev. B **104**, 195149 (2021).

[76] N. Seiberg and S.-H. Shao, Majorana chain and Ising model–(non-invertible) translations, anomalies, and emanant symmetries, arXiv:2307.02534.

[77] S.-S. Lee and P. A. Lee, $U(1)$ gauge theory of the hubbard model: Spin liquid states and possible application to κ-(BEDT- TTF)$_2$Cu$_2$(CN)$_3$, Phys. Rev. Lett. **95**, 036403 (2005).

[78] M. Hermele, $SU(2)$ gauge theory of the Hubbard model and application to the honeycomb lattice, Phys. Rev. B **76**, 035125 (2007).

[79] M. E. Peskin, Mandelstam-'t Hooft duality in Abelian lattice models, Ann. Phys. **113**, 122 (1978).

[80] C. Dasgupta and B. I. Halperin, Phase transition in a lattice model of superconductivity, Phys. Rev. Lett. **47**, 1556 (1981).

[81] M. P. A. Fisher and D.-H. Lee, Correspondence between two-dimensional bosons and a bulk superconductor in a magnetic field, Phys. Rev. B **39**, 2756 (1989).

[82] Y. Ran, M. Hermele, P. A. Lee, and X.-G. Wen, Projected-wave-function study of the spin-$\frac{1}{2}$ Heisenberg model on the kagomé lattice, Phys. Rev. Lett. **98**, 117205 (2007).

[83] O. Ma and J. B. Marston, Weak ferromagnetic exchange and anomalous specific heat in $ZnCu_3(OH)_6Cl_2$, Phys. Rev. Lett. **101**, 027204 (2008).

[84] Y. Iqbal, F. Becca, S. Sorella, and D. Poilblanc, Gapless spin-liquid phase in the Kagome spin-$\frac{1}{2}$ Heisenberg antiferromagnet, Phys. Rev. B **87**, 060405(R) (2013).

[85] Y. Iqbal, F. Ferrari, A. Chauhan, A. Parola, D. Poilblanc, and F. Becca, Gutzwiller projected states for the $J_1 - J_2$ Heisenberg model on the Kagome lattice: Achievements and pitfalls, Phys. Rev. B **104**, 144406 (2021).

[86] D. Sen and R. Chitra, Large-U limit of a Hubbard model in a magnetic field: Chiral spin interactions and paramagnetism, Phys. Rev. B **51**, 1922 (1995).

[87] O. I. Motrunich, Orbital magnetic field effects in spin liquid with spinon Fermi sea: Possible application to κ-$(ET)_2Cu_2(CN)_3$, Phys. Rev. B **73**, 155115 (2006).

[88] H. Katsura, N. Nagaosa, and P. A. Lee, Theory of the thermal Hall effect in quantum magnets, Phys. Rev. Lett. **104**, 066403 (2010).

[89] P. Czajka, T. Gao, M. Hirschberger, P. Lampen-Kelley, A. Banerjee, J. Yan, D. G. Mandrus, S. E. Nagler, and N. Ong, Oscillations of the thermal conductivity in the spin-liquid state of α-$RuCl_3$, Nat. Phys. **17**, 915 (2021).

[90] J. Bruin, R. Claus, Y. Matsumoto, J. Nuss, S. Laha, B. Lotsch, N. Kurita, H. Tanaka, and H. Takagi, Origin of oscillatory structures in the magnetothermal conductivity of the putative Kitaev magnet α-$RuCl_3$, APL Mater. **10**, 090703 (2022).

[91] S. Suetsugu, Y. Ukai, M. Shimomura, M. Kamimura, T. Asaba, Y. Kasahara, N. Kurita, H. Tanaka, T. Shibauchi, J. Nasu, Y. Motome, and Y. Matsuda, Evidence for a phase transition in the quantum spin liquid state of a Kitaev candidate α-$RuCl_3$, J. Phys. Soc. Jpn. **91**, 124703 (2022).

[92] É. Lefrançois, J. Baglo, Q. Barthélemy, S. Kim, Y.-J. Kim, and L. Taillefer, Oscillations in the magnetothermal conductivity of α-$RuCl_3$: Evidence of transition anomalies, Phys. Rev. B **107**, 064408 (2023).